Diagenetic and Mineralogical Effects in Clumped Isotope Thermometry and Application to Last Interglacial Climate

by

Ian Zacharia Winkelstern

A dissertation submitted in partial fulfillment
of the requirements for the degree of
Doctor of Philosophy
(Earth and Environmental Sciences)
in the University of Michigan
2016

Doctoral Committee:

Professor Kyger C. Lohmann, Chair
Professor George W. Kling
Associate Professor Nathan A. Niemi
Professor Christopher J. Poulsen

Acknowledgements

A great many people made the following work possible, and I would not have completed this project without the help, support, and guidance of too many people to name. I will first thank my committee for their time and effort put towards making this dissertation better. I also appreciate the research support from GSA, AAPG, SEG, the Turner Fund, and Rackham Graduate School that made many of the needed analyses and field work possible. My advisor Kacey Lohmann facilitated funding as well, but more importantly gave me a shot, taught me how to work a mass spectrometer, made me a much better scientist, and bought a beer or two along the way. Thanks to Lora Wingate for letting me get my hands on everything in the lab and for lending an ear. To Will Defliese, Sierra Petersen, Kyle Meyer, and Brice Lacroix: I would not have made it without your advice, help, and conversation, scientific and otherwise. Petr Yakovlev, Collin Ward, Alyssa Abbey, and many others also kindly listened to my issues along the way. I also appreciate Steven Clark, Christian Smith, and Gage Clark allowing me to talk about and do something other than geochemistry once in a while.

The support of my parents and stepparents has been unwavering and indispensable. Thanks for being my biggest cheerleaders. Finally, Colleen Long deserves as much credit as I do for bringing this dissertation together. You are the best editor, fan, mentor, counselor, and escape I could ask for, and I cannot wait to start the next adventure with you. Thanks.

Table of Contents

List of Figures

Figure

List of Tables

Table

List of Equations

Equation

List of Appendices

Appendix

Abstract

The relatively new clumped isotope thermometer shows great promise for paleoclimate reconstruction, as it allows for measurement of carbonate formation temperature without assuming water isotopic composition. This dissertation focuses on how mineralogical differences affect original clumped isotope (Δ_{47}) values and how they are changed through diagenesis. A primary motivation for this work was to understand the geologic conditions under which the clumped isotope thermometer can be applied with confidence to paleoclimatic problems.

To place empirical constraints on the conditions under which Δ_{47} alteration can occur, samples from a ~4500 m long drill core from Andros Island, Bahamas were analyzed. These limestones and dolomites formed under near-surface temperature conditions, but for samples below ~1.3 km in depth, calculated Δ_{47} temperatures increase by ~10° C. This indicates a shift from preserved near-surface temperatures to diagenetically modified values. Importantly, this shift is not accompanied by changes in common diagenetic indicators, and thus raises the possibility of solid-state clumped isotope alteration occurring at much lower temperatures than previously thought. Similar Δ_{47} temperatures recorded by each carbonate phase suggest that fine-grained dolomites and calcites are equally viable materials for recording surface temperature conditions, but both are also equally susceptible to alteration of their primary clumped isotope abundances when buried.

A challenge remaining in clumped isotope thermometry was the lack of an empirical calibration for dolomite, which had been theoretically predicted to differ from established calibrations. Here, analysis of a set of synthetic and natural dolomites formed at known temperatures results in a calibration line statistically indistinguishable from calcite clumped isotope calibrations. This supports the idea of a universal calibration for carbonate clumped isotope thermometry and enables new investigations into conditions of dolomite formation.

For example, many of the Early Paleozoic carbonate buildups of the Wabash Platform in the American Midwest are now entirely dolomitized, but the Pipe Creek Junior Quarry in central Indiana exposes a unique bioherm with only minor dolomite. Petrographic and stable isotope analyses demonstrate a fresh-saline mixed water origin for this dolomite and facilitate development of a diagenetic model. Clumped isotope and fluid inclusion temperature analyses of late calcite spars indicate hot fluids were transported through the complex, apparently altering the clumped isotope composition of original dolomite and calcite.

Finally, the clumped isotope thermometer can be applied to key intervals for investigating paleoclimate and testing paleoclimate questions. To determine sea surface temperatures and water composition in Bermuda during the onset of Last Interglacial sea level rise, conventional and clumped isotope measurements of fossil shells were conducted. These results suggest meltwater influence and temperatures as much as 10° C colder than modern, requiring explanations that allow for major changes in North Atlantic surface ocean circulation. They also illustrate extreme sensitivity of Bermudian climate to broad-scale climate and ocean circulation changes.

Chapter 1

Introduction

Since the first measurements by Urey (1948), McCray (1950) and Epstein et al. (1951), analyses of oxygen isotopes in carbonates have been the foundation of paleoceanographic and paleoclimatic research. Such measurements of microfossil shells in oceanic sediment cores have produced especially important data. By studying changes in the ratio of heavier to lighter isotopes (^{18}O and ^{16}O) in these fossils, we have learned much about global climate changes and patterns over the last ~70 million years (e.g., Zachos et al. 1994 and 2001). This is because the oxygen isotope ratio of a carbonate, measured as $\delta^{18}O$, is a function of temperature and the isotopic composition of the water it formed in. The latter variable, however, changes based on a variety of poorly constrained factors (e.g. local evaporation, local fresh water input, and global ice volume), thus limiting the scope of paleotemperature data that can be obtained using $\delta^{18}O$ measurements.

Many approaches and techniques have been designed to circumvent this problem. Examples include measurement of Mg/Ca ratios in microfossils (Nürnberg et al. 1996), and analyses of organic compounds in sediment known as 'TEX_{86}' (Brassell et al. 1986). These approaches, however, have significant limitations. Their shortcomings are especially apparent when applied to deeper geologic time, as ocean Mg/Ca ratios and empirical organic compound-temperature relationships are poorly constrained beyond a few tens of millions of years ago. It is

for this reason that the development of carbonate clumped isotope thermometry by Eiler and Schauble (2004) and Ghosh et al. (2006) is transformative. This approach is based on the abundance of rare carbonate isotopologues containing both a heavy carbon isotope (^{13}C) and a heavy oxygen isotope (^{18}O), relative to the calculated randomized abundance of these species. Using clumped isotopes allows for measurement of formation temperature of carbonates without any assumptions about the isotopic composition of the water in which they formed, and clumped isotopes can ostensibly be applied to any carbonate – including those formed in terrestrial or estuarine environments. The clumped isotope thermometer may therefore revolutionize the study of climate evolution of the Earth's surface, perhaps even over deep geological time spanning tens to hundreds of millions of years.

The development and refinement of clumped isotope thermometry has been challenging and is ongoing. The approach is analytically difficult, as extraordinary measurement precision is required. These 'clumped' isotopologues containing heavy isotopes of carbon and oxygen represent about 0.0048 % of all carbonate molecules (Eiler and Schauble, 2004). This tiny fraction means that obtaining a statistically significant data point requires at least six hours of mass spectrometer measurement time. As described below, many questions also remain about how carbonate mineralogy affects clumped isotope temperatures, and how different carbonates are affected by a range of diagenetic processes after original formation. A better understanding of alteration during burial is especially needed. Theoretical models and experimental data show that, at elevated temperatures, solid-state isotope reordering can occur within the carbonate crystal lattice (Passey and Henkes, 2012; Stolper and Eiler, 2015). This means that diagenetic screening techniques previously applied to studies of $\delta^{18}O$ are insufficient for clumped isotope research.

Much of this dissertation focuses on placing constraints on these problems. This thesis specifically investigates clumped isotopes in dolomite, an understudied carbonate relative to calcite and aragonite. The possibility of temperature constraints on dolomite formation is exciting because the mineral's formation mechanisms remain poorly understood. Much of Earth's dolomite forms at or near the surface (Given and Wilkinson, 1986), and thus potential also exists for use of dolomite as a proxy for the reconstruction of paleotemperature. It has been proposed that clumped isotope signals in dolomite might be better preserved than in other carbonates because of the material's different crystal structure and its inherently diagenetic nature (Eiler, 2011).

Chapter 2[1] begins to address these issues by evaluating how clumped isotope compositions vary in a ~4.5 km long core collected from Andros Island in The Bahamas. The Great Bahama Bank has remained a tropical shallow water carbonate platform since at least the Cretaceous, so this core material is almost entirely fine grained carbonate rock originally formed at ~25° to ~30° C. Varying mineralogies allow for sampling of calcites and dolomites over a range of shallow to deep burial conditions. My results show apparent preservation of original clumped isotope signals in both mineralogies over ~40 million years and to ~1.3 km burial depth. Below that point, however, clumped isotope inferred temperatures increase beyond reasonable Earth surface conditions. The clumped isotope composition of fine grained dolomites and limestones below this threshold demonstrate strong sensitivity to diagenetic alteration, and raise the possibility of solid-state alteration occurring at temperatures well below the 100° C threshold proposed by Passey and Henkes (2012). These observations also indicate that dolomite is not a

[1] Winkelstern, I., and Lohmann, K., *in review*. Geology.

more resilient proxy than other minerals and is equally prone to resetting of its primary paleotemperature signal.

The goal of Chapter 3[2] is to improve the accuracy of dolomite clumped isotope thermometry by developing the first dolomite-specific empirical temperature calibration. Small differences in calcite and dolomite clumped isotope calibrations have been theorized (Guo et al. 2009), but the results of Chapter 2 do not indicate a mineralogical difference. Dolomite is notoriously difficult to precipitate in a laboratory at temperatures below ~150° C (e.g., Land, 1998). I therefore targeted a set of natural dolomites formed under relatively well-constrained low temperature conditions ranging from ~17° – ~70° C. I also measured the clumped isotope value of a suite of synthetic dolomites grown over a range of 200° – 250° C. When compared against calcites and aragonites formed at known temperatures and analyzed in the same laboratory, my dolomite data indicate no statistical difference between calibrations.

Chapter 4[3] provides an example of how dolomite and calcite clumped isotope thermometry can contribute to understanding the diagenetic evolution of a carbonate system. Much of the Great Lakes region of the United States was a tropical shallow water carbonate platform during the Silurian (~430 Ma). Of the many Silurian buildups that dot the area, the Pipe Creek Junior carbonate complex in central Indiana is exceptional in that it is only partially dolomitized (Devaney et al. 1986). Because most comparable deposits have been overprinted by complete dolomitization, Pipe Creek Junior offers a unique opportunity to examine its diagenetic evolution and to evaluate the processes that have likely affected sediments throughout the region. Based on petrographic evaluation as well as conventional and clumped isotope analyses, I show that partial dolomitization occurred during the Silurian via the mixing of fresh and marine

[2] Winkelstern, I., Kaczmarek, S., Lohmann, K., Humphrey, J., *in review*. Geochimica et Cosmochimica Acta.

[3] Winkelstern, I., Lohmann, K., and Breining, K., *in prep*. Journal of Sedimentary Research.

waters. Much later, hot saline brines, likely derived from the Michigan Basin, passed through the complex. These brines altered original marine calcite and dolomite clumped isotope compositions and also precipitated fluid-inclusion rich calcite spars.

As perhaps a contrast to these diagenetic and methodological studies, Chapter 5[4] showcases the potential of the clumped isotope paleothermometer for paleoclimate reconstruction when applied to unaltered materials. The Last Interglacial, ~125 thousand years ago, is the most recent geologic interval during which global temperatures were 1° – 2° C warmer than preindustrial conditions (i.e., similar to today; Crowley and Kim, 1994). It is therefore an important interval for testing climate models and for understanding climate processes that may be relevant for anthropogenic warmth. Ocean sediment core records suggest that a warmer-than-modern North Atlantic contrasted with cooler-than-modern tropics, implying increased poleward heat transport (Rahmstorf, 2002). Because the climate of Bermuda is largely controlled by the warm nearby Gulf Stream, I sought to measure the paleoclimate of Bermuda and therefore also evaluate Last Interglacial ocean current heat transport. I did this by analyzing fossil gastropod shells from ~125 ka deposits on the island, combining clumped isotope-derived water $\delta^{18}O$ compositions and high-resolution carbonate $\delta^{18}O$ measurements taken along each shell's growth. These data permit construction of multi-year records of Last Interglacial sea surface temperature in Bermuda. Surprisingly, they indicate temperatures as much as 10° C colder than today, seemingly requiring dramatic changes in North Atlantic circulation. When combined with calculated water $\delta^{18}O$ values that indicate lowered salinities, these data likely indicate shutdown of the Gulf Stream during rapid ice sheet collapse. Such events are known to

[4] Winkelstern, I., Lohmann, K., Rowe, M., Defliese, W., Brewer, A. *in review*. Proceedings of the National Academy of Sciences.

have occurred during the last deglaciation (~17 ka; Hill and Condron 2014), but this is the first paleotemperature record documenting such an event in a previous interglacial.

Finally, Chapter 6 summarizes these findings and discusses possibilities for future work.

References

Brassell, S.C., Eglinton, G., Marlowe, I.T., Pflaumann, U., Sarnthein, M., 1986. Molecular Stratigraphy – A New Tool for Climatic Assessment. Nature 320, 129–133.

Crowley, T. J. and Kim, K.-Y., 1994. Milankovitch forcing of the last interglacial sea level. Science, 265, 1566–1568.

Devaney, K.A., Wilkinson, B.H., and Van der Voo, R., 1986. Deposition and compaction of carbonate clinothems: the Silurian Pipe Creek Junior complex of east-central Indiana: Geological Society of America Bulletin, 97, 37-38.

Eiler, J. M., 2011. Paleoclimate reconstruction using carbonate clumped isotope thermometry: Quaternary Science Reviews, 30, 3575–3588, doi:10.1016/j.quascirev.2011.09.001.

Eiler, J. M., and Schauble, E., 2004. $^{18}O^{13}C^{16}O$ in Earth's atmosphere. Geochimica et Cosmochimica Acta, 68, 4767-4777.

Epstein, S., Buchsbaum, R., Lowenstam, H., and Urey, H. C., 1951. Carbonate-Water Isotopic Temperature Scale, *Geological Society of America Bulletin*, *62*(4), 417-426.

Ghosh, P., Adkins, J., Affek, H., Balta, B., Guo, W., Schauble, E. A., Schrag, D., and Eiler, J. M., 2006. 13C-18O bonds in carbonate minerals: A new kind of paleothermometer: Geochimica et Cosmochimica Acta, 70, p. 1439–1456, doi:10.1016/j.gca.2005.11.014.

Given, R.K., Wilkinson, B.H., 1987. Dolomite abundance and stratigraphic age; constraints on rates and mechanisms of Phanerozoic dolostone formation. J. Sediment. Res., 57, 1068–1078

Guo, W., Mosenfelder, J. L., Goddard III, W. A., and Eiler, J. M., 2009. Isotopic fractionations associated with phosphoric acid digestion of carbonate minerals: Insights from first-principles theoretical modeling and clumped isotope measurements: Geochimica et Cosmochimica Acta, 139, 7203-7225, doi:10.1016/j.gca.2009.05.071.

Hill, J. C. & Condron, A., 2014. Subtropical iceberg scours and meltwater routing in the deglacial western North Atlantic. Nat Geosci, 7.

Land, L.S., 1998. Failure to precipitate dolomite at 25° C from dilute solution despite 1000-fold oversaturation after 32 years. Aquatic Geochemistry, 4, 361-368.

McCrea, J. M., 1950. On the Isotopic Chemistry of Carbonates and a Paleotemperature Scale. The Journal of Chemical Physics, 18, 849-857.

Nurnberg, D., Bijma, J., Hemleben, C., 1996, Assessing the reliability of magnesium in foraminiferal calcite as a proxy for water mass temperatures. Geochimica et Cosmochimica Acta, 60, 803-814.

Passey, B. H., and Henkes, G. A., 2012. Carbonate clumped isotope bond reordering and geospeedometry: Earth and Planetary Science Letters, 351, 223–236, doi:10.1016/j.epsl.2012.07.021.

Rahmstorf, S., 2002. Ocean circulation and climate during the past 120,000 years. Nature, 419**,** 207–214.

Stolper, D. A., and Eiler, J. M., 2015. The kinetics of solid-state isotope-exchange reactions for clumped isotopes: A study of inorganic calcites and apatites from natural and experimental samples: American Journal of Science, 315, 363-411, doi: 10.2475/05.2015.01.

Urey, H.C., 1948. Oxygen Isotopes in Nature and in the Laboratory. Science, 108, 489-496.

Zachos, J. C., Pagani, M., Sloan, L., Thomas, E., and Billups, K., 2001. Trends, Rhythms, and Aberrations in Global Climate 65 Ma to Present. Science, 292, 686-693.

Zachos, J.C., Stott, L. D., Lohmann, K. C, 1994. Evolution of early Cenozoic marine temperatures. Paleoceanography, 9, 353-387.

Chapter 2

Shallow Burial Alteration of Dolomite and Limestone Clumped Isotope Geochemistry[5]

2.1 Abstract

Carbonate clumped isotope paleothermometry is a promising method for paleoclimate reconstructions and understanding diagenetic processes, however, clumped isotope compositions (measured as Δ_{47} values) can be altered by recrystallization and thermal resetting. Several studies have investigated the effects of deep burial and exhumation on Δ_{47} values; here I present Δ_{47} values of still-buried samples from a ~4500 m long drill core from Andros Island, Bahamas that represent the spectrum from shallow to deep burial conditions. These limestones and dolomites originally formed under near-surface temperature conditions, which are reflected by ~27° C Δ_{47} temperatures in samples buried to less than ~1.3 km depth. Below this threshold, calculated Δ_{47} temperatures increase by ~10° C, indicating a shift from preserved near-surface temperatures to diagenetically modified values. Importantly, this shift is not accompanied by a change in $\delta^{18}O$, $\delta^{13}C$, or cathodoluminescence, and non-uniform μm-scale crystallization is observed in both Δ_{47}-altered and unaltered rocks. Similar Δ_{47} temperatures recorded by each carbonate phase suggest that fine-grained dolomites and calcites are equally viable materials for recording surface temperature conditions, both are also equally susceptible to alteration of their primary clumped

[5] Winkelstern, I., and Lohmann, K., *in review*. Geology.

isotope abundances when subjected to burial diagenesis. These results demonstrate that original Δ_{47} values of fine-grained and micritic carbonates (e.g., lacustrine carbonates and soil nodules) can be altered under mild diagenetic conditions.

2.2 Introduction

Carbonate clumped isotope thermometry is a relatively new technique used to determine the formation temperature of carbonates. It is a rapidly expanding field with applications for paleoclimate, tectonics, diagenesis, and paleontology (Eiler, 2011). The clumped isotopic composition of CO_2 liberated from carbonate dissolution, Δ_{47}, refers to the degree to which ^{18}O and ^{13}C are uniquely bonded in CO_2 molecules relative to their stochastic abundance (Ghosh et al., 2006). Measurement of Δ_{47} can potentially answer many long-standing geologic questions because it solely reflects the formation temperature of a sample independent of other factors, e.g., the $\delta^{18}O$ value of the water from which the carbonate precipitated (Ghosh et al., 2006; Eiler, 2011).

Carbonate Δ_{47} values demonstrate a greater sensitivity to diagenetic alteration than conventional $\delta^{18}O$ and $\delta^{13}C$, and the conditions under which alteration can occur are not fully understood (e.g., Eiler, 2011; Passey and Henkes, 2012; Shenton et al., 2015). Resetting of clumped isotopes in buried carbonates can occur without bulk recrystallization (Dennis and Schrag 2010), as solid-state reordering of C-O bonds in carbonates exposed to temperatures >100° C can alter Δ_{47} compositions without changing typical diagenetic indicators such as $\delta^{18}O$ and $\delta^{13}C$, trace and major elemental concentrations, or mineral texture (Passey and Henkes, 2012; Henkes et al., 2014; Stolper and Eiler, 2015). It is known that the magnitude of these changes varies with crystal structure. For example, calcite spar resets more easily than

brachiopod shell carbonate (Shenton et al., 2015), but such changes have not been evaluated for other carbonate mineralogies, such as dolomite.

The clumped isotopic composition of a carbonate can also be altered by fluid mediated diagenesis and recrystallization. This may explain why many fine-grained and micritic carbonates have provided unreasonably high clumped isotope temperatures that are difficult to reconcile with either surface or diagenetic conditions. Quade et al. (2013), for example, observed a consistent increase in Δ_{47} temperatures with modeled depth in exhumed soil nodule samples buried > 3 km deep at geothermal temperatures > 75° C. Similarly, Huntington et al. (2014) found inferred temperatures above 40° C for Himalayan lake carbonates, despite measuring surface-like Δ_{47} temperatures for coeval fossils. Such results raise questions about the applicability of the clumped isotope paleothermometer to fine-grained carbonates. It is imperative to constrain the conditions under which the clumped isotope composition of fine grained carbonates can be altered by burial and diagenesis in order to confidently use these materials for surface temperature reconstructions or other applications.

I analyzed samples collected at depth from the Andros I drill core from Andros Island, Bahamas (Fig. 2.1) in contrast to previous studies which examined clumped isotopes of exhumed materials (e.g., Shenton, 2015). The relatively continuous sedimentation of the Great Bahama Bank carbonate platform provides ideal compositional conditions to evaluate the sensitivity of Δ_{47} values in co-occurring calcite and dolomite never exposed to geothermal temperatures > 100° C. I specifically tested: (1) how lithification and shallow-burial diagenesis is reflected in near surface clumped isotope values, (2) how clumped isotope values are altered as depth increases under a relatively shallow geothermal gradient, and (3) differences between calcite and

dolomite Δ_{47} values formed and altered under similar temperature conditions, both in near-surface carbonates and at depth.

2.3 Material and Methods

The sedimentary environments documented in the Andros core are interpreted to have remained broadly unchanged since deposition began in the Cretaceous (Goodell and Garman, 1969; Eberli and Ginsburg, 1987). Tropical climate has not varied drastically over the Cenozoic (Pearson et al., 2001), and growth of the Andros Bank has likely kept water depths shallow (Schlager and Ginsburg, 1981).

Diagenetic studies suggest that lithification and dolomitization on the Great Bahama Bank occur relatively soon after deposition. Limestones 35 – 75 m below Andros Island are well lithified via submarine cementation (Beach, 1993), and dolomite occurs in the shallow subsurface coincident with hiatuses, as minor cement in void spaces, and as massive dolomite formed via circulation of marine waters (Swart and Melim, 2000). Multiple dolomitization phases via different subsurface flow mechanisms are known to occur in the upper 160 m of the Great Bahama Bank (Swart et al., 1987; Vahrenkamp and Swart, 1994). To a depth of 3250 m, dolomites in the core are also roughly coincident with erosion surfaces suggested by Goodell and Garman (1969), with completely dolomitized horizons interspersed with pure limestone and mixed mineralogies (Fig. 2.S1). Essentially all of this material is fine grained (< 0.1 mm) and macrofossils were not observed. The combination of this near-surface diagenesis, dolomitization, and lithification should ultimately result in bulk rock Δ_{47} temperatures that roughly equal mean annual water temperatures (~27° C) for both limestone and dolomite.

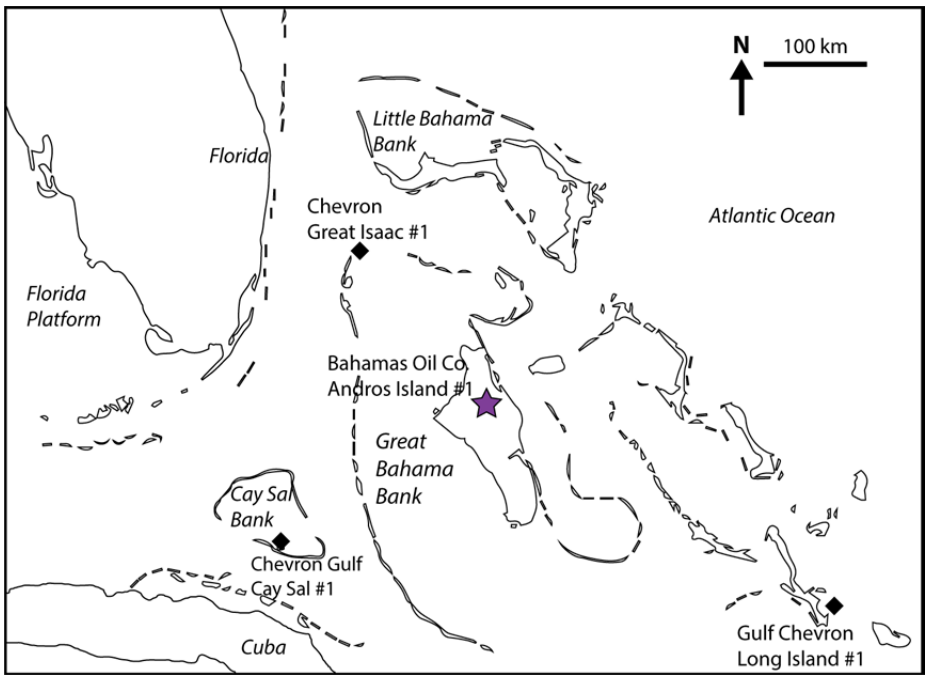

Figure 2.1. Map of the Bahamas, with the Andros Island I well location (star). Diamonds indicate other regional deep wells (used for geothermal gradient estimation, see Fig. 2.2).

Ten samples of 80% – 100% dolomite and eight samples of 80% – 100% calcite (indicated by XRD; see Appendix 2.1) were taken at depths of 122 to 4413 m. Calcite and dolomite subsamples were milled from the same rock sample at depths of 1859 and 3240 m. I studied the petrology and cathodoluminescence of fifteen thin sections at depth intervals ranging from 206 to 4413 m, eight of which overlapped with clumped isotope samples. Goodell and Garman (1969) studied the petrography of the entire Andros I core, and our petrographic assessment is concordant with their findings (see Appendix 2.1). I observed no cathodoluminescence in any sample. This is a common indicator of recrystallization, but local rocks may not have provided a necessary Mn source.

Carbonate samples were measured three to five times for their stable and clumped isotopic composition following methods described by Defliese et al. (2015; see Appendix 2.2). A minimum of 4 mg was used for each measurement. I applied the 75° C phosphoric acid correction of +0.067 ‰ to all Δ_{47} data, based on the identical calcite and dolomite clumped isotope fractionation factors of Defliese et al. (2015). For each depth horizon where samples were measured for clumped isotopes, one additional sample was measured for $\delta^{18}O$ and $\delta^{13}C$ using a Kiel IV automated preparation device coupled to a Thermo Scientific MAT 253 mass spectrometer (with analytical precision better than 0.1 ‰). As a test for heterogeneous recrystallization, three to four cm-spaced samples were also milled from three limestones and three dolomites at 122, 499, 1330, 1859 (2 samples), and 4413 m depth and measured via the Kiel IV method. Even though sample powders were not identical, there is general consistency of $\delta^{18}O$ and $\delta^{13}C$ results by either clumped or Kiel IV preparation.

Clumped isotope temperatures were calculated using the combined Δ_{47}-temperature high temperature acid calibration of Defliese et al. (2015) because: (1) it is based on compiled data

from several calibration studies; (2) it uses only data from samples reacted in a common acid bath at 75° C or greater (the method used in this study); and (3) it incorporates data measured on the same apparatus as these samples, thereby reducing the impacts of any method-specific effects. The same calibration was applied to dolomite and calcite samples; this is discussed below.

2.4 Results

Calculated temperatures from clumped isotope analysis of samples above 1300 m depth range from 26° to 32° C, with an average of 28° ± 1° C. This compares well with modern mean annual sea surface temperatures of ~27° C. Below this depth, I find a consistent offset of Δ_{47} values as indicated by an abrupt increase of ~10° C in calculated temperature (Fig. 2.2). All samples taken from a depth of 1330 m or below show temperatures > 35° C. Variability also increases with depth; the standard deviation for Δ_{47} temperatures is 2.1° C above 1300 m and 9.5° C below 1300 m. All samples record temperatures colder than geothermal temperatures. Carbonate Δ_{47} values therefore reflect varying mixtures of original and burial signatures.

$\delta^{18}O$ values decrease downcore while maintaining consistent variability, with the deepest dolomite samples ~2.5 ‰ more negative than near-surface samples and deep calcites ~1 ‰ more negative than the shallowest calcites (Fig. 2.2). $\delta^{13}C$ values in contrast do not show trends or increased variability downcore. The ~2 ‰ spread in $\delta^{18}O$ values for dolomite at 1859 m depth is likely due to variable amounts of calcite incorporated into powders sampled from the rock.

Using combined carbonate clumped isotope $\delta^{18}O$ and Δ_{47} data, calculated dolomite $\delta^{18}O_{water}$ values increase by ~2 ‰ downcore, while calcite values do not show consistent trend.

All samples with unaltered Δ_{47} values (above 1300 m depth) have water $\delta^{18}O$ values ranging from -0.3 to +1.9 ‰ VSMOW (Fig. 2.2).

2.5 Discussion

2.5.1 Shift in Δ_{47}

Consistent Δ_{47} values to 1300 m depth seem to indicate relative climate stability in the Bahamas since at least the Eocene. Calculated water $\delta^{18}O$ values for these samples also compare well with modern $\delta^{18}O_{water}$ values measured near Andros Island (+0.7 to +2.8 ‰ VSMOW; Swart et al., 2009). The abrupt ~10° increase in Δ_{47} temperatures indicated by a sample at 1330 m depth does not reflect a climate signal, as these conditions exceed reasonable Bahamian conditions, even during the climatically warm Cretaceous (Pearson et al., 2001). Increased variability of Δ_{47} values below 1300 m relative to values above further suggests heterogeneous alteration. This alteration, due to recrystallization or solid-state reordering, begins at a remarkably shallow depth and is unexpectedly consistent downcore.

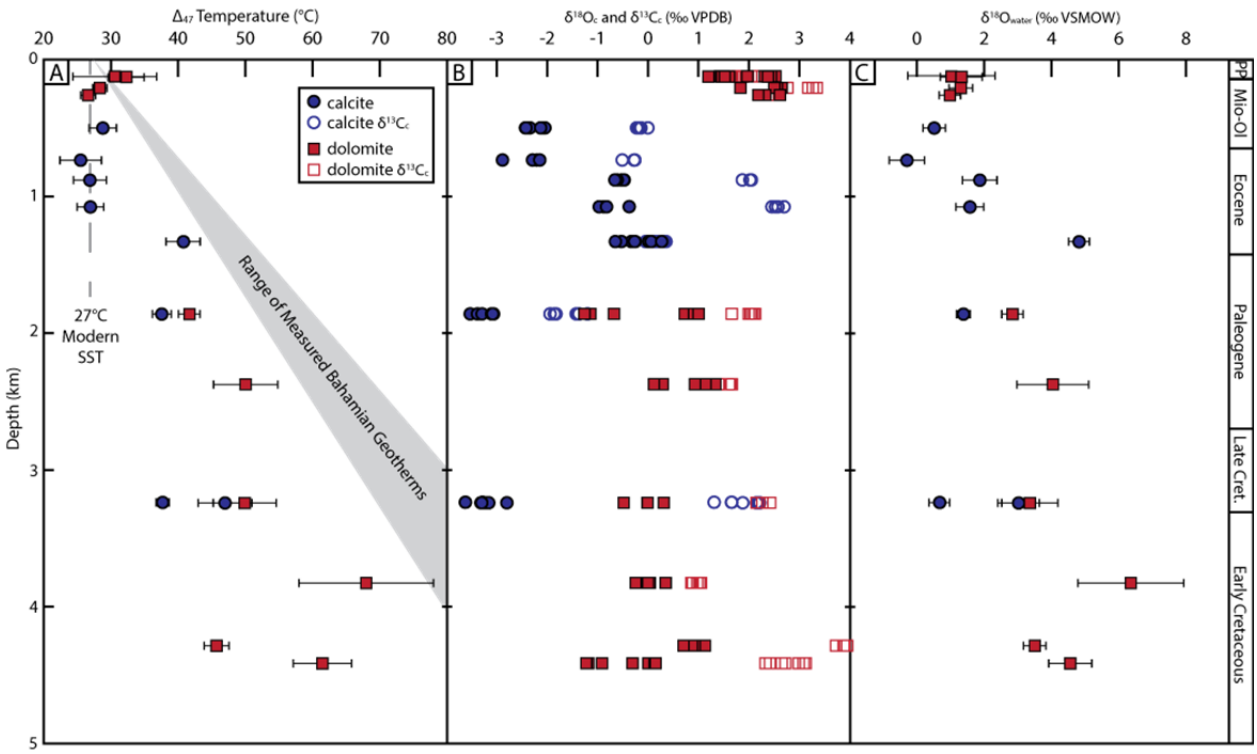

Figure 2.2. A) Clumped isotope temperatures relative to sample depth. The range of measured regional geotherms is from data from the three additional wells shown in Fig. 2.1. B) Conventional carbonate isotope data. Analytical errors are smaller than symbol size. C) Water $\delta^{18}O$ (‰ VSMOW) calculated from clumped isotope temperatures and concurrent carbonate $\delta^{18}O$ measurements, via the fractionation factors of Kim and O'Neil (1997) for calcite and Horita (2014) for dolomite. All error bars reflect one standard error of the mean.

2.5.2 Dolomite Clumped Isotope Thermometry

There is little difference between corresponding dolomite and calcite Δ_{47} values. Where calcite and dolomite were subsampled from the same interval (at 1859 m and 3240 m), calcite Δ_{47} temperatures are on average ~2° C degrees cooler than dolomites sampled from the same rock. Above 1300 m, average dolomite and calcite Δ_{47} temperatures are the same within one standard error (29.7° ± 1.8° and 27.0° ± 1.3° C, respectively). In other studies (Ferry et al., 2011) a +0.02 ‰ Δ_{47} adjustment has been applied to dolomite Δ_{47} values to account for theoretical differences between the dolomite and calcite Δ_{47}-temperature calibrations of Guo et al. (2009). Conversely, the apparent overlap between empirically derived temperature calibrations of siderite, apatite, and calcite suggest that mineralogical effects on the calibration are minor (Fernandez et al., 2014; Stolper and Eiler, 2015). Adding +0.02 ‰ to my dolomite data would lower calculated temperatures by ~8° C, implying that near-surface dolomites record significantly cooler conditions than both modern sea surface temperatures and underlying limestones. There is no physical reason why this should be the case. Assuming co-existing calcite and dolomite actually formed at nearly the same temperature, our results imply that the same Δ_{47} temperature calibration can be used for both mineralogies.

It has been suggested that dolomite and calcite could have different susceptibilities to Δ_{47} alteration (e.g., Eiler, 2011). I do not find evidence for significantly different degrees of alteration, although the variability in dolomite and calcite Δ_{47} values below 1300 m is large. The abrupt shift in Δ_{47} at depth does not coincide with a mineralogical change. Dolomite and calcite Δ_{47} values are similar throughout the core and provide no evidence that either mineralogy is more resistant to diagenetic alteration or thermal resetting of the Δ_{47} values.

2.5.3 Alteration of Δ_{47}

Carbonate Δ_{47} is susceptible to thermally-induced reformation of C – O bonds within the solid mineral lattice. Based on experimental data, approximately 100° C has been suggested as the minimum temperature under which solid-state reordering can alter primary Δ_{47} values over the ~100 million year timescale evaluated here (Passey and Henkes, 2012; Henkes et al., 2014; Stolper and Eiler, 2015). Under no realistic geothermal scenario have samples above 1500 m depth experienced temperatures of 100°C, and measurements suggest this threshold is reached closer to 4 km depth (Epstein and Clark, 2009).

If solid-state reordering caused the observed shift in clumped isotope composition, downcore I would expect a step-like Δ_{47} temperature increase followed by an increasing trend in temperature. I essentially observe this pattern, but the sharp increase in Δ_{47} temperature occurs at geothermal temperatures below the ~100° C reordering threshold. This means that either solid-state alteration is possible at lower temperatures than predicted, or that subtle diagenetic recrystallization has altered clumped isotope temperatures. It is also possible that fine grained samples can more easily undergo reordering, as Shenton et al. (2015) argued that micrite was more susceptible to such alteration at high temperatures (>140° C) relative to the skeletal calcite of brachiopods. However, because our samples underwent recrystallization during lithification, early diagenesis, and (in some cases) dolomitization, the amount of recrystallization during later burial diagenesis is difficult to constrain. Although no clear petrographic transition coincides with the Δ_{47} temperature increase, this uncertainty does not permit a true test of low temperature reordering effects. Still, these results raise the possibility of solid-state reordering at temperatures below 50° C.

Samples below ~4 km depth have almost certainly experienced >100° C conditions and would be expected to no longer record surface temperatures. However, given the measured geothermal gradient range and a simple burial model based on stratigraphic thickness for each epoch, the Passey and Henkes (2012) resetting model predicts Δ_{47} temperatures at least 20° C lower than the maximum observed temperature of 68° ± 10° C (Fig. 2.S2). The Stolper and Eiler (2015) isotopologue reordering model also would not replicate the observed Δ_{47} change, and neither model would predict any reordering above ~4 km. This again signifies either the impact of recrystallization or a greater susceptibility to solid-state reordering than previously predicted.

Carbonate $\delta^{18}O$ values do not conclusively indicate alteration and do not increase in variability downcore (a common indication of heterogeneous recrystallization). Cretaceous through Eocene values must be corrected for changes in the composition of ocean water in an ice-free world (-1.04 ‰ VSMOW; Petersen and Schrag, 2015) and possible small increases in mean annual temperature relative to today. Given these conditions one would expect downcore dolomite and calcite $\delta^{18}O$ values to be roughly 1-2 ‰ lighter than core top values (i.e., the magnitude of change observed in most samples). It is also possible to evaluate diagenetic alteration by estimating the $\delta^{18}O$ of porewaters utilizing the reconstructed Δ_{47} temperatures. For most samples below 1300 m, restimated$\delta^{18}O_w$ values are all extremely positive relative to seawater and are unrealistic for evolved porewater compositions. What this implies is that the $\delta^{18}O$ of the carbonate remains relatively unaltered while the Δ_{47} temperatures have been reset. This in turn argues against significant diagenetic recrystallization occurring within the core at elevated temperatures unless alteration occurred in a rock-dominated diagenetic system where porewaters reach isotopic equilibrium with surrounding rock. Such rock dominated diagenetic systems have been described in other micritic low porosity units (e.g., Czerniakowski et al.,

1984). Just as I observe, in such a system $\delta^{18}O$ may be altered only slightly and $\delta^{13}C$ is invariant (Swart, 2015). The lack of a clear agreement between shifts in petrographic texture and Δ_{47} may be indicative of shallow-burial crystallization masking any contrast with later recrystallization. In that case, Δ_{47} values would serve as a proxy for closed-system recrystallization at depth, with warmer temperatures indicating increased alteration.

Previous clumped isotope studies that have used shallowly buried fine-grained carbonate materials have produced temperatures in the 35 – 50° C range (Quade et al., 2013; Huntington et al., 2014). The results of this study show that these high calculated temperatures could be due to recrystallization of the primary material, but also show that solid-state reordering of fine grained material at low temperatures is possible. Taken together, it is unlikely that clumped isotope analyses of micritic carbonates buried more than ~1 km can be consistently relied on as a temperature proxy. Resetting of Δ_{47} values can occur under mild geothermal conditions without distinct changes in the petrologic texture or conventional stable isotope values. Irrespective of origin, these hot Δ_{47} temperatures from shallowly buried carbonates suggest that the micritic component of samples should be used with extreme caution in clumped isotope studies seeking original composition and realistic primary environmental temperatures.

2.6 Acknowledgements

I thank Sierra Petersen, Kyle Meyer, William Defliese, and Lora Wingate for discussion and lab assistance. This manuscript was improved by thoughtful reviews from Ethan Grossman and an anonymous reviewer. Work was supported by AAPG and SEG grants to IZW and NSF EAR grant 1123733 awarded to KCL.

References

Beach, D. K., 1993, Submarine Cementation of Subsurface Pliocene Carbonates from the Interior of Great Bahama Bank. Journal of Sedimentary Research 63, 1059–1069, doi:10.1306/D4267C99-2B26-11D7-8648000102C1865D.

Czerniakowski, L. A., Lohmann, K. C., Wilson, J., 1984. Closed-system marine burial diagenesis: isotopic data from the Austin Chalk and its components. Sedimentology 31, 863–877, doi:10.1111/j.1365-3091.1984.tb00892.x.

Defliese, W. F., Hren, M. T., Lohmann, K. C., 2015. Compositional and temperature effects of phosphoric acid fractionation on Δ47 analysis and implications for discrepant calibrations. Chemical Geology 396, 51–60, doi:10.1016/j.chemgeo.2014.12.018.

Dennis, K. J., and Schrag, D. , 2010. Clumped isotope thermometry of carbonatites as an indicator of diagenetic alteration. Geochimica et Cosmochimica Acta 74, no. 14, 4110–4122, doi:10.1016/j.gca.2010.04.005.

Dennis, K. J., Affek, H. , Passey, B. H., Schrag, D. , Eiler, J. M., 2011. Defining an absolute reference frame for "clumped" isotope studies of CO2. Geochimica et Cosmochimica Acta 75, 7117–7131, doi:10.1016/j.gca.2011.09.025.

Eberli, G. , and Ginsburg, R. N., 1987. Segmentation and coalescence of Cenozoic carbonate platforms, northwestern Great Bahama Bank. Geology 15, 75–79, doi:10.1130/0091-7613.

Eiler, J. M., 2011. Paleoclimate reconstruction using carbonate clumped isotope thermometry. Quaternary Science Reviews 30, 3575–3588, doi:10.1016/j.quascire2011.09.001.

Epstein, S. A., and Clark, D., 2009. Hydrocarbon Potential of the Mesozoic Carbonates of the Bahamas. Carbonates and Evaporites 24, 97–138.

Fernandez, A., Tang, J., Rosenheim, B. E., 2014. Siderite "clumped" isotope thermometry: A new paleoclimate proxy for humid continental environments: Geochimica et Cosmochimica Acta, 126, 411–421, doi:10.1016/j.gca.2013.11.006.

Ferry, J. M., Passey, B. H., Vasconcelos, C., Eiler, J. M., 2011. Formation of dolomite at 40-80 °C in the Latemar carbonate buildup, Dolomites, Italy, from clumped isotope thermometry. Geology 39, 571-574, doi:10.1130/G31845.1.

Ghosh, , Adkins, J., Affek, H., Balta, B., Guo, W., Schauble, E. A., Schrag, D., Eiler, J. M., 2006. 13C-18O bonds in carbonate minerals. A new kind of paleothermometer. Geochimica et Cosmochimica Acta, 70, 1439–1456, doi:10.1016/j.gca.2005.11.014.

Goodell H.G., and Garman R.K., 1969. Carbonate Geochemistry of Superior Deep Test Well, Andros Island, Bahamas. American Association of Petroleum Geologists Bulletin 53, 513–536, doi:10.1306/5D25C697-16C1-11D7-8645000102C1865D.

Guo, W., Mosenfelder, J. L., Goddard III, W. A., and Eiler, J. M., 2009. Isotopic fractionations associated with phosphoric acid digestion of carbonate minerals: Insights from first-principles theoretical modeling and clumped isotope measurements. Geochimica et Cosmochimica Acta 139, 7203-7225, doi:10.1016/j.gca.2009.05.071.

Henkes, G. A., Passey, B. H., Grossman, E. L., Shenton, B. J., Pérez-Huerta, A., Yancey, T. E., 2014.Temperature limits for preservation of primary calcite clumped isotope paleotemperatures. Geochimica et Cosmochimica Acta 139, 362–382, doi:10.1016/j.gca.2014.04.040.

Horita, J., 2014. Oxygen and carbon isotope fractionation in the system dolomite-water-CO2 to elevated temperatures. Geochimica et Cosmochimica Acta 129, 111–124, doi:10.1016/j.gca.2013.12.027.

Huntington, K. W., Saylor, J., Quade, J., Hudson, A. M., 2014. High late Miocene-Pliocene elevation of the Zhada Basin, southwestern Tibetan Plateau, from carbonate clumped isotope thermometry. Geological Society of America Bulletin 127, 181-199, doi:10.1130/B31000.1.

Huntington, K. W., Eiler, J. M., Affek, H. , Guo, W., Bonifacie, M., Yeung, L. Y, Thiagarajan, N., Passey, B., Tripati, A., Daeron, M., Came, R., 2009. Methods and limitations of "clumped" CO2 isotope (Δ47) analysis by gas-source isotope ratio mass spectrometry. Journal of Mass Spectrometry 44, 1318–1329, doi:10.1002/jms.1614.

Illing, L. , 1954. Bahaman calcareous sands. American Association of Petroleum Geologists Bulletin 38, 1-95.

Kim, S.-T., and O'Neil, J. R., 1997. Equilibrium and nonequilibrium oxygen isotope effects in synthetic carbonates. Geochimica et Cosmochimica Acta 61, 3461–3475, doi:10.1016/S0016-7037(97)00169-5.

Melim, L. A., Westphal, H., Swart, K., Eberli, G. , Munnecke, A., 2002. Questioning carbonate diagenetic paradigms: Evidence from the Neogene of the Bahamas Marine Geology 185, 27–53, doi:10.1016/S0025-3227(01)00289-4.

Melim, L. A., Swart, K., Maliva, R.G., 2001. Meteoric and marine-burial diagenesis in the subsurface of the Great Bahama Bank, in Ginsburg, R. N., ed., Subsurface Geology of a Prograding Carbonate Platform Margin, Great Bahama Bank: Results of the Bahamas Drilling Project. SEPM Special Publication 70, 137-161.

Passey, B. H., and Henkes, G. A., 2012. Carbonate clumped isotope bond reordering and geospeedometry. Earth and Planetary Science Letters 351-352, 223–236, doi:10.1016/j.epsl.2012.07.021.

Pearson, N., Ditchfield, W., Singano, J., Harcourt-Brown, K. G., Nicholas, C. J., Olsson, R. K., Shackleton, N. J., Hall, M. A., 2001. Warm tropical sea surface temperatures in the Late Cretaceous and Eocene epochs. Nature 413, 481–487, doi:10.1038/35106617.

Petersen, S. V., Winkelstern, I. Z., Lohmann, K. C., Meyer, K. W., 2015. The effects of Porapak trap temperature on δ18O, δ13C, and Δ47 in preparing samples for clumped isotope analysis: Rapid Communications in Mass Spectrometry 30, 1-10.

Petersen, S. V., and Schrag, D. P., 2015. Antarctic ice growth before and after the Eocene-Oligocene Transition: New estimates from clumped isotope paleothermometry: Paleoceanography 30, 1305 – 1317.

Quade, J., Eiler, J., Daëron, M., Achyuthan, H., 2013. The clumped isotope geothermometer in soil and paleosol carbonate. Geochimica et Cosmochimica Acta 105, 92–107, doi:10.1016/j.gca.2012.11.031.

Rosenbaum, J., and Sheppard, S. M., 1986. An isotopic study of siderites, dolomites and ankerites at high temperatures. Geochimica et Cosmochimica Acta 50, 1147–1150, doi:10.1016/0016-7037(86)90396-0.

Schlager, W., and Ginsburg, R.N., 1981. Bahama carbonate platforms- The deep and the past. Marine Geology, 44, 1-24.

Shenton, B. J., Grossman, E. L., Passey, B. H., Henkes, G. A., Becker, T. P., Laya, J. C., Perez-Huerta, A., Becker, S. P., Lawson, M., 2015. Clumped isotope thermometry in deeply buried sedimentary carbonates: The effects of bond reordering and recrystallization. Geological Society of America Bulletin, p. 1–16, doi:10.1130/B31169.1.

Stolper, D. A., and Eiler, J. M., 2015. The kinetics of solid-state isotope-exchange reactions for clumped isotopes: A study of inorganic calcites and apatites from natural and experimental samples. American Journal of Science 315, 363-411, doi: 10.2475/05.2015.01.

Spencer, M., 1967. Bahamas Deep Test: American Association of Petroleum Geologists Bulletin, 51, 263-268.

Swart, P. K., 2015. The Geochemistry of Carbonate Diagenesis: The Past, Present and Future. Sedimentology, doi:10.1111/sed.12205.

Swart, P.K.., Reijmer, J.J., Otto, R., 2009. A reevaluation of facies on Great Bahama Bank II: Variations in the $\delta^{13}C$, $\delta^{18}O$ and mineralogy of surface sediments: in Swart, P.K., Eberli, G.P., McKenzie, J.A., eds., Perspectives in Carbonate Geology: A Tribute to the Career of Robert Nathan Ginsburg. IAS Special Publication, 47-60.

Swart, P. K., and Melim, L. A., 2000. The Origin of Dolomites in Tertiary Sediments from the Margin of Great Bahama Bank. Journal of Sedimentary Research 70, 738–748, doi:10.1306/2dc40934-0e47-11d7-8643000102c1865d.

Swart, P.K., Ruiz, J., Holmes, C.W., 1987. Use of strontium isotopes to constrain the timing and mode of dolomitization of Upper Cenozoic sediments in a core from San Salvador, Bahamas. Geology 15, 262-265.

Vahrenkamp, V.C., and Swart, P.K., 1994. Late Cenozoic dolomites of the Bahamas: metastable analogues for the genesis of ancient platform dolomites. In: Purser, B.H., Tucker, M.E., Zenger, D.H. (Ed.), Dolomieu Conference on Carbonate Platforms and Dolomitization, 133-153.

Whitaker, F. F., Smart, P. L., Vahrenkamp, V. C., Nicholson, H., Wogelius, R. A., 1994. Dolomitization by near-normal seawater? Field evidence from the Bahamas, in Purser, B., Tucker, M., and Zenger, D., eds., Dolomites: A Volume in Honour of Dolomieu. IAS Special Publication 21, 111-131.

Appendix 2.1 Geology of the Sample Site

Andros Island, the largest island on the Great Bahama Bank, sits atop more than six kilometers of nearly 100% carbonate rock. The 4442-meter-long Andros Number 1 well was drilled into north-central Andros Island by the Stafford and Bahamas Oil companies in 1947. The core is now housed by the Florida State Geological Survey in Tallahassee, FL. The core spans the Pleistocene through the Early Cretaceous according to approximate microfossil dating and correlation with the stratigraphy of Florida (Spencer, 1967).

The core material was discussed by Illing (1954) and Spencer (1967) and petrographically and geochemically described by Goodell and Garman (1969; Fig. 2.S1). The foraminifera and bivalve fossils, occasional reefal debris, and common pelletal muds found in the core support the interpretation of marine deposition for the entire sedimentary sequence.

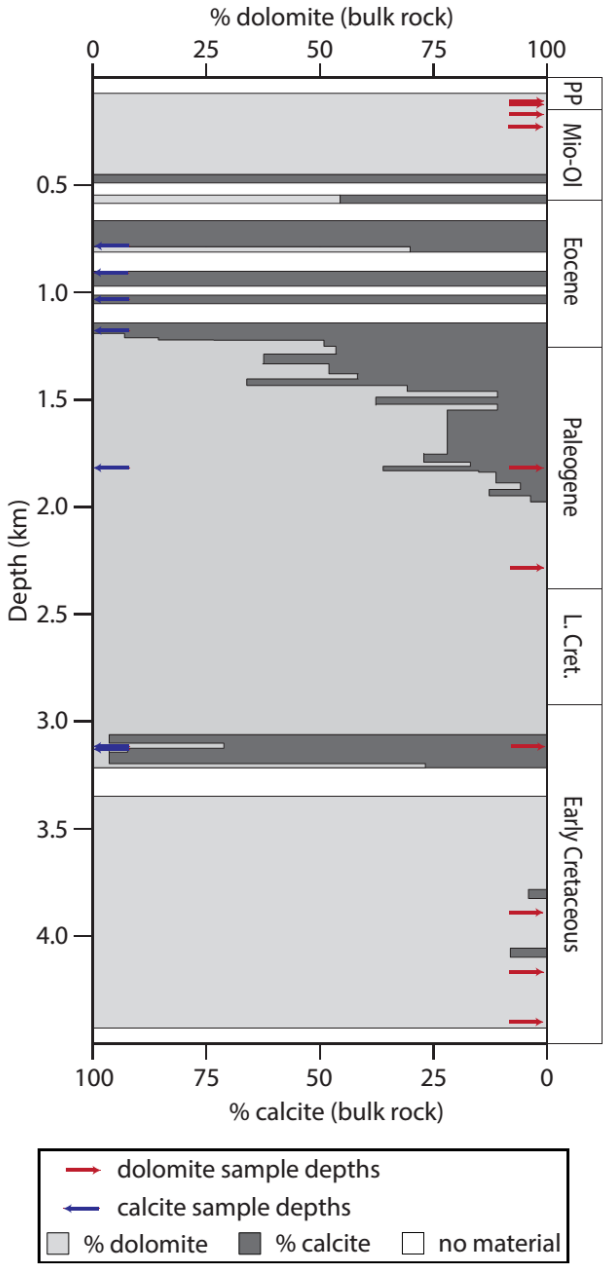

Figure 2.S1. Mineralogy of all Andros Island #1 core material, via XRD analyses of this study and Goodell and Garmin (1969). Dolomite and calcite sample depths are indicated with squares and circles, respectively. All samples analyzed were >80% pure dolomite or calcite, as indicated by XRD. PP = Plio-Pleistocene; Mio-Ol = Miocene-Oligocene.

Table 2.S1. Mineralogies calculated from XRD for each sample. Analytical error is ~5%. Letters (d or c) indicate dominant mineralogy.

Depth (m)	Sample	% dolomite
122	AC30d	100
125	AC31d	100
206	AC27d	100
259	AC33d	100
499	AC32c	3
735	AC29c	8
880	AC37c	0
1076	AC23c	0
1330	AC26c	0
1859	AC18c	17
1859	AC18d	90
2373	AC15d	89
3236	AC6d	100
3240	AC7c	3
3240	AC7d	99
3825	AC5d	100
4284	AC2d	100
4413	AC1d	100

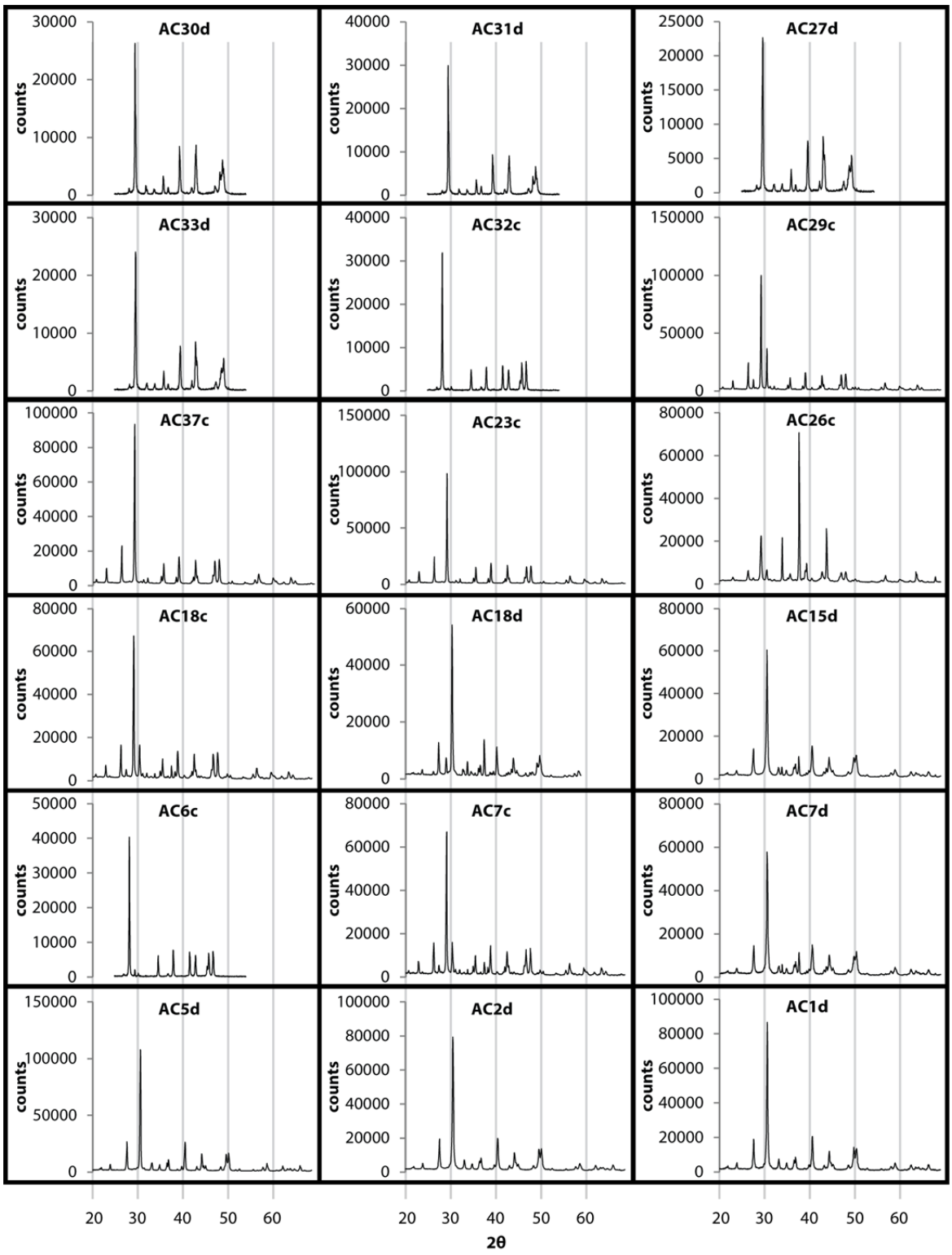

Figure 2.S2. Raw XRD data for all samples. Organized by sample depth.

Some faulting and uplift occurred within the Great Bahama Bank during the Early Cretaceous, however, it is likely that the burial history of all samples from the Andros core follows an essentially linear increasing depth and temperature trend (Elberli and Ginsburg, 1987). While it is true that periods of erosion are observed in core sediments, their magnitude is likely minor and no tectonic uplifts are known to have occurred (Goodell and Garman, 1969; Elberli and Ginsburg, 1987).

Today, deposits on the interior of the Great Bahama Bank are generally oolitic and coralgal sands in higher-energy areas that grade into pelletal muds (Illing, 1954). Most of this modern material is aragonitic, but early diagenesis has resulted in no aragonite present below ~35 m depth (Goodell and Garman, 1969; Beach, 1993). All material studied from this core is 100% carbonate, but the mineralogy varies from calcite to dolomite.

Offshore cores analyzed by Melim et al. (2002) indicate a shift from aragonite-dominated mud to mature microsparitic limestone and complete alteration by marine pore fluids within 100 – 150 m of sea level. Recrystallization of material at ~250 m depth indicates complete dolomitization and a degree of diagenetic stabilization relatively soon after deposition, consistent with diagenetic models (Beach, 1993; Whitaker et al., 1994; Melim et al., 2001; Melim et al., 2002). Marine waters have been shown to flow consistently through the upper ~400 m of the Great Bahama Bank (from the center of the platform outward) and are likely agents of lithification as well as dolomitization (e.g., Whitaker et al. 1994).

Appendix 2.2 Sample Characterization

Samples taken from the core's uppermost layers are entirely micritic dolomite with no visible grains. By 250m depth, dolomite is entirely recrystallized with dolomitic microspar, which is the likely result of near-surface diagenesis and lithification as described above. Foraminifera, bivalve, and coral fragments are still visible within the entirely recrystallized micritic matrix. From ~450 m to 3500 m depth, limestone beds are interbedded with dolomite, with both commonly preserving pellet traces and fossil outlines. Specifically in sample AC7 at 3240 m depth, calcitic algal grains are encased in a dolomite rhomb matrix. Such preservation further suggests that dolomitization above this depth was not the result of deep burial fluids but instead early diagenesis.

Samples below 3500 m depth are largely homogenous, showing microcrystalline dolomite rhombs with little variation. These near-uniform microcrystalline rocks with no apparent preservation of original features mark a petrographic transition between relatively unaltered near-surface material and material that may have been wholly recrystallized at depth. Rare, 10 μm-scale fractures are filled with additional dolomite rhombs; these were too small to independently sample and thus were avoided for isotopic analysis. Minor calcite fractions indicated in Figure 2.S1 (Goodell and Garman 1969) were not observed in my coarser analysis.

XRD results agreed with high resolution XRD and XRF analyses conducted by Goodell and Garman (1969; Fig. 2.S1, Fig. 2.S2). Eleven samples analyzed were 100% calcite or 100% dolomite. Specific mineralogies are indicated below (Table 2.S1). Porosity roughly decreases downcore but is qualitatively highly variable. Sr concentrations are consistently below 200 ppm throughout the entire core, except for a specific interval between ~800 and ~1200 m where concentrations are ~400 ppm (Goodell and Garman, 1969).

Appendix 2.3 Stable and Clumped Isotope Measurements

Carbonate samples were measured for their stable and clumped isotopic composition. All stable isotope work was conducted at the University of Michigan Stable Isotope Laboratory. Carbonate material was sampled using a mounted Dremel hand drill at lowest speed settings to prevent overheating of a given sample.

CO_2 was extracted from each carbonate sample using an offline sample preparation procedure (see Defliese et al., 2015; based on Huntington et al., 2009). Each ~5 mg aliquot was reacted individually in anhydrous phosphoric acid in a common acid bath at 75° C. Calcites were reacted for 20 minutes and dolomites were reacted for 1 hour or until completion. Residual water vapor was removed from resultant CO_2 via cryogenic procedures under vacuum conditions. To eliminate hydrocarbon and halocarbon contaminants, gas was passed through Porapak^{TM} resin held at -15° C for 10 minutes (AC sample numbers 5, 6, 23, 29, 33, 37) or at -30° C for 15 minutes (all other samples; Petersen et al., 2015). Volume of CO_2 before and after this process was monitored to ensure quantitative collection of all sample gas. Clean CO_2 was then transferred to a Thermo Scientific MAT 253 Stable Isotope Ratio Mass Spectrometer for Δ_{47} analysis, where masses 44 through 49 were measured for 60-80 cycles. As described by Dennis et al. (2011), heated CO_2 with stochastic isotopologue distributions and CO_2 equilibrated with water at 25° C were used to monitor machine conditions and establish the absolute reference frame.

$\delta^{18}O$ and $\delta^{13}C$ measurements are a byproduct of clumped isotope analysis but have lower multi-replicate precision than when measured using the Kiel method, at least in part because much more heterogeneous material (>4 mg) is incorporated into each replicate measurement. For

those samples passed through the cold (-30° C) Porapak^{TM}, corrections of +0.36 ‰ for $\delta^{18}O$ and +0.10 ‰ for $\delta^{13}C$ were applied to account for measured method-specific fractionation effects (Petersen et al. 2015). All clumped $\delta^{18}O$ values were then corrected for acid fractionation via Kim and O'Neil (1997) (calcites) or Rosenbaum and Shepard (1986) (dolomites). The isotopic composition of the fluid from which the carbonates precipitated was calculated using the fractionation factor of Kim and O'Neil (1997) for calcite and Horita (2014) for dolomite (Table 2.S1). All carbonate $\delta^{18}O$ and $\delta^{13}C$ values are reported relative to the Vienna Pee Dee Belemnite standard (VPDB), and all $\delta^{18}O$ water values ($\delta^{18}O_w$) are reported relative to the Vienna Standard Mean Ocean Water standard (VSMOW).

Table 2.S2. Summary of isotopic data for all samples.

Depth (m)	Sample	Mineralogy	$\delta^{13}C$ (‰ VPDB)[1]	$\delta^{18}O$ (‰ VPDB)[1]	Δ^{47} (‰ ARF)[2]	Δ^{47} °C[3]	$\delta^{18}O_{H2O}$[4] (‰ VSMOW)
122	AC30	dolomite	1.88 ± 0.05	1.64 ± 0.14	0.6811 ± 0.0162	30.6° ± 6.3°	1.0 ± 1.3
125	AC31	dolomite	1.83 ± 0.02	1.45 ± 0.08	0.6754 ± 0.0069	32.3° ± 2.7°	1.3 ± 0.6
206	AC27	dolomite	3.13 ± 0.15	2.30 ± 0.19	0.6856 ± 0.0034	28.4° ± 1.3°	1.3 ± 0.4
259	AC33	dolomite	2.32 ± 0.02	2.38 ± 0.10	0.6903 ± 0.0031	26.6° ± 1.1°	1.0 ± 0.3
499	AC32	calcite	-0.18 ± 0.02	-2.33 ± 0.08	0.6845 ± 0.0057	28.8° ± 2.1°	0.5 ± 0.4
735	AC29	calcite	-0.35 ± 0.07	-2.44 ± 0.18	0.6938 ± 0.0089	25.5° ± 3.2°	-0.3 ± 0.5
880	AC37	calcite	2.00 ± 0.04	-0.57 ± 0.03	0.6899 ± 0.0069	26.9° ± 2.5°	1.9 ± 0.5
1076	AC23	calcite	2.52 ± 0.03	-0.89 ± 0.03	0.6895 ± 0.0058	27.0° ± 2.1°	1.6 ± 0.4
1330	AC26	calcite	0.13 ± 0.07	-0.30 ± 0.14	0.6543 ± 0.0061	40.8° ± 2.6°	4.8 ± 0.3
1859	AC18c	calcite	-1.33 ± 0.06	-3.16 ± 0.05	0.6618 ± 0.0036	37.6° ± 1.5°	1.4 ± 0.2
1859	AC18d	dolomite	2.10 ± 0.01	0.97 ± 0.02	0.6519 ± 0.0040	41.7° ± 1.7°	2.8 ± 0.3
2373	AC15	dolomite	1.52 ± 0.06	0.62 ± 0.21	0.6337 ± 0.0106	50.0° ± 4.9°	4.0 ± 1.1
3236	AC6	calcite	1.54 ± 0.09	-3.89 ± 0.22	0.6614 ± 0.0024	37.7° ± 1.0°	0.7 ± 0.4
3240	AC7c	calcite	2.12 ± 0.07	-3.14 ± 0.10	0.6402 ± 0.0092	47.0° ± 4.1°	3.0 ± 0.6
3240	AC7d	dolomite	2.33 ± 0.07	1.45 ± 0.19	0.6337 ± 0.0104	49.9° ± 4.8°	3.4 ± 0.9
3825	AC5	dolomite	0.98 ± 0.04	0.04 ± 0.11	0.5996 ± 0.0179	68.0° ± 10.1°	6.4 ± 1.6
4284	AC2	dolomite	3.85 ± 0.05	0.83 ± 0.05	0.6425 ± 0.0045	45.7° ± 1.9°	3.5 ± 0.4
4413	AC1	dolomite	2.53 ± 0.08	-0.91 ± 0.18	0.6096 ± 0.0088	61.5° ± 4.4°	4.6 ± 0.7

[1]Conventional isotopic data as measured in clumped isotope analyses. All uncertainties are one standard error based on 3 or 4 replicate measurements.
[2]Δ_{47} values are reported in the absolute reference frame of Dennis et al. (2011).
[3]Δ_{47} temperatures via the Defliese et al. (2015) calibration.
[4]Water $\delta^{18}O$ calculated from clumped isotope temperatures and carbonate $\delta^{18}O$, via fractionation factors of Kim and O'Neil (1997) for calcite and Horita (2014) for dolomite.

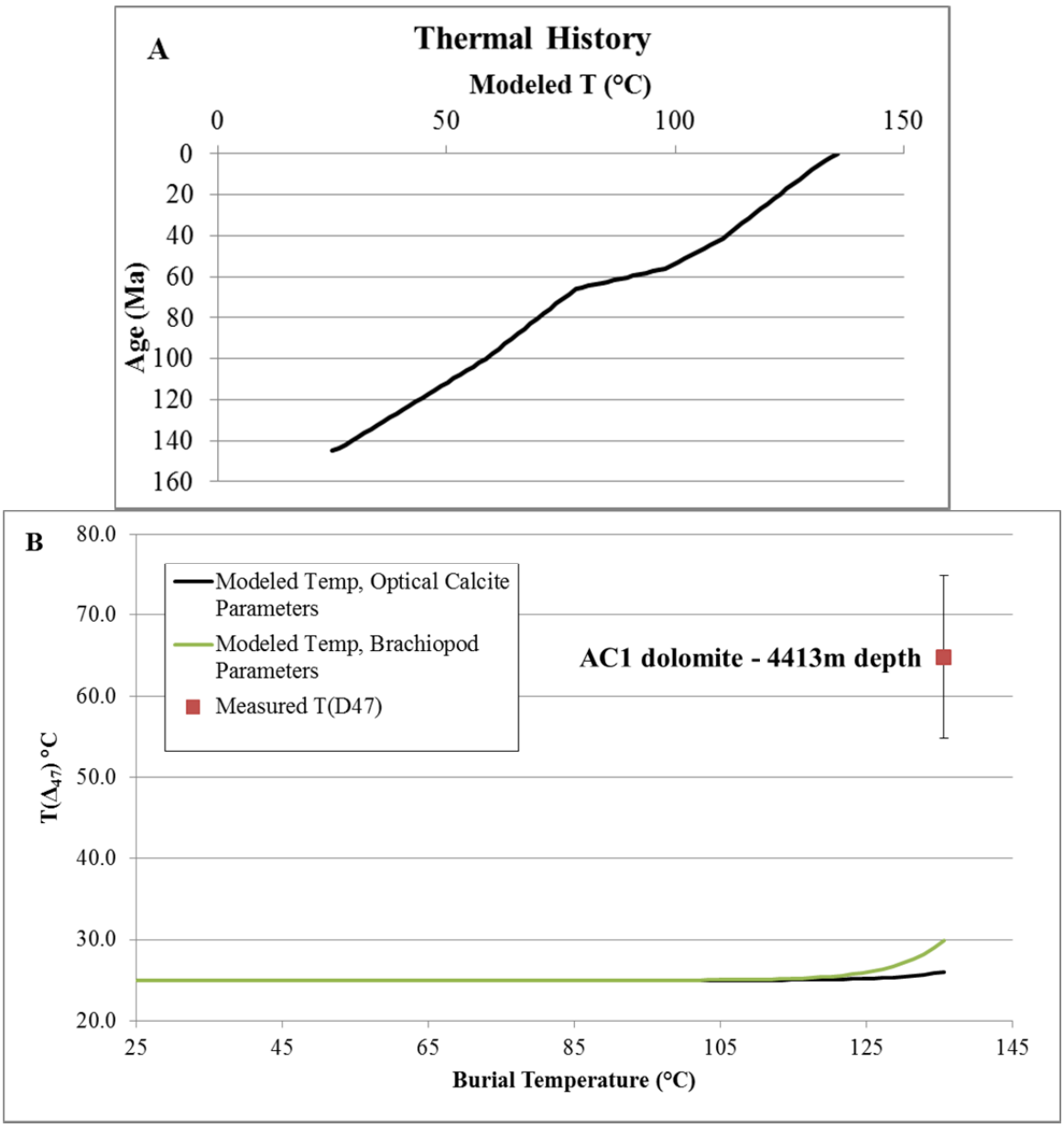

Figure 2.S3. A) Temperature change over time for the lower most sample (AC1, 4413 m depth) given a ~30° C/km geothermal gradient (hotter than measurements indicate) and a burial model based on stratigraphic thickness for each epoch. B) Passey and Henkes (2012) model output given the conditions outlined in (A). Under this hotter-than-measured geothermal scenario, the Stolper and Eiler (2015) model would predict similar temperature change to that observed, although much less change (<10 °C) would be predicted under the measured geothermal range. The Stolper and Eiler (2015) model would predict essentially no Δ_{47} change for all other samples.

Chapter 3

Calibration of Dolomite Clumped Isotope Thermometry[6]

3.1 Abstract

Use of the clumped isotope thermometer to understand the conditions of dolomite formation has been inhibited by the absence of a Δ_{47}-temperature calibration based on empirical data from dolomites formed at known temperatures. Empirical calibrations for aragonite, calcite, siderite, and carbonate apatite indicate that a single Δ_{47} – temperature relationship may exist across all carbonate-bearing mineral phases. However, theoretical modeling and proposed acid fractionation differences suggest that dolomite may have elevated Δ_{47} values relative to calcite precipitated at the same temperature. To resolve this issue, I analyzed five synthetic and four natural dolomites formed at known temperatures. I used synthetic dolomites grown in Mg-Ca-Cl solutions at temperatures of 200 – 250 °C, and natural samples constrained by fluid inclusion analyses (~70 °C), climate (~28° and ~27 °C), and deep ocean borehole temperature (~17° C). When using calcite Δ_{47} acid fractionation values, these data result in a Δ_{47} –temperature calibration that is statistically indistinguishable from other carbonate clumped isotope calibrations. With current measurement capabilities no evidence for a consistent dolomite Δ_{47} offset was found, while a possible relationship between the degree of dolomite cation ordering and Δ_{47} is present. These results support a single Δ_{47}-temperature calibration for carbonate clumped isotope thermometry. Furthermore, extension of this calibration enables new

[6] Winkelstern, I., Kaczmarek, S., Lohmann, K., and Humphrey, J. *in review*. Geochimica et Cosmochimica Acta.

investigations into conditions of dolomite formation and its application as a proxy for paleotemperature determination.

3.2 Introduction

Dolomite is common throughout the geologic record, but the usefulness of dolomite as a paleoenvironmental and diagenetic proxy has been inhibited by a general lack of understanding about the precise geochemical settings of its formation (e.g., Machel 2004). Because clumped isotope measurements provide temperature data that are independent of water isotopic composition (Ghosh et al. 2006), and thus can be used to exploit dolomite as a proxy tool, while also helping to solve long-standing questions about how the mineral forms. Understanding mineral-specific differences in dolomite clumped isotope thermometry, if any, will enable further studies on the temperature conditions of dolomite formation, help constrain the isotopic composition of formation waters, and in turn constrain the inferred environments of precipitation.

Recent work has demonstrated the usefulness of the clumped isotope paleothermometer for determining formation temperatures of other carbonate minerals, as well as in carbonate ions within biogenic apatites (Eagle et al., 2010; Fernandez et al., 2014; Stolper and Eiler, 2015). The clumped isotope thermometer is based on the idea that the heavier oxygen (^{18}O) and carbon (^{13}C) isotopes preferentially bond to each other within a carbonate mineral lattice (e.g., Eiler, 2011). The abundance of ^{13}C–^{18}O bonds in CO_2 resulting from phosphoric acid digestion of a carbonate mineral, relative to their expected abundance from a stochastic isotope distribution, is expressed as a Δ_{47} value (Eiler and Schauble, 2004). Using a suite of calcite and aragonite samples formed

at known temperatures and reacted with phosphoric acid at 25° C, Ghosh et al. (2006) empirically demonstrated that Δ_{47} is dependent on carbonate formation temperature.

Many Δ_{47} - temperature calibrations have been published since Ghosh et al. (2006). In general, these more recent calibrations roughly follow either the lower slope of the Dennis and Schrag (2010) relationship, or the original Ghosh et al. (2006) calibration (Fernandez et al., 2014; Defliese et al., 2015). Although corrections are applied for the acid digestion fractionation at temperatures above the 25° C as used in Ghosh et al. (2006) (e.g., Passey et al., 2010), these calibration differences may be attributable to unaccounted-for effects of phosphoric acid digestion methodology (Fernandez et al., 2014). This is because compiled data produced via acid digestion at 75° C or higher gives a calibration line with a lower slope that is statistically distinct from the calibration produced from compiled data produced with 25° C acid (Defliese et al., 2015).

Within this framework, no differences in the mineral-specific Δ_{47} - temperature relationships have been empirically found between calcite, aragonite, siderite, or biogenic apatite (Ghosh et al., 2006; Eagle et al., 2010; Fernandez et al., 2014). Acid fractionation of Δ_{47} values may also be mineral-independent, as suggested by Defliese et al. (2015), who observed statistically identical acid fractionation factors for dolomite, calcite, and aragonite over an acid temperature range of 25 to 90° C. More recently however, Murray et al. (2015) reported a significantly different acid fractionation factor for dolomite compared to calcite and aragonite, indicating ongoing uncertainty regarding mineral-specific effects in clumped isotope thermometry.

Quantum mechanical models suggest that the acid fractionation factor is independent of mineralogy but that small differences between Δ_{47} -.temperature –calibrations should exist (Guo

et al., 2009). In theory, calcite Δ_{47} is expected to be ~0.02‰ lower than dolomite Δ_{47} under Earth surface temperatures (Guo et al., 2009). No dolomite-specific calibration has empirically tested this model, perhaps largely because dolomite is difficult to produce in a laboratory at sub-150° C temperatures (e.g., Usdowski, 1994; Land, 1998). Despite the lack of empirical data, several studies have applied clumped isotope thermometry to natural dolomite samples (e.g., Ferry et al., 2009; Loyd et al., 2012; Lechler et al., 2013; Van de Velde et al., 2013; Dale et al., 2014; Sena et al., 2014). The Δ_{47} temperatures reported by these studies (albeit in some cases with various dolomite-specific correction schemes) have been generally reasonable, suggesting that calcite and dolomite calibrations do not greatly differ. The similarity between other mineral-specific clumped isotope calibrations further suggests that a single Δ_{47} - temperature relationship may exist. The lack of empirical calibration data for dolomite, however, means that all dolomite clumped isotope interpretations are assuming this to be the case.

In this study, I used five synthetic dolomites formed at known temperatures between 200 and 250° C and four natural dolomites formed under well-constrained, lower-temperature conditions to develop the first calibration for dolomite clumped isotope thermometry. By direct comparison with calcites and aragonites reacted at the same acid temperature in the same laboratory, I am able to explicitly test for mineral-specific differences in the Δ_{47} - temperature relationship. These data will enable more precise use of dolomite clumped isotope thermometry for diagenetic and paleoenvironmental questions, as well as for insight into the formation of dolomite itself.

3.3 Methods

3.3.1 Synthetic Dolomites

Synthetic dolomites were prepared as in Kaczmarek and Sibley (2014), with the exception that natural aragonite ooids harvested from the Ambergris Shoal (Caicos platform, BWI) were used as the starting material rather than crushed calcite. In summary, 100 mg whole ooids sieved to obtain the 300-354 μm size fraction and 15 ml 0.875 M Mg-Ca-Cl solution with a Mg/Ca of 1.0 were loaded into Teflon-lined stainless steel acid-digestion Parr bombs. Sealed bombs were placed in a laboratory oven heated to temperatures ranging from 200.0° to 250.0° C (see Table 3.1). Upon completion of the experiment, bombs were removed from the oven, and allowed to air-cool to room temperature. Fluids were decanted and solid products were rinsed with DI water, filtered and dried. All solid products were prepared for powder X-ray diffraction (XRD) analysis.

Three parameters were quantified for each sample via XRD (Table 3.1): (1) percent dolomite relative to the starting aragonite ooids, (2) mol % $MgCO_3$ of the dolomite products (i.e., dolomite stoichiometry) as determined by position of the 104 reflection, and (3) the degree of Mg-Ca cation ordering as determined by the relative heights of the 015 and 110 reflections. These parameters were determined following the approach described by Kaczmarek and Sibley (2011, 2014). In general, high-temperature dolomitization reactions proceed via replacement of aragonite by very-high magnesium calcite (VHMC), which is then replaced by poorly-ordered dolomite, and finally well-ordered dolomite. Evidence of cation ordering was present only in the samples synthesized at temperatures of 200° C and above.

3.3.2 Natural Samples

3.3.2.1 Bonneterre Formation, Viburnum Trend, Missouri

I analyzed dolomite spar collected from the Ozark Lead Mine in southeastern Missouri. This cement formed within the upper Bonneterre Formation, part of the Viburnum Trend Mississippi Valley Type lead-zinc deposit (Braunsdorf and Lohmann, 1983; Frank and Lohmann 1986). These are petrographically identified as 100 % gangue spar dolomites and are indicated by XRD to have near-perfect ordering (Gregg and Shelton 1990). I base temperature "error" estimates for this sample of 70° ± 10° C on homogenization temperature- relationships of Shelton et al. (1992) that indicate this dolomite likely precipitated from ~60° to ~80° C saline waters.

3.3.2.2 Barbados

I analyzed sample 1.10A of Humphrey (1988, 2000), from the late Pleistocene of Barbados. This is 100% calcium-rich dolomite with ~43 mol % $MgCO_3$. XRD analysis shows an attenuated (015) ordering reflection, indicating some degree of dolomite ordering. This dolomite has been interpreted to specifically have formed from the mixing of fresh and marine waters (Humphrey 1988, 2000). It must have formed during a late Pleistocene sea-level high stand, and thus formed under tropical conditions similar to today. I thus assign a formation temperature of 28° C to this sample, based on local modern sea surface temperature (SST) (Locarnini et al., 2009). I assign an "error" on this temperature estimate of ± 5° C, which likely exceeds realistic tropical climate change during the Cenozoic (Pierson et al. 2001). The calibration effects of such a shift in temperature are discussed below.

3.3.2.3 Andros Island

I also used core sample AC30 from 122 m below Andros Island, Bahamas. XRD analysis indicates this sample is >95 % dolomite, and based on the presence of the (015) ordering peak has some degree of cation ordering. By similar logic to that applied to the Barbados dolomite, I assigned a 27° ± 5° C formation temperature to the Andros dolomite based on local SST (Locarnini et al., 2009). Because it also formed during a high stand just north of the tropics, it is unlikely that Plio-Pleistocene local temperatures differed dramatically from modern mean annual temperatures.

3.3.2.4 Deep ocean

Sample DSDP is from a Deep Sea Drilling Project drillcore in the southern Gulf of California (Leg 64, core 29, hole 479; water depth 440 m). Based on two core temperature logs, this dolomite formed under shallow burial conditions at a maximum of 20 – 24° C. If dolomite precipitation began at shallower depths during burial, formation temperature would be biased toward slightly cooler values, as current bottom waters are ~10 ºC. I assigned the average of these extremes, 17° C, as the formation temperature of this sample. My "error" bars thus extend from 10° to 24° C. Dolomitization of this material is described by Kelts et al. (1984) as the result of active methanogenesis. Via XRD, the composition of the material analyzed was 100% dolomite with 46 to 48 mol % $MgCO_3$ (Kelts et al. 1984). Ordering peaks in XRD spectra are attenuated but present (Kelts et al. 1984).

3.3.3 Clumped Isotope Analysis

3.3.3.1 Isotopic Analytical Methods

All stable isotope work was conducted at the University of Michigan Stable Isotope Laboratory. Dolomites were powdered using mortar and pestle. The Δ_{47} value of each sample was replicated at least three times, with a minimum of 4 mg used for each measurement. CO_2 was extracted from each dolomite using an offline sample preparation procedure identical to that of Defliese et al. (2015), who provide additional details. Each aliquot was reacted individually in anhydrous 105 wt % phosphoric acid in a common acid bath at 75° C for 1 hour or until completion. Residual water vapor was removed from resultant CO_2 via cryogenic distillation under vacuum conditions. To eliminate hydrocarbon and halocarbon contaminants, gas was passed through Porapak^{TM} resin held at -15° C for 10 minutes or, in the case of sample AC30, at -30° C for 15 minutes. The pressure of CO_2 before and after this process was measured to ensure collection of all sample gas (± 1%).

Purified CO_2 was then transferred to a Thermo Scientific MAT 253 Isotope Ratio Mass Spectrometer for Δ_{47} analysis, where masses 44 through 49 were measured for 60-80 cycles. As described by Dennis et al. (2011), heated CO_2 with stochastic isotopologue distributions and CO_2 equilibrated with water at 25° C were used to monitor machine conditions and establish the absolute reference frame (see Appendix 6.1). Carrara marble and an internal aragonitic ooid standard were measured every other day as additional checks on reference frame consistency. $\delta^{18}O$ and $\delta^{13}C$ measurements are a byproduct of clumped isotope analysis; for sample AC30 passed through the cold (-30° C) Porapak^{TM}, corrections of +0.36 ‰ for $\delta^{18}O$ and +0.10 ‰ for $\delta^{13}C$ were applied to account for measured method-specific fractionation effects (Petersen et al. 2015; Table 3.2). All carbonate $\delta^{18}O$ and $\delta^{13}C$ values are reported relative to the Vienna Pee Dee

Belemnite standard (VPDB), and all $\delta^{18}O$ water values ($\delta^{18}O_w$) are reported relative to the Vienna Standard Mean Ocean Water standard (VSMOW).

3.3.3.2 Acid fractionation

Because measurement of carbonate clumped isotope species was initially developed by reacting samples with phosphoric acid at 25° C, an acid factor must be applied to account for the lower Δ_{47} value of samples reacted with acid at higher temperatures. Reaction at higher temperatures is required because complete reaction of dolomite powder at 25° C takes multiple days. The analysis of dolomite standard NIST-88b by Defliese et al. (2015), using identical analytical methods as this study, found an acid fractionation factor of +0.067 ‰ at 75° C, with no significant difference between dolomite, calcite, and aragonite Δ_{47} acid fractionation factors. The recent work of Murray et al. (2015), however, suggested that the acid fractionation factor for a dolomite reacted at 90° C should instead be 0.137 (and 0.125 for a dolomite reacted at 75° C). I report results using both fractionation factors (Table 3.2), and this is discussed in detail below.

3.4 Results

When using the +0.067 (at 75° C) acid fractionation factor of Defliese et al. (2015) and through least square linear regression of dolomite Δ_{47} values and temperature ($10^6/T^2$, K), I obtained the following relationship ($R^2 = 0.97$; 1 standard error of the slope and intercept; Fig. 3.1):

(3.1) $\Delta_{47} = (0.0364 \pm 0.0011) * 10^6 / T^2 + (0.290 \pm 0.008)$

When instead applying the +0.125 (at 75° C) acid fractionation factor of Murray et al. (2015), I obtained an offset calibration (with identical slope and R^2 values) of:

(3.2) $\Delta_{47} = (0.0364 \pm 0.0011) * 10^6 / T^2 + (0.348 \pm 0.008)$

The slopes of these equations are statistically indistinguishable (within 95% confidence intervals) from those of other non-dolomite calibrations, including: the Defliese et al. (2015) compiled ≥75° C acid calibration, the Defliese et al. (2015) calibration using only University of Michigan data, the Dennis and Schrag (2010) calibration, and the Fernandez et al. (2014) siderite calibration. The intercept of equation (3.1) is also within the range of intercepts of these other calibrations, while the intercept of equation (3.2) is statistically unique amongst all published temperature – Δ_{47} calibrations.

Because all Defliese et al. (2015) calcite and aragonite samples measured using 75° C acid were processed with essentially identical analytical procedures and equipment as those used here, all acid fractionation factors can be removed from these data to enable direct aragonite, calcite, and dolomite calibration comparison. As shown in Figure 3.2, the synthetic calcites and aragonites of Defliese et al. (2015) are statistically indistinguishable from our data when acid fractionation factors are removed.

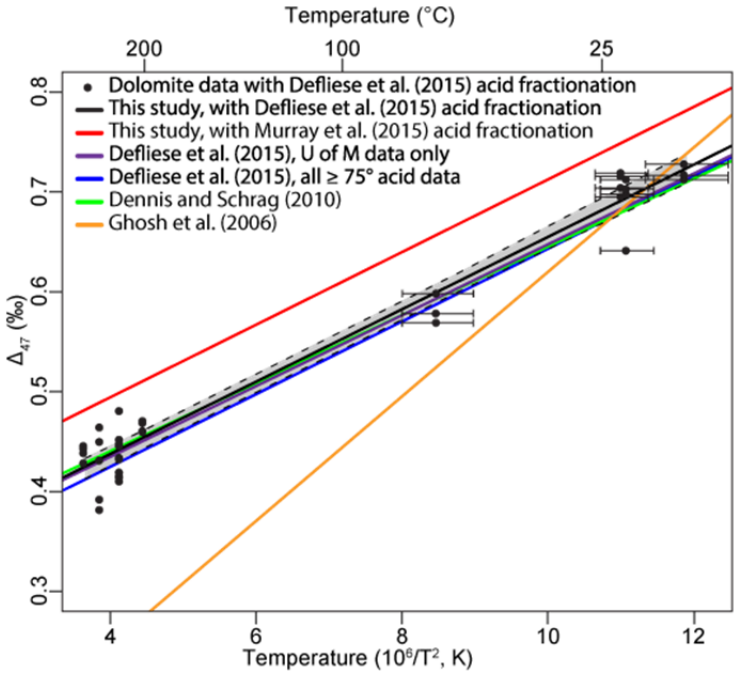

Figure 3.1. Linear regression of the dolomite clumped isotope results and temperature, with each clumped isotope replicate measurement plotted separately. The 95% confidence interval for this calibration is shown in grey. This figure also includes calibration lines from Defliese et al. (2015), Dennis and Schrag (2010), and Ghosh et al. (2006). Dashed lines and grey region shows 95% confidence interval for the dolomite regression. Instrumental (vertical) error is smaller than symbol size; horizontal error bars are defined as described in the text.

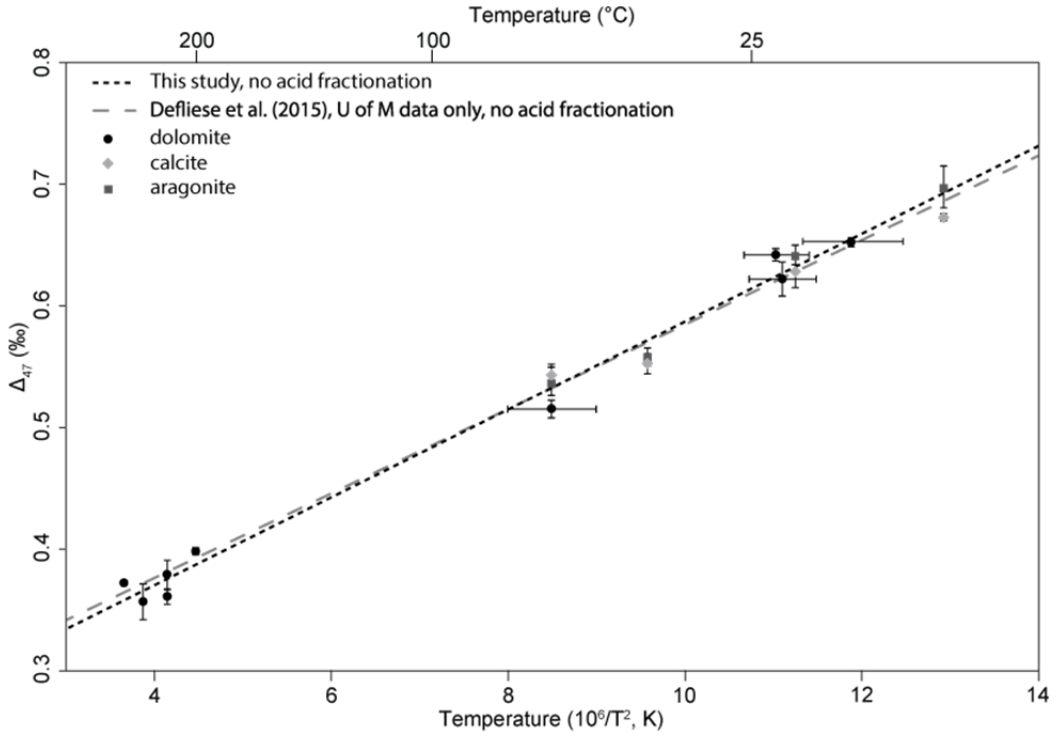

Figure 3.2. Average Δ_{47} values for each dolomite sample, along with synthetic calcite and aragonite data from Defliese et al. (2015), plotted against temperature with acid fractionation corrections removed. All samples were measured in the same laboratory with the same acid digestion method, though dolomites were given additional reaction time (≥ 1 hour). Linear regressions shown were calculated using average Δ_{47} values for each sample, with vertical error bars indicating one standard error of the mean.

3.5 Discussion

3.5.1 Effect of Dolomite Ordering

Samples O-H-2 and O-T-5 were each synthesized at 218° C but have different degrees of Mg-Ca cation ordering within the crystal lattice (0.08 and 0.25, respectively; Table 3.1). This refers to the degree to which the lattice structure of the product consists of alternating layers of Mg^{2+} and Ca^{2+} interspersed with CO_3^{2-} groups oriented normal to the c-axis. The Mg/Ca composition and the degree of cation order of dolomite in nature and in the laboratory can deviate from ideality. With poorly-ordered dolomites, cation ordering reflections (XRD) are attenuated, because cations occupy increasingly random positions within the lattice. In the extreme case, a truly random distribution of cations within the lattice results in the complete disappearance of the principle ordering reflections (e.g., the (015) peak) and the product is thus referred to as VHMC because it belongs to the calcite, rather than dolomite space group (see Gregg et al. 2015).

Using +0.067 ‰ acid fractionation and at one standard error, the average Δ_{47} values of O-H-2 (0.4461 ‰ ± 0.0116 ‰) and O-T-5 (0.4281 ‰ ± 0.0062 ‰) are statistically distinct (Table 3.2). This indicates that the degree of dolomite ordering may have an effect on final Δ_{47} value. Further study is required to validate and measure the magnitude of this effect, though the good correspondence between expected formation temperature of our natural samples and Δ_{47} temperatures calculated using calcite calibrations suggests that ordering effects must be small.

Sample ID	Formation Temperature (°C)	% 'Dolomite'	Mole % $MgCO_3$	Cation Order
250-I-7	250	93	47.8	0.12
235-O-12	235	94	46.5	0.08
O-H-2	218	95	45.8	0.08
O-T-5	218	99	50.5	0.25
200-P-30	200	91	40.8	0.00*

Table 3.1. Composition of synthetic dolomite samples. 'Dolomite' is in quotes because some samples lack cation order; * indicates sample is VHMC as indicated by lack of cation order; see Gregg et al. (2015) for details.

Sample ID	n	Formation Temp. (°C)	$\delta^{13}C$ (‰, PDB)	$\delta^{18}O$ (‰, PDB)	Δ_{47} (‰, Defliese et al. acid fractionation)	Δ_{47} (‰, Murray et al. acid fractionation)
250-I-7	4	250	+4.23	-27.51	0.4393 ± 0.0032	0.4973 ± 0.0032
235-O-12	5	235	+4.13	-26.54	0.4239 ± 0.0144	0.4819 ± 0.0144
O-H-2	4	218	+4.34	-26.12	0.4461 ± 0.0116	0.5041 ± 0.0116
O-T-5	6	218	+3.51	-26.44	0.4281 ± 0.0062	0.4861 ± 0.0062
200-P-30	4	200	+4.55	-24.37	0.4653 ± 0.0024	0.5233 ± 0.0024
MIZd	3	70 ± 10	-0.36	-8.84	0.5823 ± 0.0070	0.6403 ± 0.0070
Barb110	4	28 ± 5	-7.41	+1.65	0.7089 ± 0.0048	0.7669 ± 0.0048
AC30	4	27 ± 5	+1.89	+1.83	0.6891 ± 0.0139	0.7471 ± 0.0139
DSDP	3	17 ± 7	+12.57	-1.98	0.7193 ± 0.0037	0.7773 ± 0.0037

Table 3.2. Stable isotope data for all samples. Δ_{47} values are reported in the absolute reference frame of Dennis et al. (2011). Precision on $\delta^{13}C$ measurements is ± 0.1 ‰ or better, and precision on $\delta^{18}O$ measurements is ± 0.2 ‰ or better. All errors are one standard error based on the number of replicates (n), except for formation temperature of natural samples which are determined as explained in the text.

3.5.2 Natural Samples

When simply applying the Defliese et al. (2015) or Dennis and Schrag (2010) calibration to natural samples, each records a Δ_{47} temperature similar to their expected formation temperature (Table 3.3). This qualitatively suggests that all calcites and dolomites formed at the same temperature will have the same Δ_{47} value.

This agreement includes Andros Island, Bahamas sample AC30, which likely has a similar formation history to the San Salvador, Bahamas sample analyzed by Murray et al. (2015). Both AC30 and the San Salvador dolomite of Murray et al. (2015) are Plio-Pleistocene dolomites (now buried < 150 m depth) that are interpreted to have formed in waters similar to seawater and in temperature conditions similar to modern mean annual seawater temperature of ~27° C (e.g., Vahrenkamp et al., 1991). My results are in good agreement with these conditions, while Murray et al. (2015) reported a Δ_{47} temperature of 34° ± 3° C with their dolomite-specific acid fractionation and a temperature >50° C without it. The reason for the warmer than climate Δ_{47} temperature recorded by their sample is unknown, but I find no evidence in the natural sample data for a consistent offset between dolomite and calcite Δ_{47} values.

Sample ID	Formation Temp. (°C)	Δ_{47} °C, Defliese et al. (≥ 75° C acid) calibration	Δ_{47} °C, Dennis and Schrag calibration	Δ_{47} °C, Ghosh et al. calibration
MIZd	70 ± 10	76 ± 4	80 ± 4	56 ± 2
Barb110	28 ± 5	21 ± 2	22 ± 2	25 ± 1
AC30	27 ± 5	28 ± 5	29 ± 6	30 ± 3
DSDP	17 ± 7	17 ± 1	18 ± 1	23 ± 1

Table 3.3. Comparison between formation temperatures of natural samples and selected calcite and aragonite clumped isotope calibrations. All temperatures are based on Δ_{47} values using Defliese et al. (2015) acid fractionation. Δ_{47} temperatures using the acid fractionation factor of Murray et al. (2016) while still applying the above calcite temperature calibrations would be > 10 °C colder.

3.5.3 Dolomite Δ_{47} Acid Fractionation

The focus of my study was not to determine the temperature dependence of acid fractionation, but the results narrow the possible effects of dolomite acid fractionation to two options:

1) If the mineral-specific acid fractionation factor of Murray et al. (2015) is valid for all laboratories, equation (3.2) can be used to calculate temperature from corrected dolomite Δ_{47} values if they are reacted in 75° C acid. The intercept of this equation would be different if these dolomites were reacted at a different acid temperature because a different corresponding value would be added to account for acid fractionation.

2) Alternatively, based on the measurements of Defliese et al. (2015) that suggest no dolomite-specific acid fractionation factor is necessary, equation (3.1) can be used to calculate temperature from acid-corrected dolomite Δ_{47} values. Significantly, this calibration is statistically indistinguishable from several other calibrations.

In either case, my Δ_{47} - temperature –regression equations can be used with the corresponding acid fractionation factor to calculate formation temperature from dolomite Δ_{47}. My results are inconsistent with the assertion of Murray et al. (2015) that an increased acid fractionation factor means previously measured dolomites (e.g., Loyd et al. 2012; Lechler et al. 2013; Van de Velde et al. 2013; Dale et al. 2014; Sena et al. 2014) should be interpreted as having cooler formation temperatures. When applying the fractionation factor of Murray et al. (2015) to my Δ_{47} values, I

simply find that dolomite Δ_{47} values are expected to be larger than those of calcites formed at the same temperature.

The agreement of equation (3.1) with other calibrations suggests no difference in dolomite and calcite Δ_{47} acid fractionation factors. The reason for the apparently inconsistent results of Murray et al. (2015) require further study, but may be attributable to still unaccounted for laboratory-specific methodology effects on Δ_{47}. For example, the fundamental reasons underlying ongoing disparity between data approximately fitting the Ghosh et al. (2006) and Dennis et al. (2010) calibrations has yet to be resolved.

3.5.4 Dolomite – Calcite Δ_{47} Calibration Differences

Given ongoing uncertainty regarding inter-laboratory clumped isotope data comparison, my most important finding is to clearly demonstrate a lack of mineralogical effect on Δ_{47}. Using essentially the same methodology as Defliese et al. (2015), I found a statistically indistinguishable clumped isotope calibration relationship for dolomite when compared with the regression through all synthetic calcite and aragonite data measured at the University of Michigan at the same acid temperature. This remains true with acid fractionation factors removed, thus any mineralogical difference is below levels of analytical precision. The error on our calibration and calcite calibrations means the approximate +0.02 ‰ Δ_{47} enhancement of dolomite relative to calcite predicted by Guo et al. (2009) cannot be ruled out, but I find no empirical evidence for an offset.

The precision of my calibration is affected by inherently imprecise control on the formation temperature of natural samples. The exact mean annual temperature for the Barbados and Bahamas samples, for example, has not been determined. However, a ± 5° C shift in their

formation temperatures would not affect the basic conclusion that dolomite and calcite calibrations are indistinguishable, but would affect the parameter values of the linear regression. I therefore recommend that existing calibrations are used to interpret dolomite Δ_{47} data without mineral-specific corrections. At this time, laboratory-specific calibrations in particular may be the most reliable way to empirically account for analytical effects.

3.6 Conclusions

My data show that dolomite and calcite Δ_{47} values for a given formation temperature are indistinguishable when using identical sample preparation and analytical techniques. These data, when combined with published calibrations for siderite and apatite, suggest that there are no mineral-specific calibration differences in carbonate clumped isotope thermometry, at least at current levels of precision. This suggests that carbonate clumped isotope temperatures from samples of mixed mineralogy can be interpreted with confidence (if the effects of mixing are accounted for; Defliese and Lohmann, 2014). It also implies that the clumped isotope thermometer can be used in future work to better understand dolomite formation in a variety of geochemical settings.

3.7 Acknowledgements

I thank William Defliese and Sierra Petersen for helpful discussions of the manuscript, and Lora Wingate and Kyle Meyer for assistance in the laboratory. This work was funded by student research grants from the American Association of Petroleum Geologists and the Society of Economic Geology awarded to IZW, and by NSF EAR grant 1123733 awarded to KCL.

References

Braunsdorf , N.R., Lohmann, K.C, 1983. Isotopic trends in gangue carbonates from the Viburnum Trend: Implications for Mississippi Valley-Type mineralization. M.S. Thesis, University of Michigan.

Dale, A., John, C.M., Mozley, P.S., Smalley, P.C., Muggeridge, A.H., 2014. Time-capsule concretions: Unlocking burial diagenetic processes in the Mancos Shale using carbonate clumped isotopes. Earth and Planetary Science Letters 394, 30-37.

Defliese, W.F., Hren, M.T., Lohmann, K.C., 2015. Compositional and temperature effects of phosphoric acid fractionation on Δ_{47} analysis and implications for discrepant calibrations. Chemical Geology 396, 51-60.

Defliese, W.F., Lohmann, K.C, 2014. Non-linear mixing effects on mass-47 CO_2 clumped isotope thermometry: Patterns and implications. Rapid Communications in Mass Spectrometry 29, 901-909.

Dennis, K.J., Schrag, D.P., 2010. Clumped isotope thermometry of carbonatites as an indicator of diagenetic alteration. Geochimica et Cosmochimica Acta 74, 4110-4122.

Dennis, K.J., Affek, H., Passey, B.H., Schrag, D.P., Eiler, J.M., 2011. Defining an absolute reference frame for 'clumped' isotope studies of CO_2. Geochimica et Cosmochimica Acta 75, 7117-7131.

Eagle , R.A., Schauble, E.A., Tripati, A.K., Tutken, T., Hulbert, R.C., Eiler, J.M., 2010. Body temperatures of modern and extinct vertebrates from ^{13}C-^{18}O bond abundances in bioapatite. Proceedings of the National Academy of Sciences 107, 10377-10382.

Eiler, J.M., Schauble, E., 2004. $^{18}O^{13}C^{16}O$ in Earth's atmosphere. Geochimica et Cosmochimica Acta 68, 4767-4777.

Eiler, J.M., 2011. Paleoclimate reconstruction using carbonate clumped isotope thermometry. Quaternary Science Reviews 30, 3575-3588.

Fernandez, A., Tang, J., Rosenheim, B.E., 2014. Siderite 'clumped' isotope thermometry: A new paleoclimate proxy for humid continental environments. Geochimica et Cosmochimica Acta 126, 411-421.

Ferry, J.M., Passey, B.H., Vasconcelos, C., Eiler, J.M., 2011. Formation of dolomite at 40-80° C in the Latemar carbonate buildup, Dolomites, Italy, from clumped isotope thermometry. Geology 39, 571-574.

Frank, M.H., Lohmann, K.C, 1986. Textural and chemical alteration of dolomite: interaction of mineralizing fluids and host rock in a Mississippi Valley-Type deposit, Bonneterre Formation, Viburnum Trend. Process Mineralogy 6, 103-116.

Ghosh, P., Adkins, J., Affek, H., Balta, B., Guo, W., Schauble, E.A., Schrag, D., Eiler, J.M., 2006. ^{13}C-^{18}O bonds in carbonate minerals: A new kind of paleothermometer. Geochimica et Cosmochimica Acta 70, 1439-1456.

Gregg, J.M., Bish, D.L., Kaczmarek, S.E., and Machel, H.G., 2015. Mineralogy, nucleation and growth of dolomite in the laboratory and sedimentary environment: A review. Sedimentology 62, 1749-1769.

Gregg, J.M., and Shelton, K.I., 1990. Dolomitization and dolomite neomorphism in the back reef facies of the Bonneterre and Davis Formations (Cambrian), southeastern Missouri. Journal of Sedimentary Petrology 60, 549-562.

Guo, W., Eiler, J.M., 2007. Temperature of aqueous alteration and evidence for methane generation on the parent bodies of the CM chondrites. Geochimica et Cosmochimica Acta 71, 5565-5575.

Humphrey, J.D., 1988. Late Pleistocene mixing zone dolomitization, southeastern Barbados, West Indies. Sedimentology 35, 327-348.

Humphrey, J.D., 2000. New geochemical support for mixing-zone dolomitization at Golden Grove, Barbados. Journal of Sedimentary Research 70, 1160-1170.

Kaczmarek, S.E., Sibley, D.F., 2014. Direct physical evidence of dolomite recrystallization. Sedimentology 61, 1862-1882.

Kaczmarek, S.E., Sibley, D.F., 2011. On the evolution of dolomite stoichiometry and cation order during high-temperature synthesis experiments: an alternative model for the geochemical evolution of natural dolomites. Sedimentary Geology 240, 30-40.

Kelts, K., McKenzie, J.A., 1984. 10. Diagenetic dolomite formation in Quaternary anoxic diatomaceous muds of Deep Sea Drilling Project Leg 64, Gulf of California. Initial Reports DSDP 64, 553-569.

Land, L.S., 1998. Failure to precipitate dolomite at 25° C from dilute solution despite 1000-fold oversaturation after 32 years. Aquatic Geochemistry 4, 361-368.

Lechler, A.R., Niemi, N.A., Hren, M.T., Lohmann, K.C., 2012. Paleoelevation estimates for the northern and central proto-Basin and Range from carbonate clumped isotope thermometry. Tectonics 32, 295 - 316.

Locarnini, R.A., Mishonov, A.V., Antonov, J.I., Boyer, T.P., Garcia, H.E., Baranova, O.K., Zweng, M.M., and Johnson, D.R., 2010. World Ocean Atlas 2009, Volume 1: Temperature.

In *NOAA Atlas NESDIS 68* (ed. S. Levitus). U.S. Government Printing Office, Washington, D.C., pp. 184.

Loyd, S.J., Corsetti, F.A., Eiler, J.M., Tripati, A.K., 2012. Determining the diagenetic conditions of concretion formation: Assessing temperatures and pore waters using clumped isotopes. Journal of Sedimentary Research 82, 1006-1016.

Machel, H., 2004. Concepts and models of dolomitization: a critical reappraisal. Geological Society London, Special Publications 235, 7-63.

Murray, S.T., Arienzo, M.M., Swart, P.K., 2016. Determining the Δ_{47} acid fractionation in dolomites. Geochimica et Cosmochimica Acta 174, 42-53.

Passey, B.H., Levin, N.E., Cerling, T.E., Brown, F.H., Eiler, J.M., 2010. High temperature environments of human evolution in East Africa based on bond ordering in paleosol carbonates. Proceedings of the National Academy of Sciences 107, 11245 - 11249.

Petersen, S.V., Winkelstern, I.Z., Lohmann, K.C, Meyer, K.W., 2016. The effects of Porapak™ trap temperature on $\delta^{18}O$, $\delta^{13}C$, and $\Delta47$ values in preparing samples for clumped isotope analysis. Rapid Communications in Mass Spectrometry 30, 1-10.

Pearson, P. N., Ditchfield, P. W., Singano, J., Harcourt-Brown, K. G., Nicholas, C. J., Olsson, R. K., Shackleton, N. J., and Hall, M. A., 2001. Warm tropical sea surface temperatures in the Late Cretaceous and Eocene epochs. Nature 413, 481–487.

Rosenbaum, J., Sheppard, S.M., 1986. An isotopic study of siderites, dolomites and ankerites at high temperatures. Geochimica et Cosmochimica Acta 50, 1147-1150.

Sena, C.M., John, C.M., Jourdan, A.-L., Vandeginste, V., Manning, C., 2014. Dolomitization of Lower Cretaceous peritidal carbonates by modified seawater: Constraints from clumped isotopic paleothermometry, elemental chemistry, and strontium isotopes. Journal of Sedimentary Research 84, 552 - 556.

Shelton, K.L., Bauer, R. M., Gregg, J.M., 1992. Fluid-inclusion studies of regionally extensive epigenetic dolomites, Bonneterre Dolomite (Cambrian), southeast Missouri: Evidence of multiple fluids during dolomitization and lead-zinc mineralization. Geological Society of America Bulletin 104, 675-683.

Stolper, D.A., Eiler, J.M., 2015. The kinetics of solid-state isotope-exchange reactions for clumped isotopes: A study of inorganic calcites and apatites from natural and experimental samples. American Journal of Science 315, 363-411.

Usdowski, E., 1994. Synthesis of dolomite and geochemical implications. Special Publication of the International Association of Sedimentologists 21, 345-360.

Vahrenkamp, V.C., Swart, P.K., Ruiz, J., 1991. Episodic dolomitization of late Cenozoic

carbonates in the Bahamas: Evidence from strontium isotopes. Journal of Sedimentary Petrology 61, 1002-1014.

Van De Velde, J.H., Bowen, G.J., Passey, B.H., Bowen, B.B., 2013. Climatic and diagenetic signals in the stable isotope geochemistry of dolomitic paleosols spanning the Paleocene-Eocene boundary. Geochimica et Cosmochimica Acta 109, 254-267.

Chapter 4

Mixing-zone dolomitization and diagenetic evolution of the Pipe Creek Junior carbonate complex, Indiana, USA[7]

4.1 Abstract

The Pipe Creek Junior Quarry in central Indiana exposes a four square kilometer Silurian carbonate bioherm formed in the shallow seas of the Wabash Platform. The formation history of the buildup has been relatively well studied, but the unique partial dolomitization of the complex has not been explained. Quarry and core samples reveal Pipe Creek dolomitization to have occurred only in its central and upper portions, contrasting with hundreds of other completely dolomitized regional bioherms. Here I use petrographic and stable isotope analysis to demonstrate a fresh-saline mixed water origin for this dolomite and to develop a diagenetic model for the complex.

Following marine cementation, multiple episodes of aerial exposure resulted in development of a freshwater lens and progressive microbial reduction documented by $\delta^{13}C$ values as high as +8.1 ‰. Within this sequence, a minor influx of seawater generated porewaters capable of dolomite precipitation. This dolomite occurs as mm-scale void-filling rhombs, is sometimes replacive of corroded calcites, and occurs on a small spatial scale (< 2 km^2 area); all are characteristics of other known mixing-zone dolomites.

[7] Winkelstern, I., Lohmann, K., and Breining, K. *in prep.* Journal of Sedimentary Research.

Ubiquitous late spar precipitation and hydrocarbon emplacement demonstrate subsequent late diagenetic fluid flow through this system. Clumped isotope and fluid inclusion temperature analyses of late calcite spars indicate that basinal fluids at > 70°C were transported through the complex. Clumped isotope temperatures of approximately 40° to 54°C in marine calcites and 65° to 85°C in dolomites clearly indicate resetting by these brines. Calculated $\delta^{18}O$ water values from calcites precipitated from these fluids are consistent with sourcing from the Michigan Basin. Based on these observations I describe the diagenetic evolution of the Pipe Creek complex, from marine cementation, to freshwater diagenesis, dolomitization, and finally brine influx. More broadly, these results demonstrate consistent alteration of clumped isotope values of Paleozoic carbonates in a relatively low temperature, shallow burial environment.

4.2 Introduction

The shallow, warm seas that covered the United States Great Lakes region during the Silurian provided favorable conditions for widespread development of carbonate bioherms. The area is dotted with thousands of such buildups, with about 200 described in some detail (Textoris and Carozzi, 1964). Of these, the Pipe Creek Junior carbonate complex is one of the largest that has not been completely dolomitized (Devaney et al., 1986). It therefore provides a unique opportunity to evaluate the timing and mechanisms of dolomitization that may have affected other regional Silurian carbonate systems.

The complex is partially exposed in the Pipe Creek Junior Quarry, located ~14 km southwest of Marion, Indiana, USA (Fig. 4.1). Like the entire Wabash Platform, it is largely structurally undeformed (Shaver and Sunderman, 1982; Devaney et al., 1986). Its maximum thickness is about 50 m, with ~45 m of section exposed in the quarry (Devaney et al., 1986).

Only minor amounts of original thickness were removed by subsequent erosion (Devaney et al., 1986). Based on conodont data, carbonate deposition began in the late Wenlockian (Silurian) and continued through the Ludlovian, concurrent with the uppermost Louisville Limestone and the Mississinewa Shale and Liston Creek Limestone members of the Wabash Formation (Shaver and Sunderman, 1982; Devaney et al., 1986).

The Pipe Creek complex has been referred to as a reef, but is more accurately a buildup of thinly bedded, graded carbonate units surrounding a micritic core. These thinly bedded sections are tilted up to 45°, largely the result of deposition on prograding bench-margin slopes at angles of repose (Devaney et al., 1986). Frank et al. (1993) showed that the entire buildup is made of allochthonous material generated upslope on wave-swept platforms and that local bioaccumulation was insignificant. It is therefore not a true reef but a broad carbonate bioherm formed in a high energy shallow environment. Although disagreement with this model exists (e.g., Shaver and Sunderman, 1989), here I address only the development of the Pipe Creek complex after original deposition.

This developmental history is complex. As shown here, multiple sea level changes and diagenetic fluids have resulted in a complicated sequence of carbonate precipitation and dissolution, beginning immediately after deposition and continuing throughout the burial history. The partial dolomitization of the Pipe Creek complex is the focus of this study because it sharply contrasts with the total dolomitization of most other Wabash Platform bioherms. This dolomite was briefly described by Lehmann (1978), Shaver and Sunderman (1982), and others, but the mechanism and precise timing of dolomitization has been poorly constrained. Dolomite is confined to the central portions of the Pipe Creek complex (Fig. 4.2), and any explanation for its occurrence must allow for the majority of local carbonate being entirely unaffected.

One plausible mechanism for partial dolomitization is fresh-saline water mixing. Mixed water dolomitization is the result of thermodynamic supersaturation with respect to dolomite in mixed fresh and ocean waters with 10 to 50 % normal seawater salinity (Machel, 2004). Once proposed as the main dolomitization mechanism in a variety of contexts (e.g., Humphrey and Quinn, 1989), massive dolomitization by this method is now understood to be unlikely (Melim et al., 2003). However, small-scale dolomitization on platform margins by mixed waters has been demonstrated (e.g., Land, 1973; Ward and Halley, 1985; Humphrey, 2000).

Mixing zone dolomites are chemically and petrologically distinct from other dolomites. Crystals tend to be stoichiometric, relatively clear, well-ordered rhombs on the order of millimeters in size (Machel, 2004). It generally occurs as a void-filling cement and is intergrown with calcites as water chemistry and salinity changes (Ward and Halley, 1985). Dolomite formed from fresher waters will also have more negative $\delta^{18}O$ values relative to those derived from pure or slightly modified seawater (Humphrey, 2000). Here I present geochemical and petrographic evidence for mixed water dolomitization by describing the diagenetic evolution of the Pipe Creek Junior system. I also use stable isotopes and the clumped isotope paleothermometer to describe the isotopic composition of diagenetic fluids and to evaluate isotopic alteration of original dolomite and calcite.

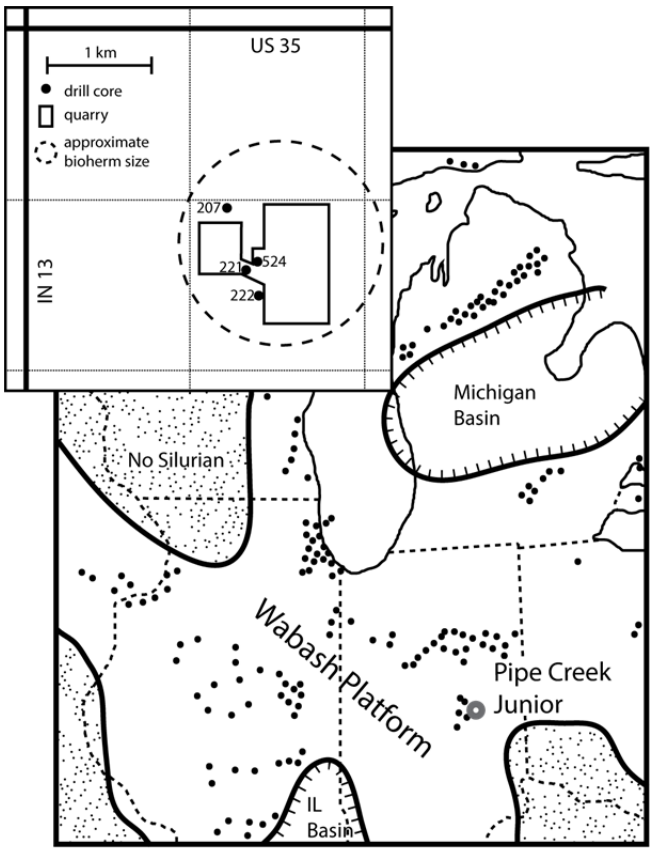

Figure 4.1. Generalized Silurian paleogeography of the Great Lakes region with known reefs and bioherms indicated by black dots. The Pipe Creek Junior complex is indicated by an open grey circle. Inset shows approximate aerial extent of the complex and sites of cores used in this study. Modified from Lehmann (1978) and Frank et al. (1993).

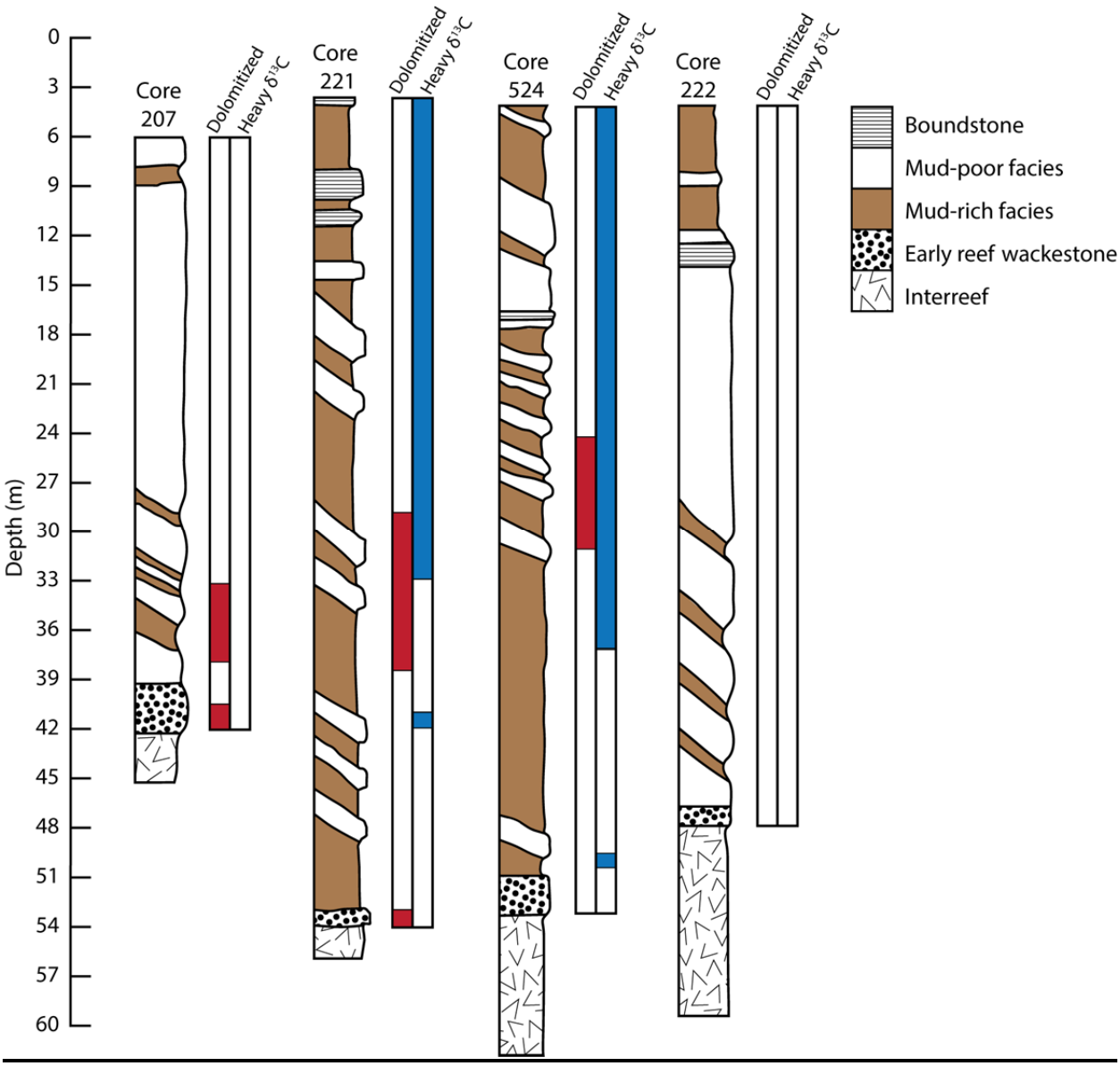

Figure 4.2. Visual description of four cores drilled into the Pipe Creek Junior complex. See Figure 4.1 for map view of each core's location.

4.3 Petrography

4.3.1 Methods

156 samples were selected for petrographic and isotopic analysis from core material housed at the Core Library of the Indiana State Geological Survey. An additional 17 samples were obtained from outcrop and float within the Pipe Creek Junior Quarry, east-northeast of the bioherm center. Samples were cut and polished, and thin and thick sections were prepared. Cathodoluminescence was examined on a Nuclide Corporation Luminoscope using an acceleration potential of 12 kilovolts with a 0.85 to 0.95 milliamp beam current. Phase transition measurements for fluid inclusion analysis on thick sections were performed on a modified heating-freezing stage of Werre et al. (1979). Concentrations of Mg, Mn, Fe, Sr, and Ca were measured in a single < 2cm thick section from the quarry exposures at the University of Michigan Electron Microprobe Analysis Laboratory using a Cameca SX100 electron microprobe coupled to a wavelength-dispersive x-ray spectroscopy (WDS) detector. Operating conditions were based on the carbonate microprobe work of Reeder and Grams (1987). A 25 kV accelerating voltage with a beam current of 15 nA and a ~15 μm spot size was used. A minimum of 5 replicate measurements were performed on internal calcite, dolomite, and sulfate standards to ensure accuracy, with 399 ppm precision or better.

4.3.2 Description

The first lithification of the Pipe Creek system is indicated by an isopachous syntaxial calcite cement and a fibrous or prismatic cloudy calcite cement. These phases line voids, biogenic fragments, and tension fractures throughout and are each at times overlain by fossil material, indicating a synsedimentary origin (Fig. 4.3A). Earlier syntaxial cements exhibit

multiple growth zones parallel to crystal faces . Fibrous calcites possess radiaxial optic extinction and are likely neomorphic products of former high-Mg calcite cements, with original prisms now intergrown and coalesced along irregular boundaries. This idea is further supported by the presence of microdolomites in both cements (Lohmann and Meyers, 1977). WDS measurements of Mg concentration in syntaxial cements range from ~1000 ppm to ~2500 ppm, confirming that these calcites are no longer high-Mg. Fibrous cements and underlying syntaxial cements are both of marine origin on the basis of intimate association with internal marine sediments, original mineralogic metastability, original high-Mg composition, and stable isotopic evidence discussed below.

The marine cements are occasionally intruded by finely zoned luminescent calcite along corroded intracrystalline regions. These later calcites more commonly occlude primary and secondary pore spaces. Several generations of equant calcite (and a single dolomite) can be discriminated petrographically and separated based on crystal morphology, inclusions, luminescence, and stratigraphic distribution. The earliest of these calcites is a fluid-inclusion free clear spar that partially occludes primary pore spaces. It is luminescently zoned, with initial growth typically indicated by a 10 – 50 μm wide bright yellow band. I interpret this phase to be the result of phreatic freshwater precipitation on the basis of its restriction to uppermost portions of the bioherm and reduced iron content, as shown by potassium ferrocyanide staining. Furthermore, rare geopetal red calcitic silts deposited in these upper regions are bracketed by marine cements and these inclusion-free calcites (Fig. 4.3A). These oxidized silts further suggest subaerial exposure and imply freshwater availability. Clear calcite cement precipitation in subsequently deformed intraskeletal porosity also demonstrates that its occurrence predates significant burial.

The petrography of Pipe Creek Junior dolomite has been previously evaluated by other workers (e.g., Suchomel, 1975; Lehmann 1978; Shaver and Sunderman, 1982). Our core evaluations suggest that overall dolomitization is more extensive than reported by Lehmann (1978) and is most intense in the upper central portions of the complex (Fig. 4.2). There selective dolomitization of micrites is common, though discrete calcitic horizons remain. Replacive dolomite and dolomite cement are both present. Intense dolomitization (>80%) generally favors wackestones and packstones and crinoidal grainstones are occasionally affected. Overall, however, dolomite distribution is more a function of stratigraphic position than lithologic type.

Irregular replacement of calcite by dolomite commonly occurs along interprismatic boundaries, substrate contacts, or growth bands, often resulting in partial retention of original crystallographic orientation. Euhedral dolomite cements occur as cloudy centered, clear-rimmed crystals less than one mm in size with an outer ferroan zone surrounding an iron-poor core (Fig. 4.3B). Up to 2400 ppm Fe was detected via WDS this outer zone, while Fe measurements in the core were below detection limits. Replacive dolomite is identifiable under cathodoluminescence as bright red-orange crystal mosaics (Fig. 4.3C). Dolomites are commonly followed by precipitation of minor amounts of pyrite and marcasite, as shown in Figure 4.3B.

In the upper central portions of the Pipe Creek complex, precipitation of inclusion-free clear calcite cement resumed. This finely zoned calcite has alternating bright yellow-orange luminescence and non-luminescence. The phase is more abundant in relatively deeper core samples where continued precipitation resulted in wider zones of orange luminescence. Potassium ferrocyanide staining revealed elevated reduced iron content. This second clear cement is similar in appearance to the first and also is restricted to upper and central complex

regions, implying that it too is meteoric in origin. Dolomitization is often bracketed by both of these meteoric calcites (Figs. 4.3D and 4.3E).

Most of the remaining porosity throughout the bioherm was infilled with fluid inclusion-rich equant calcite spars (Fig. 4.3F). These phases are especially prevalent in distal flank beds and stratigraphically lower areas where phreatic calcite did not occur. There were at least two phases of spar emplacement. The earlier spar has luminescent zoning and common two-phase (liquid and vapor) inclusions, whereas the later spar luminesces as a uniform brown and more often also contains birefringent daughter salts within fluid inclusions. Phase transition measurements on the latest spar inclusions indicate diagenetic fluid salinities greater than 20 %, as evidenced by final fluid melting from -22° to -19° C. Heating to homogenization resulted in a minimum entrapment temperature of approximately 94° C. These observations and results clearly indicate the late spars were precipitated by warm saline brines and are diagenetic in origin.

Such fluids are likely also responsible for minor corrosion and calcitization of some dolomites, observed especially where late calcite cements are in contact with replacive dolomite (e.g., along fractures). De-dolomitization is evidenced by calcitized dolomite rhomb interiors, corroded rhomb margins, and partial rhombs isolated within calcite matrices (Budai et al., 1984). Lehman (1978) suggested that this process was associated with near-surface weathering, but cathodoluminescence of calcitized regions is a uniform brown identical to that of the latest spar described above. De-dolomitization thus likely occurred via the same saline burial brines that precipitated the void-filling spar.

I therefore describe the paragenetic sequence as: 1) marine cementation; 2) neomorphism of marine cements and precipitation of early meteoric calcite; 3) corrosion of preceding cements;

4) partial dolomitization of preceding cements and precipitation of luminescent dolomite cement; 5) subsequent precipitation of ferroan non-luminescent dolomite cement rims; 6) minor iron sulfide emplacement; 7) precipitation of later meteoric calcite cement; and 8) two phases of diagenetic calcite spar precipitation, along with hydrocarbon emplacement and corrosion of preceding phases with minor de-dolomitization.

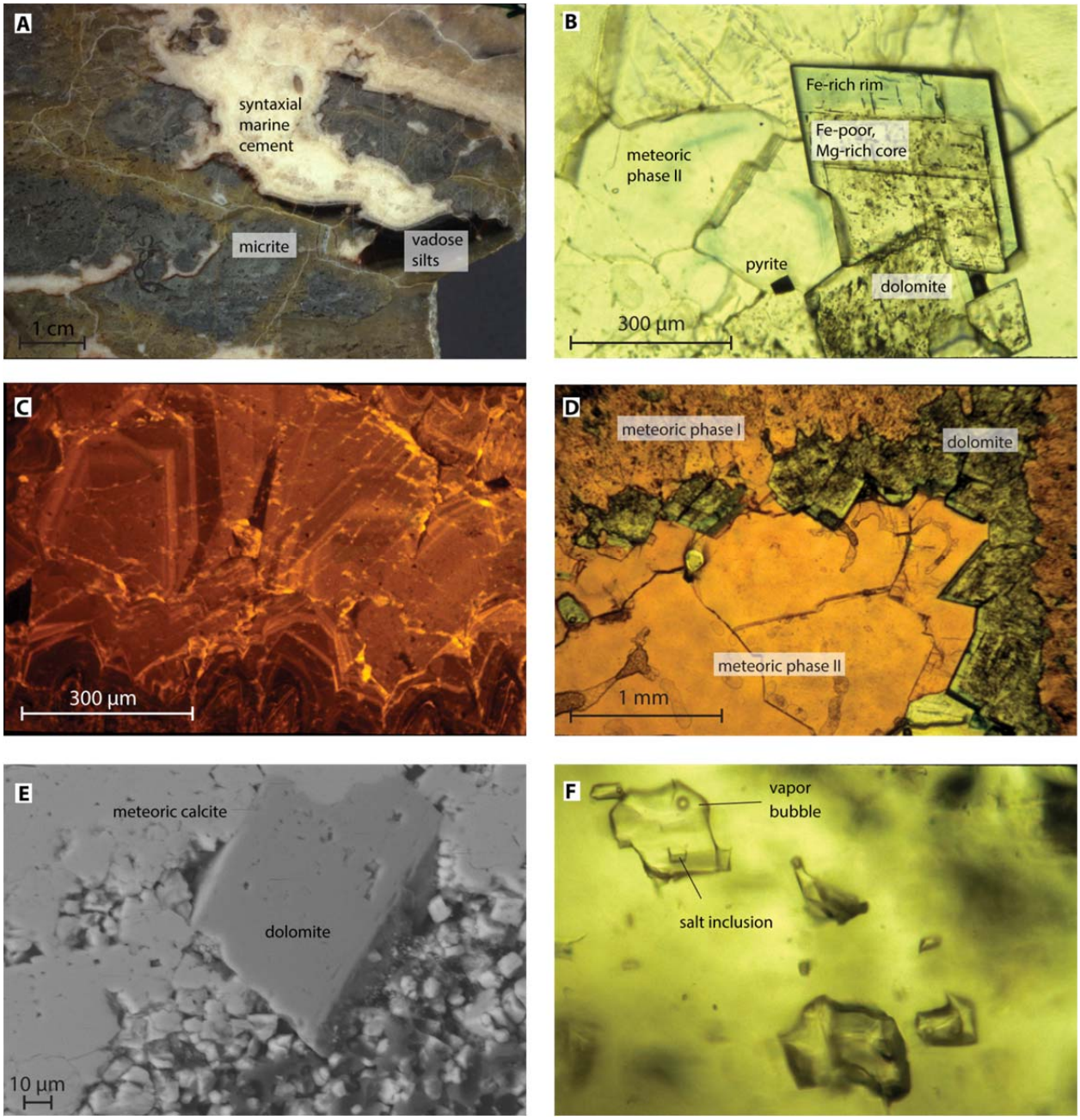

Figure 4.3 A) Hand sample from core material showing emplacement of vadose red silts between original marine micrite and syntaxial marine cements. B) Photomicrograph of dolomite rhomb in inclusion-free meteoric calcite matrix. The opaque crystal in the lower-center is pyrite, indicative of reducing conditions. Blue staining indicates iron-rich dolomite rim surrounding the Fe-poor, Mn-rich core. C) Cathodoluminescence photomicrograph illustrating zonation in meteoric calcite cements. D) Dolomite overgrowth on syntaxial marine cement and later (phase II, post-dolomite) meteoric calcite. E) Electron microscope image of dolomite rhomb growing on corroded phase I meteoric calcite. F) Example of two-phase fluid inclusions in late spar calcite.

4.4 Stable Isotopes

4.4.1 Methods

To constrain the formation conditions of the marine calcite, dolomite, and late spar described above I used conventional $\delta^{18}O$ and $\delta^{13}C$ along with the carbonate clumped isotope paleothermometer. This technique relies on the temperature dependence of $^{13}C - ^{18}O$ bond abundance within the carbonate crystal lattice. The frequency of these bonds between rare isotopes (i.e., "clumped isotopes") is solely a function of temperature and is independent of carbonate or formation water stable isotope ($\delta^{18}O$, $\delta^{13}C$) compositions (see Eiler, 2011). By measuring the mass 44, 45, 46, and 47 isotopologues of CO_2, the amount of isotope 'clumping' can be measured relative to an expected random distribution. These deviations are expressed as a Δ_{47} value, with units of per mille (Huntington et al., 2009). A unique temperature measurement provided by this technique can constrain the oxygen isotope composition for water in equilibrium with a given carbonate. In multiple studies, clumped isotopes have helped to describe the temperature and composition of diagenetic fluids (e.g., Budd et al., 2013; Dale et al., 2014; Chapters 2 and 3). Based on the findings of Chapters 2 and 3, I apply the Defliese et al. (2015) acid fractionation factor and temperature calibration to all dolomite and calcite clumped isotope data.

In all, 296 stable isotope analyses were conducted on material from the 156 studied samples. A subset of seven core and float samples were chosen for eleven clumped isotope analyses. All stable isotope work was conducted at the University of Michigan Stable Isotope Laboratory. Carbonate samples of at least 20 mg for clumped isotope analysis were sampled using a mounted Dremel hand drill kept at low speeds. The Δ_{47} value of each sample was measured three to four times, with a minimum of 4.5 mg used for each measurement.

Δ_{47} analyte CO_2 was extracted using a specific offline procedure to ensure purity (see Defliese et al., 2015). Each sample replicate was loaded into a multisample carousel that dropped individual carbonate powders into a common anhydrous phosphoric acid bath held at 75° C. Calcites were reacted for 20 minutes, while dolomites were reacted for 1 hour or until completion. Residual water vapor was removed from resultant CO_2 via cryogenic procedures under vacuum conditions as outlined by Huntington et al. (2009). To eliminate hydrocarbon and halocarbon contaminants, gas was passed through Porapak^{TM} resin held at -30° C for 20 minutes. To correct for known fractionations in this method, +0.36 ‰ was added to $\delta^{18}O$ values and +0.10 ‰ was added to $\delta^{13}C$ measurements made as a byproduct of clumped isotope analyses (Petersen et al., 2015). CO_2 pressures were measured before and after this process to ensure quantitative recovery (within 1%). Remaining gas was trapped in an evacuated glass vessel and transferred for Δ_{47} analysis. Masses 45 through 49 were measured on a dual-inlet Thermo MAT 253 mass spectrometer following the methods of Huntington et al. (2009). As described by Dennis et al. (2011), heated CO_2 with stochastic isotopologue distributions and CO_2 equilibrated with waters at 25° C were used to establish equilibration lines for data reporting in the empirical reference frame. Heated CO_2 gases were held at 1000° C in a muffle furnace for at least two hours and then quenched at room temperature.

$\delta^{18}O$ and $\delta^{13}C$ measurements resulting from clumped isotope analysis are included in the results below. For all other conventional stable isotope data, each carbonate component was microsampled using a microscope-mounted drill assembly that allowed for sampling at scales as small as 100 microns. These samples were roasted at 380° C for one hour to remove organic contaminants and were then reacted with phosphoric acid at 50°C. Reaction times were 20 minutes for calcites and 6 hours for dolomites. Resulting CO_2 was purified in an extraction line

coupled to a VG 602E Micromass mass spectrometer. Daily measurement of NBS-20 standard indicated precision for all analyses was better than 0.2 ‰. Appropriate acid fractionation factors for calcite (Friedman and O'Neil, 1977) and dolomite (Rosenbaum, 1986) were applied for each reaction temperature (50° and 75° C) for all conventional stable isotope results. All carbonate $\delta^{18}O$ and $\delta^{13}C$ values here are reported relative to the Vienna Pee Dee Belemnite standard (VPDB), and all $\delta^{18}O$ water values are reported relative to the Vienna Standard Mean Ocean Water standard (VSMOW).

4.4.2 Conventional Stable Isotopes

Conventional stable isotope results for all phases are shown in Figure 4.4. Marine calcite components show wide variability (-3.8 to -8.9 ‰ $\delta^{18}O$, +3.2 to -0.5 ‰ $\delta^{13}C$; VPDB) but are roughly distributed along two covariant trends (Fig. 4.4A). Samples from the Pipe Creek Quarry and the uppermost portions of cores have slightly lower $\delta^{13}C$ than deeper core samples. These trends, however, converge at their heaviest end member, approximately -3.8 ‰ $\delta^{18}O$ and +1.9 ‰ $\delta^{13}C$ VPDB. This estimated Silurian marine calcite value roughly agrees with that of Lohmann and Walker (1989), and would imply a local Silurian seawater value of -0.7 ‰ (VSMOW) at 30° C.

For both trends, stable isotope values from any single hand sample show compositional variability along the entire length of the trend, i.e., isotopic heterogeneity exists on the hand sample scale. This implies that partial alteration pervades all marine cementation and that stabilization and spar intergrowth via diagenetic fluids occurred throughout the complex. Comparison of cathodoluminescence and isotopic signatures confirms that heavier values seem to correspond with unaltered components.

Stable isotope values for early, phase I (pre-dolomite) meteoric calcite cements are indicated in Figure 4.4B, again with deeper core samples tending to be more enriched in ^{13}C. Overall, values are nearly identical to those of marine cements, ranging from -4.6 to -8.0 ‰ $\delta^{18}O$ and +1.8 to -0.2 ‰ $\delta^{13}C$. Post-dolomite phase II meteoric calcite cements have a similar range of $\delta^{18}O$ values (-6.5 to -8.3 ‰), but have a dramatically wider $\delta^{13}C$ range (+8.1 to +1.7 ‰) than any other phase, with deeper samples yielding heavier carbon values (Fig. 4.4B). Relatively depleted (< 3.0 ‰) $\delta^{13}C$ values are only observed in post-dolomite meteoric calcite samples collected from the uppermost exposures.

$\delta^{18}O$ values for dolomite are slightly more negative (-5.1 to -9.3 ‰) than those for meteoric calcites, and $\delta^{13}C$ values (+2.5 to +0.9 ‰) lie between values for the meteoric cements that bracket it (Fig. 4.4C). The bulk of more enriched carbon values come from later ferroan dolomites. Late calcite spar stable isotope values range from -7.6 ‰ to -10.7 ‰ $\delta^{18}O$ and +1.8 ‰ to 0.0 ‰ $\delta^{13}C$ (Fig. 4.4D). These burial phases are the most ^{18}O depleted of all studied phases.

4.4.3 Clumped Isotopes

Clumped isotope temperatures for each phase are shown in Table 4.1 and Figure 4.5, along with calculated $\delta^{18}O$ of formation porewaters. Late spar calcites are presumably unaltered and were emplaced at high temperature (>70 °C), which is roughly in agreement with fluid inclusion data. Neither marine calcite nor dolomite samples preserve realistic Silurian Earth surface conditions, with dolomites representing ambient conditions ranging between 65° ± 3° C and 85° ± 7° C, and marine calcites ranging between 40° ± 4° C and 54° ± 4° C.

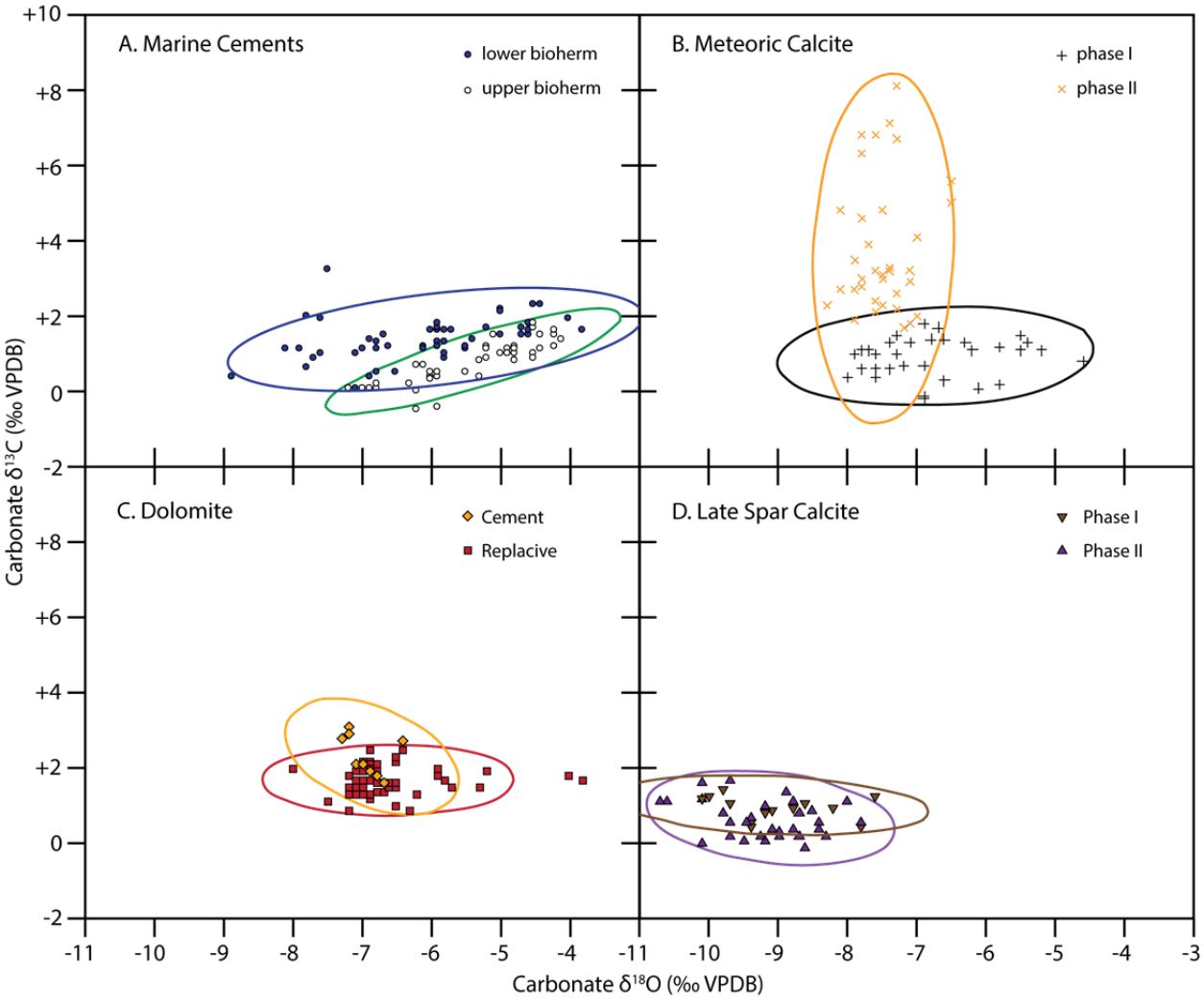

Figure 4.4. $\delta^{18}O$ and $\delta^{13}C$ values of separate carbonate phases. Outlines designate 95% confidence ellipses around the median. A) Syntaxial and fibrous marine cements follow two separate trends, with deeper rocks on average having more positive $\delta^{13}C$. The trends merge at the approximate original marine calcite value, -3.8 ‰ $\delta^{18}O$ and +1.9 ‰ $\delta^{13}C$. B) Pre-dolomite (phase I) and post-dolomite (phase II) meteoric calcites plot along different trajectories. Phase I calcites largely match marine calcite values, while phase II calcites are dramatically enriched in carbon. C) Replacive dolomite and dolomite cements have nearly identical compositions and have slightly more positive $\delta^{13}C$ than preceding meteoric calcite. D) Late diagenetic spar calcites have the most negative $\delta^{18}O$ of any phase.

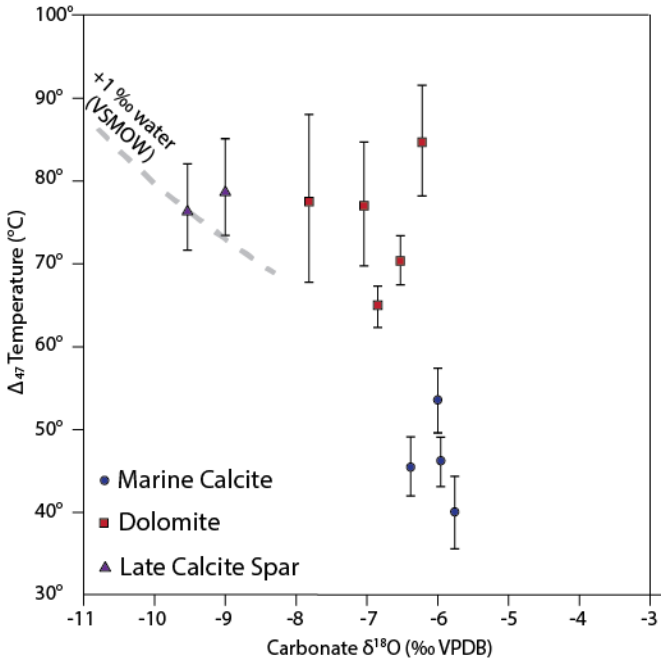

Figure 4.5. Δ_{47}-derived temperatures plotted against $\delta^{18}O$ carbonate values (VPDB) for marine cements, dolomites, and the late spar calcite. The approximate calculated $\delta^{18}O$ value (VSMOW) of late spar formation waters is also shown, as these Δ_{47} temperatures are presumed to be unaltered.

Sample	$\delta^{18}O$ (PDB)	$\delta^{13}C$ (PDB)	Δ_{47}	°C, Defliese et al. (2015)
Dolomite A	-7.8	+1.8	0.5795 ± 0.0176	77 ± 10
Dolomite B	-7.0	+2.1	0.5803 ± 0.0131	77 ± 8
Dolomite C	-6.8	+1.7	0.6025 ± 0.0049	65 ± 3
Dolomite D	-6.2	+1.2	0.5675 ± 0.0110	85 ± 7
Dolomite E	-6.5	+1.8	0.5923 ± 0.0055	70 ± 3
Marine Calcite A	-6.4	+1.1	0.6433 ± 0.0084	46 ± 4
Marine Calcite B	-6.0	+1.0	0.6250 ± 0.0078	54 ± 4
Marine Calcite C	-6.0	+1.5	0.6420 ± 0.0070	46 ± 3
Marine Calcite D	-5.8	+1.0	0.6565 ± 0.0108	40 ± 4
Late Spar A	-9.0	+0.9	0.5767 ± 0.0101	79 ± 6
Late Spar B	-9.5	+1.0	0.5808 ± 0.0092	76 ± 5

Table 4.1. Stable isotope data and Δ_{47} derived temperatures using the calibration of Defliese et al. (2015). All errors are one standard error via three (Dolomite E) or four replicate analyses (all others).

4.5 Discussion

4.5.1 Marine Cementation

Marine syntaxial and fibrous calcite cements caused initial lithification of the Pipe Creek complex. Syntaxial cements are not commonly interpreted as having a marine origin, but these are epitaxially overlain by, and have $\delta^{18}O$ values completely concurrent with, the fibrous cements. Each cement also possesses a similar fabric, with underlying syntaxial cement typically being less corroded. Diagenetic calcite intergrowth into the marine phases likely occurred during meteoric and late spar emplacement, with both affecting stable isotope results.

4.5.2 Progressive Reduction and Mixed Water Dolomitization

Meteoric cements in the Pipe Creek complex are volumetrically minor but are key to understanding its early diagenesis and dolomitization. Early (phase I, pre-dolomite emplacement) and later (phase II, post-dolomite emplacement) meteoric calcites typically can be differentiated based on their alternating bright-dark luminescence and are also isotopically distinct. Depleted $\delta^{13}C$ values less than +2.0 ‰ in early meteoric calcites may reflect water recharge through a soil zone where soil CO_2 (< -20 ‰ $\delta^{13}C$; Cerling et al., 1991) locally contributes light carbon to the porewater system. Higher $\delta^{13}C$ values thus likely reflect increased rock-water interaction with marine components (which have an approximate +2.0 ‰ composition) or reduced soil development. This contrasts with the uniquely positive $\delta^{13}C$ values of late meteoric calcites (ranging between +1.7 ‰ and +8.1 ‰) which clearly indicate the introduction of a new carbon source.

A likely explanation for heavy $\delta^{13}C$ values in meteoric calcites is fermentation of organic carbon in lower central portions of the complex. As originally described by Kelts and McKenzie

(1982), the large fractionations in breakdown of formaldehyde ($2CH_2O$ —> $CH_4 + CO_2$) result in heavy carbon HCO_3 coexisting with light carbon methane. Organic fermentation can thus result in introduction of ^{13}C-enriched bicarbonate to the system. Because this can occur at depths as shallow as 10 m, this is consistent with calcite (and dolomite) precipitation occurring near the surface (Kelts and McKensie 1982; Gunatilaka et al., 1984).

This fermentation represents the culmination of progressive reduction of porewaters. As documented in other work (e.g., Sayles 1981), consumption of dissolved oxygen by the degradation of organic matter initiates a predictable reduction series where shifts in terminal electron acceptors result in reductions of oxidized Mn, Fe, and S, producing increased concentrations of reduced Mn^{2+}, Fe^{2+}, and S^- in porewaters. The luminescent zoning of early meteoric calcite indicates initial reduction (Fig. 4.3C). Following corrosion, luminescence of replacive dolomite and rhomb cores signifies continued Mn^{2+} enrichment, with iron-rich dolomite rims documenting a shift to Fe^{2+} enrichment (Fig. 4.3B). $\delta^{13}C$ of dolomites (ranging from +0.9 ‰ to +3.1 ‰) fit between earlier and later meteoric calcites and begin to document carbon enrichment in the system. Occasional precipitation of iron sulfides in the complex's core then signifies a shift to sulfate reduction. The final shift to fermentation is then documented by large $\delta^{13}C$ values as well as luminescent zonation of later meteoric calcites.

The progressive reduction of porewaters and bracketing by meteoric calcites therefore constrains the timing of dolomitization to within a freshwater diagenetic sequence. Corrosion of marine and phreatic calcites preceding dolomite emplacement further indicate fresh-saline water mixing, as such waters can become undersaturated with respect to calcite and supersaturated with respect to dolomite (Machel, 2004). Mixed water dolomitization, occurring via seawater intrusion during subaerial exposure, is thus the most likely mechanism for dolomite occurrence

in the Pipe Creek complex. The apparently reset Δ_{47} temperatures and largely altered $\delta^{18}O$ values in Pipe Creek dolomites inhibit quantitative measurement of original formation water composition. However, if the heaviest measured dolomite $\delta^{18}O$ values (approaching -5 ‰ VPDB, see Fig. 4.4B) are assumed to be original, at 30° C freshwater-influenced formation waters lighter than -5 ‰ (VSMOW) are indicated when using the water-dolomite fractionation factor of Horita (2014).

The extent of mixing zone dolomitization in the geologic record is controversial, but the process has been proposed for the origins of a variety of near-recent and Paleozoic dolomites (Machel, 2004). Although geologically recent examples of mixing zone dolomitization are somewhat uncommon, several reports of small-scale Holocene or Pleistocene dolomitization via mixed waters demonstrate the model's viability (e.g., Land, 1973; Ward and Halley, 1985; Gill et al., 1995; Humphrey 2000). Specifics of their hydrology and dolomite composition vary, but in each case dolomitization, like that described here, typically occurs as mm-scale void-filling stoichiometric rhombs or as replacive of corroded calcites. Isolated patches of dolomitization are also commonly indicative of mixed-water processes (Machel, 2004). The dolomitization conditions in the Pipe Creek complex were likely somewhat analogous to those described for the Late Pleistocene of the northwest Yucatan Peninsula (Ward and Halley, 1984). There, too, a brief high stand of sea level enhanced mixing of fresh and marine water and caused dolomitization between intervals of fresh water precipitation and diagenesis.

Seawater-derived dolomitization (e.g., Purser et al., 1994) is unlikely for the Pipe Creek system based on the small scale and patchy occurrence of dolomite (and because of clear evidence for freshwater influence before and after dolomite emplacement). The available evidence also does not support evaporative lagoon or sabkha-style dolomitization (e.g., Aharon

et al., 1977; Gunatilaka et al., 1984). This is because no positive (evaporation-related) $\delta^{18}O$ values were measured in any phase, no evaporite deposits have been observed, and the distribution of Pipe Creek dolomite is unlike the thin, laterally extensive layers observed in modern sabkhas. Positive $\delta^{18}O$ values for overlying middle Devonian dolomites may be indicative of this mechanism (Breining, 1985).

4.5.3 Late Diagenesis and Clumped Isotopes

Clumped isotope-derived temperatures are clearly influenced by diagenesis, as Silurian water temperatures in excess of 50° C are unrealistic (Munnecke et al., 2010). Solid state reordering has been experimentally shown to alter carbonate Δ_{47} values when samples are exposed to temperatures exceeding 100° C (Passey and Henkes, 2012). The Pipe Creek Jr. complex was never deeply buried (Frank et al., 1993), however, and therefore the solid-state reordering model of Passey and Henkes (2012) would not predict Δ_{47} alteration as a result of burial. The most likely source for Δ_{47} alteration of these phases are the hot basinal brines that flowed through the system and precipitated late calcite spar.

The reasons for significantly hotter and more altered dolomite Δ_{47} temperatures are unclear. Previous work has established that calcite and dolomite clumped isotope temperature calibrations are statistically identical (Chapter 3) and that both minerals seem equally susceptible to alteration of clumped isotope compositions (Chapter 2). One plausible explanation is that dolomites were more exposed to hot temperatures than marine calcites. If hot fluid transport through the Pipe Creek complex was indeed the cause of Δ_{47} alteration, then areas with more porosity would be expected to have been exposed to more continuously elevated temperatures and to have experienced more thermal alteration. Dolomites corrosively overlay meteoric calcite

cementation and therefore likely were more often adjacent to pore spaces (Fig. 4.3E). Nevertheless, more investigation is needed into the clumped isotope temperature response of different carbonate phases in diagenetic systems.

Calculated $\delta^{18}O$ water values from (presumably unaltered) late calcite spar are around +1.0 ‰ (VSMOW), and are consistent with the idea that a series of brines was exported from an adjoining basin through the Pipe Creek complex. These values fit within the range of measurements (-3.9 ‰ to +2.9 ‰ VSMOW) of Michigan basin brines in Silurian strata (McNutt et al., 1987; Wilson and Long, 1993). The most likely scenario, therefore, is that a series of externally-sourced fluids progressively altered Δ_{47} and eventually $\delta^{18}O$ of original calcites and dolomites.

4.5.4 Diagenetic Model

The evolution of the modern Pipe Creek complex proceeded in three main phases: 1) deposition and marine cementation, 2) subaerial exposure, freshwater diagenesis and dolomitization, and 3) burial diagenesis.

Following original marine phreatic cementation, the Pipe Creek Junior complex underwent several phases of subaerial exposure. As a result, meteoric calcite cements were precipitated under reducing conditions. Marine waters mixed with these reducing porewaters to then form a zone of meteoric-marine mixing undersaturated with respect to calcite and supersaturated with respect to dolomite, resulting in partial corrosion of older calcite components and dolomite replacement and precipitation (Fig. 4.6). Continued reduction of porewaters precipitated clear outer rims of relatively iron-rich dolomite and later pyrite. A second generation

of carbon-enriched meteoric calcite was precipitated afterwards, closely associated with decomposing organic material.

At some time following final burial, the Pipe Creek Junior complex was intruded by a series of hot saline brines most likely sourced from the Michigan Basin. These fluids precipitated at least two generations of calcite spar, further infilling porosity. Hydrocarbon emplacement then occurred. Based on identical sterane (hydrocarbon) classes, Lehmann and Simo (1989) interpreted the stratigraphically higher Devonian New Albany shale as the source for approximately 11 million barrels of oil being emplaced in the complex (though most of these hydrocarbons are no longer present). Finally, Pleistocene glaciation truncated a small portion (<10 m) of the top of the Pipe Creek complex (Frank et al., 1993).

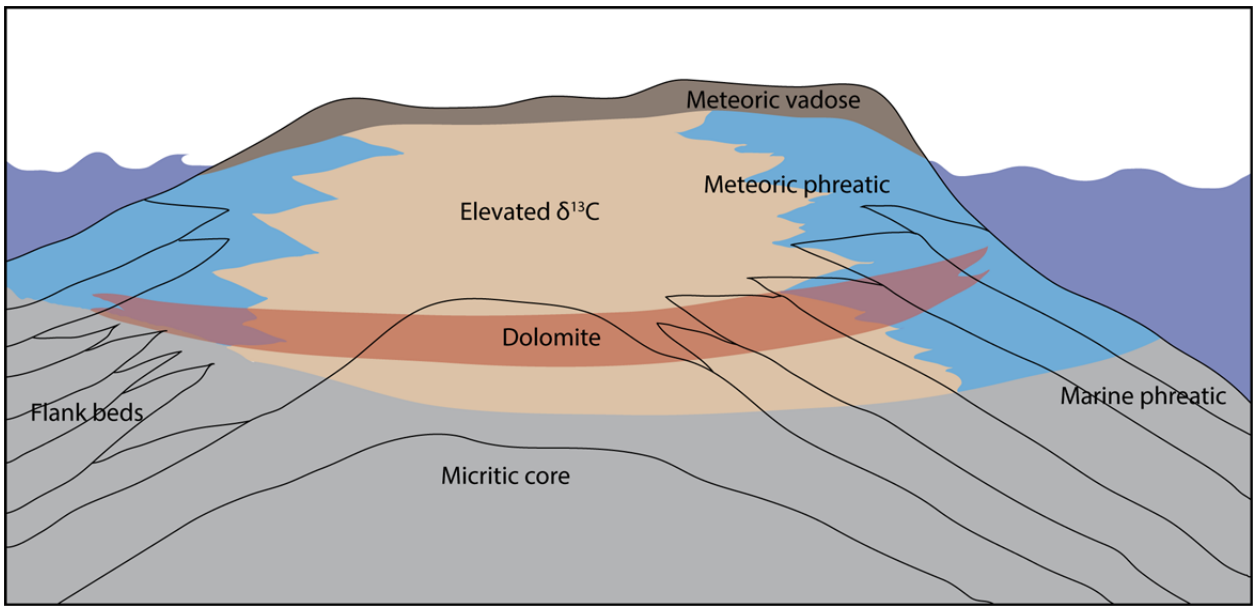

Figure 4.6. Model for the Pipe Creek Junior complex prior to final burial (and late spar emplacement). Note that dolomite is present only in a relatively thin lens near the freshwater-marine groundwater interface.

4.5 Conclusions

The timing of dolomitization in the Pipe Creek complex is tightly constrained within a freshwater calcite diagenetic sequence defined by subaerial exposure and development of a freshwater lens. Petrographic and geochemical evidence suggests stagnation of these waters resulted in increasingly anoxic and reducing conditions, ultimately resulting in organic fermentation of organic matter leading to precipitation of ^{13}C-enriched carbonates. Dolomite formation occurred when a mix of ~10 – 50% seawater was temporarily achieved.

The fabrics and relationships between the carbonates resulting from these events are remarkably preserved, but conventional $\delta^{18}O$ has been progressively altered and Δ_{47} values have been reset by late-stage diagenesis. Although the lack of original isotopic compositions prohibits the gathering of Silurian paleotemperature information, this unique set of preservation conditions has permitted an understanding of the early and late diagenesis of the Pipe Creek Junior complex. The resetting of calcite and dolomite Δ_{47} has shown that higher temperature brines must have played a role in late sequence diagenesis. Their $\delta^{18}O$ compositions match with brines in the Michigan Basin today and thus document basin outflow events that could have altered other Wabash Platform systems.

This fact that the relatively low temperature diagenetic conditions undergone by the Pipe Creek complex have altered Δ_{47} values provides further evidence that the technique must be applied carefully when attempting deep time paleoenvironmental reconstruction. Clumped isotope paleothermometry remains useful for diagenetic studies as it can constrain the temperature and fluid conditions under which rocks are altered.

References

Aharon, P., Kolodny, Y., Sass, E., 1977. Recent hot brine dolomitization in the "Solar Lake" Gulf of Elat isotopic, chemical, and mineralogical study. Journal of Geology, 85, 27-48.

Breining, K.A., 1985. Stable isotopic and cathodoluminescence study of a Silurian shelf reef. evaluation of the timing and mechanism of dolomitization [unpublished M.S. thesis]. Ann Arbor, Michigan, University of Michigan, 1-37.

Budd, D.A., Frost, III, E.L., Huntington, K.W., Allwardt, P.F., 2013. Syndepositional deformation features in high-relief carbonate platforms: Long-lived conduits for diagenetic fluids. Journal of Sedimentary Research 82., 12-36, doi. 10.2110/jsr.2013.3

Cerling, T.E., Solomon, D.K., Quade, J., Bowman, J.R., 1991. On the isotopic composition of carbon in soil carbon dioxide. Geochimica et Cosmochimica Acta 55, 3403-3405.

Dale, A., John, C.M., Mozley, P.S., Smalley, P.C., Muggeridge, A.H., 2014. Time-capsule concretions: Unlocking burial diagenetic processes in the Mancos Shale using carbonate clumped isotopes. Earth and Planetary Science Letters 394, 30-37, doi. 10.1016/j.epsl.2014.03.004

Defliese, W. F., Hren, M. T., Lohmann, K. C, 2015. Compositional and temperature effects of phosphoric acid fractionation on Δ_{47} analysis and implications for discrepant calibrations. Chemical Geology, 396, 51–60, doi.10.1016/j.chemgeo.2014.12.018.

Dennis, K.J., Affek, H.P., Passey, B.H., Schrag, D.P., Eiler, J.W., 2011. Defining an absolute reference frame for 'clumped' isotope studies of CO_2. Geochimica et Cosmochimica Acta 75, 7117-7131.

Devaney, K.A., Wilkinson, B.H., Van der Voo, R., 1986. Deposition and compaction of carbonate clinothems: the Silurian Pipe Creek Junior complex of east-central Indiana. Geological Society of America Bulletin, v. 97, p. 37-38.

Eiler, J.M., 2011. Paleoclimate reconstruction using carbonate clumped isotope thermometry. Quaternary Science Reviews 30, 3575-3588.

Frank, T.D., Wilkinson, B.H., Lohmann, K.C, 1993. Origin of submarine pisoliths and the sedimentology of midwestern Silurian reefs. Journal of Sedimentary Petrology 63, 1070-1077.

Friedman, I., and O'Neil, J.R., 1977. Compilation of stable isotope fractionation factors of geochemical interest, in: Fleischer, M., ed., Data of Geochemistry. Geological Survey Professional Paper 440, 12 p.

Gill, I.P., Moore, C.H., Aharon, P., 1995. Evaporitic mixed-water dolomitization on St. Croix, U.S.V.I.. Journal of Sedimentary Research 65, 591-604.

Gunatilaka, A., Saleh, A., Al-Temeemi, A., Nassar, N., 1984. Occurrence of subtidal dolomite in a hypersaline lagoon, Kuwait. Nature 311, 450-452.

Henkes, G.A., Passey, B.H., Wanamaker Jr., A.D., Grossman, E.L., Ambrose Jr., W.G., Carroll, M.L., 2013. Carbonate clumped isotope compositions of modern marine mollusk and brachiopod shells. Geochimica et Cosmochimica Acta 106, 307-325, doi. 10.1016/j.gca.2012.12.020

Horita, J., 2014. Oxygen and carbon isotope fractionation in the system dolomite-water-CO_2 to elevated temperatures. Geochimica et Cosmochimica Acta 129, 111-124, doi. 10.1016/j.gca.2013.12.027

Humphrey, J.D., 2000. New geochemical support for mixing-zone dolomitization at Golden Grove, Barbados 70, 1160-1170.

Humphrey, J.D., and Quinn, T.M., 1989. Coastal mixing zone dolomite, forward modeling, and massive dolomitization of platform-margin carbonates. Journal of Sedimentary Petrology 59, 438-454.

Huntington, K.W., Eiler, J.M., Affek, H.P., Guo, W., Bonifacie, M., Yeung, L.Y., Thiagarajan, N., Passey, B., Tripati, A., Daëron, M., Came, R., 2009. Methods and limitations of 'clumped' CO_2 isotope (Δ_{47}) analysis by gas-source isotope ratio mass spectrometry. Journal of Mass Spectrometry 44, 1318-1329, doi. 10.1002/jms.1614

Kelts, K., and McKenzie, J.A., 1982. Diagenetic dolomite formation in Quaternary anoxic diatomaceous muds of Deep Sea Drilling Project Log 64, Gulf of California. Initial Reports of the Deep Sea Drilling Project, 64, 553-569.

Land, L.S., 1973. Contemporaneous dolomitization of middle Pleistocene reefs by meteoric water, North Jamaica. Bulletin of Marine Science 23, 64-92.

Lehmann, P.J., 1978. Deposition, porosity evolution and diagenesis of the Pipe Creek Junior reef (Silurian), Grant County, Indiana [unpublished M.S. thesis]. Madison, Wisconsin, University of Wisconsin, 234 p.

Lehmann, P.J. and Simo, 1989. Depositional facies and diagenesis of the Pipe Creek Jr. reef, Silurian, Great Lakes region, Indiana, in: Geldsetzer, H.H.J., James, N.P., and Tebbutt, G.E., eds., Reefs, Canada and Adjacent Area. Canadian Society of Petroleum Geologists, 319-329.

Lohmann, K.C., and Meyers, W.J., 1977. Microdolomite inclusions in cloudy prismatic calcites: A proposed criterion for former high magnesium calcites. Journal of Sedimentary Petrology, 47, 1078-1088.

Lohmann, K.C., and Walker, J.C.G., 1989. The $\delta^{18}O$ record of Phanerozoic abiotic marine calcite cements. Geophysical Research Letters, v. 16, p. 319-322.

Machel, H.G., 2004. Concepts and models of dolomitization. a critical reappraisal, in. Braithwaite, C.J.R., Rizzi, G., and Darke, G., eds., The Geometry and Petrogenesis of Dolomite Hydrocarbon Reservoirs. Geological Survey special publication 235, 7-63.

McNutt, R.H., Frape, S.K., Dollar, P., 1987. A strontium, oxygen, and hydrogen isotopic composition of brines, Michigan and Appalachian basins, Ontario and Michigan. Applied Geochemistry 2, 495-505.

Melim, L.A., Swart, P.K., Eberli, G.P., 2003. Mixing-zone diagenesis. separating fact from theory, in: 12th Bathurst Meeting – International Conference of Carbonate Sedimentologists, July 2003, Durham, U.K., 68.

Munnecke, A., Calner, M., Harper, D.A.T., Servais, T., 2010. Ordovician and Silurian sea-water chemistry, sea level, and climate: A synopsis. Palaeogeography, Palaeoclimatology, Palaeoecology 296, 389-413, doi. 10.1016/j.palaeo.2010.08.001

Passey, B. H., and Henkes, G. A., 2012. Carbonate clumped isotope bond reordering and geospeedometry. Earth and Planetary Science Letters 351, 223–236, doi.10.1016/j.epsl.2012.07.021.

Petersen, S. V., Winkelstern, I. Z., Lohmann, K. C., Meyer, K. W., 2015. The effects of Porapak trap temperature on $\delta^{18}O$, $\delta^{13}C$, and Δ_{47} in preparing samples for clumped isotope analysis. Rapid Communications in Mass Spectrometry 30, 1-10.

Purser, B.H., Tucker, M.E., Zenger, D.H., 1994. Dolomites – a volume in honour of Dolomieu. International Association of Sedimentologists 21.

Reeder, R.J., and Grams, J.C., 1987. Sector zoning in calcite cement crystals. Implications for trace element distributions in carbonates. Geochimica et Cosmochimica Acta 51, 187-194.

Rosenbaum, J., 1986. An isotopic study of siderites, dolomites, and ankerites at high temperatures. Geochimica et Cosmochimica Acta 50, 1147-1150.

Sayles, F.L. 1981. The composition and diagenesis of interstitial solutions; II: Fluxes and diagenesis at the water-sediment interface in the high latitude North and South Atlantic. Geochimica et Cosmochimica Acta 45, 1061-1086.

Shaver, R.H., and Sunderman, J.A., 1982. Silurian reefs at Delphi and Pipe Creek Junior quarry, Indiana, with emphasis on the question of deep vs. shallow water. Purdue University Department of Geosciences and Geological Society of America North-Central Section Guidebook 5, 1-39.

Shaver, R.H., and Sunderman, J.A., 1989. Silurian seascapes. water depth, clinothems, reef geometry, and other motifs – a critical review of the Silurian reef model. Geological Society of America Bulletin, 101, 939-951.

Suchomel, D.M., 1977. Paleoecology and petrology of Pipe Creek Jr. reef (Niagran-Cayugan), Grant County, Indiana. A.M. Thesis. Indiana Univerisy, Bloomington,38 p.

Textoris, D.A. and Carozzi, A.V., 1964. Petrography and evolution of Niagaran (Silurian) reefs, Indiana. American Association of Petroleum Geologists Bulletin 48, 397-426.

Ward, W.C., and Halley, R.B., 1985. Dolomitization in a mixing zone of near-seawater composition, Late Pleistocene, northeastern Yucatan Peninsula. Journal of Sedimentary Petrology 55, 407-420.

Werre Jr., R.W., Bodnar, R.J., Benthke, P.M., Barton Jr., P.B., 1979. A novel gas-flow fluid inclusion heating/freezing stage. Geological Society of America Abstracts with Programs 11, 539.

Wilson, T.P., and Long, D.T., 1993. Geochemistry and isotope chemistry of Ca-Na-Cl brines in Silurian strata, Michigan Basin, U.S.A. Applied Geochemistry 8, 507-524.

Chapter 5

Shifts in Last Interglacial Ocean Circulation Indicated by Cold Temperatures in Bermuda[8]

5.1 Abstract

The peak of the Last Interglacial (LIG), Marine Isotope Stage 5e (MIS 5e; 124 – 119 ka), was the last time global temperatures were elevated 1-2 °C relative to preindustrial conditions. Reconstructed sea surface temperatures (SSTs) indicate much warmer MIS 5e poles contrasted with cooler tropical conditions. One explanation for these conditions is enhanced poleward heat transport, but Atlantic Meridional Overturning Circulation was similar in strength to modern, reflecting uncertainties in how MIS 5e climate and ocean circulation changes were connected. Bermuda offers an ideal location to observe a record of change in North Atlantic circulation and the relative position of the nearby Gulf Stream, which in its modern aspect produces the island's warm climate. Here I present submonthly-resolution SST time series from two localities documenting MIS 5e temperatures ~3 °C and ~10 °C colder than today. These remarkably cold SSTs are the first quantitative measurement of local LIG paleoclimate and require explanations that allow for major deviations from modern North Atlantic surface circulation. The coldest temperatures likely reflect reductions of the Gulf Stream during rapid deglaciation. Warmer SSTs, but still cooler than modern, are perhaps the result of increased cool surface return flow of the North Atlantic Drift or Canary Current, implying an enhanced North Atlantic Gyre during

[8] Winkelstern, I., Lohmann, K., Rowe, M., Defliese, W., Brewer, A., *in review*. Proceedings of the National Academy of Sciences.

much of MIS 5e. These results are colder than current ocean-atmosphere models indicate. They also refute faunal-based qualitative estimates of local warming and illustrate extreme sensitivity of Bermudian climate to broad-scale climate and ocean circulation changes.

5.2 Last Interglacial Climate

As observed for other Late Pleistocene interglacial intervals, at the onset of the Last Interglacial (LIG) the climate warmed rapidly and large-scale ice sheet melting occurred (Lisiecki and Raymo, 2005). During the peak of this interval, identified as Marine Isotope Stage 5e (MIS5e; 124 – 119 ka), global average temperatures were similar to today, i.e., 1 – 2 °C warmer than pre-industrial conditions (Crowley and Kim, 1994). The Earth was not uniformly warmer, however, as sea surface temperature (SST) proxy records indicate cooler tropics and a warmer arctic (Rahmstorf, 2002). This suggests enhanced poleward heat transport and would seem to suggest stronger Atlantic Meridional Overturning Circulation (AMOC) relative to modern (Otto-Bliesner, 2006). Coeval benthic isotopic ratios of $^{231}Pa/^{230}Th$ and $^{143}Nd/^{144}Nd$, however, do not indicate that the deep and intermediate water components of MIS 5e AMOC were enhanced relative to the current interglacial (Böhm et al., 2015). Uncertainty regarding how LIG ocean circulation and climate were connected therefore remains.

5.3 Bermudian Climate

Because the warm modern climate of Bermuda is controlled by ocean surface circulation, it is an excellent location to examine past ocean circulation changes. Home to the northernmost coral reef communities in the Atlantic, the island today is warmed by tendrils of the Gulf Stream mixing with the relatively stagnant waters of the Sargasso Sea (Steinberg et al., 2001). It has

been proposed that local climate was slightly warmer during MIS 5e (Muhs et al., 2002), but a virtual absence of emergent, life position LIG fossil corals on Bermuda (Rowe and Bristow, 2015) may reflect cooler temperatures relative to today.

A better understanding of local paleoclimate can provide rare insight into past states of North Atlantic circulation. The wind-driven surface currents of the North Atlantic Gyre directly influence the climates of eastern North America and western Europe (Capron et al., 2014; Palter, 2015). Therefore, a possible explanation for the apparent contradiction between a warm arctic coupled with an unremarkable AMOC is enhanced surface circulation relative to modern. The resulting stronger southward return flow could perhaps bring cooler conditions to the eastern and central North Atlantic, including around Bermuda, without major changes in deep water circulation. More dramatic perturbations in North Atlantic surface currents, such as weakening or shutdown of the Gyre, would have major immediate effects on Bermudian and regional climate.

5.4 Water Isotope and Paleotemperature Analyses

I determined MIS 5e temperatures in Bermuda by applying isotope sclerochronology and clumped isotope thermometry to fossil marine gastropods. Clumped isotope thermometry enables the reconstruction of a carbonate's formation temperature based on the abundance of isotopologues containing both ^{13}C and ^{18}O relative to a stochastic distribution (Eiler, 2011). This technique provides an independent measurement of temperature while measuring shell $\delta^{18}O$, thereby leaving seawater $\delta^{18}O$ as the only remaining variable in the aragonite-water oxygen isotope fractionation equation (Grossman and Ku, 1986).

I sampled eight *Cittarium pica* fossils from two localities of the Devonshire Marine Member of the Rocky Bay Formation: Grape Bay (GB) and Rocky Bay (RB). *C. pica* was

chosen as the targeted species because it lives for multiple years, is extant in Bermuda, and is common in MIS 5e deposits on the island. The species records true SSTs because it does not live deeper than 7 m in the water column and usually lives at the surface (Welch, 2010).

The Devonshire Marine Member consists of transgressive lag deposits that represents initial flooding of a high stand interval (Rowe and Bristow, 2015). Corals from GB Devonshire Marine deposits give U-Th ages of 113 – 126 ka (Muhs et al., 2002) and are correlated with RB Devonshire Marine deposits (~2 km northeast) via amino acid racemization geochronology and a U-Th age of 125 ± 4 ka (Hearty et al., 1992), as well as by stratigraphic interpretation (Vacher and Hearty, 1989). *C pica* is not known from Bermuda during glacial intervals and is thought to colonize the island at the very onset of interglacials (Olson and Hearty, 2013). To ensure my analytical approach would faithfully reproduce temperature and water compositional variation, I also obtained two *C. pica* gastropods collected live in Bermuda in 2011. I applied the clumped isotope paleothermometer to calculate individual water $\delta^{18}O$ values for all shells (Fig. 5.1). These individual water $\delta^{18}O$ measurements for each shell were then applied to submonthly-resolution $\delta^{18}O$ measurements made along each shell's growth axis via cross sections in order to produce SST timeseries spanning a portion of the life of each animal (Fig. 5.2). Individual SST time series therefore provide multi-year insight into local MIS 5e paleoclimate.

Evaluation of fossil material indicates excellent preservation and a lack of diagenetic alteration. This is based on visible shell microstructure and consistent stable isotope values that contrast with surrounding bulk rock material, which is 3 – 5 ‰ more negative in $\delta^{18}O$ and ~7 ‰ higher in $\delta^{13}C$ than fossil shells. Clear annual ranges between maximum and minimum temperatures (i.e., seasonality) in SST time series, 100% aragonitic composition via XRD, and consistent intra-locality reconstructed water $\delta^{18}O$ values and SSTs also suggest preservation of

original isotopic composition (Fig. 5.1). Moreover, possible undetected recrystallization would bias results towards warmer SSTs because diagenetic cements in Pleistocene rocks on Bermuda record ~17° – ~55° C clumped isotope temperatures (Defliese and Lohmann, 2016). This pattern is not observed in this data set.

I found excellent correspondence between the range of calculated SSTs for modern shells and modern SSTs from local NOAA buoy data, both in bulk samples and submonthly time series (Fig. 5.2). In contrast, all fossil shells record significantly colder temperatures than modern (mean annual SST is ~24° C); with calculated MIS 5e SSTs ranging between 8° and 27° C. Relative to modern, maximum and minimum SST are ~10° C lower for GB shells and ~3° C lower for RB shells. SST time series demonstrate essentially constant seasonality between modern (~11 °C), GB (~12 °C), and RB shells (~11 °C), further suggesting that these cold reconstructed SSTs accurately reflect MIS 5e conditions.

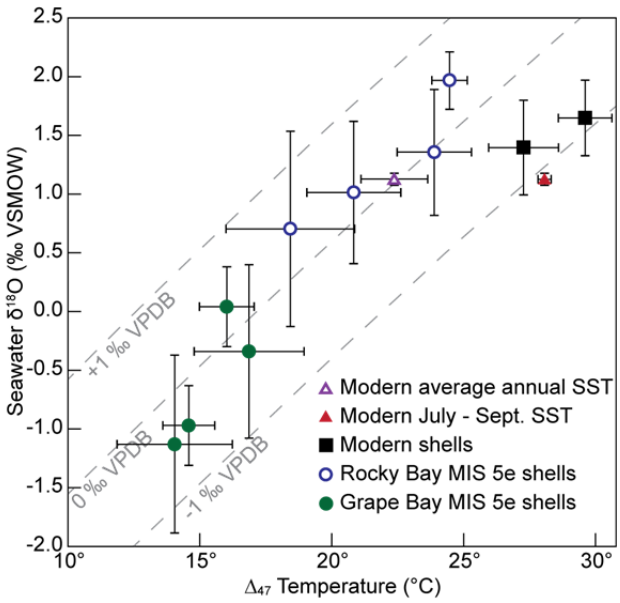

Figure 5.1. Bulk clumped isotope temperatures plotted against calculated water $\delta^{18}O$ (‰, VSMOW) for each shell. Dashed lines indicate carbonate $\delta^{18}O$ (‰, VPDB) values. Modern average annual and summer sea surface temperatures (SSTs; purple and red triangles) are from 2009 – 2011 NOAA buoy data. The range of modern water $\delta^{18}O$ values (purple and red triangles) is from the Global Seawater Oxygen-18 Database. Error bars indicate one standard error of the mean, based on four replicate measurements per fossil shell and six replicate measurements per modern shell.

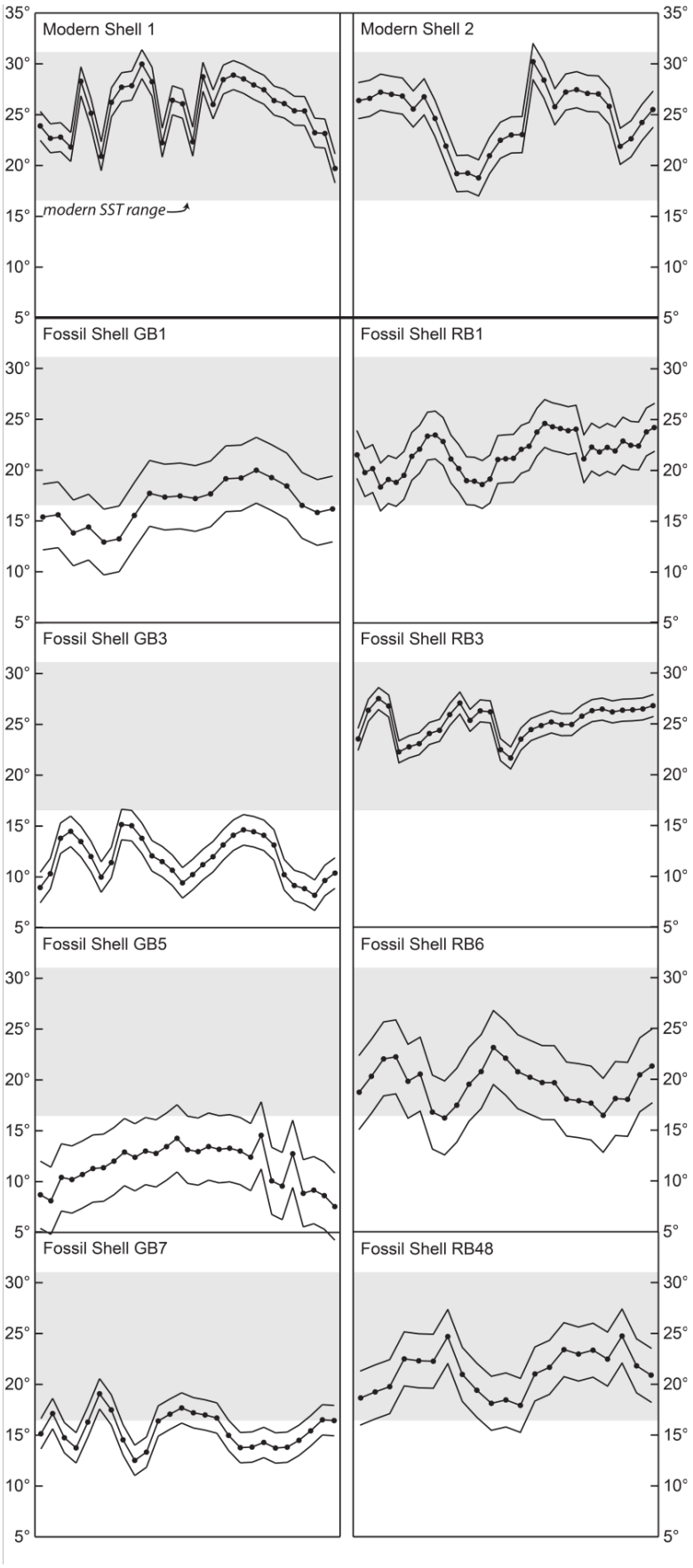

Figure 5.2. SST time series for each shell calculated from bulk clumped isotope-derived water $\delta^{18}O$ values and aragonite $\delta^{18}O$ measurements along each shell's growth axis. Horizontal axis is distance along each shell's main growth axis and is variable for each shell; youngest shell material is at right. Black lines indicate SST error based on one standard error for calculated water $\delta^{18}O$. Shaded regions indicate 2009 – 2011 SST range in Bermuda.

5.5 Cold Temperatures at Different Times Within the LIG

The relatively cold SSTs contrast with a fossil assemblage-based LIG climate reconstruction that found moderately warmer conditions relative to modern, a conclusion that was in part based on the presence of *C. pica* (assuming that the species required warmer temperatures) (Muhs et al., 2002). However, the SSTs I found, especially for the GB locality, are colder than anywhere that *C. pica* lives today (Olson and Hearty, 2013). This indicates that the modern temperature range of *C. pica* does not reflect its minimum temperature tolerance, at least in the past.

Inter-formational seawater $\delta^{18}O$ variability of > 2 ‰ VSMOW demonstrates the utility of clumped isotope thermometry to calculate local seawater $\delta^{18}O$ when applying carbonate $\delta^{18}O$ values to SST reconstruction. Shell $\delta^{18}O$ is relatively invariant across modern and fossil shells (Fig. 5.1), and thus using a constant modern seawater $\delta^{18}O$ value would have resulted in reconstructed SSTs similar to today and would not have captured the full temperature range observed. The range of water $\delta^{18}O$ values (-1.1 ± 0.8 ‰ to $+2.0 \pm 0.2$ ‰ VSMOW) illustrates the difficulty in interpreting SSTs based solely on carbonate $\delta^{18}O$. MIS 5e foraminifera $\delta^{18}O$ values around -1 ‰ VPDB from a core ~700 km northeast of Bermuda (MD95-2036; 34°N, 58°W) (Adkins et al., 1997), for example, could reflect SSTs of roughly 19° – 30° C given our seawater $\delta^{18}O$ range. This is a much wider range than would be calculated if only the modern seawater value was used (~25° C).

All of our results reveal colder than modern local conditions throughout MIS 5e. The significantly colder temperatures and lighter calculated water $\delta^{18}O$ recorded by GB shells relative to RB shells, however, suggest that these two locations are recording temperatures that are temporally distinct (Fig. 5.1). Although they have been stratigraphically correlated to each

other and ranges of radiometric dates from each site overlap, GB and RB deposits likely represent different phases of a single transgression or two separate LIG sea level high stands.

Two transgressions on Bermuda during the LIG would be consistent with large aeolian dune deposits on the Bermuda Platform (Rowe and Bristow, 2015) and global sea level reconstructions showing two sea level rise events separated by sea level fall within MIS 5e (Kopp et al., 2009). Based on geographic similarities, proximity of the GB and RB localities, and the absence of confounding factors such as rivers, local influences on SST can be eliminated. The inferred temperature difference between the two sites, therefore, indicates significantly different circulation patterns within the LIG, whether during a single or two transgressive phases. This is consistent with proxy data that suggest increased LIG climate instability relative to the Holocene (Fronval and Jansen, 1996). The different SST and water $\delta^{18}O$ conditions recorded by GB and RB shells ultimately suggests that separate paleoclimatic interpretations are required.

5.6 Gulf Stream Weakening During Sea Level Rise

Sudden massive meltwater pulses are known to have shutdown North Atlantic ocean circulation during the most recent deglaciation (Alley, 2007). During these events, icebergs drifted south of Bermuda's latitude and major freshening of waters as far south as Bermuda coincided with reduced meridional heat transport (Hill and Condron, 2014).

GB shells record remarkably consistent cold temperatures that are difficult to explain without the absence of warm Gulf Stream waters from the western North Atlantic. More critically, water $\delta^{18}O$ values from GB shells approximately match the deviation from modern (~2 ‰ VSMOW) expected for modeled salinity changes (-5 to -10 psu) for Bermuda during a melting event (Hill and Condron, 2014). These more negative water $\delta^{18}O$ values are almost

certainly reflective of ocean changes rather than local freshwater input, as fresh ground water volumes were minimal during sea level high stands (Defliese and Lohmann, 2016). Such large changes in water isotopic composition and SST require large changes in ocean circulation.

Just as occurred at the onset of the current interglacial, rapid warming at the onset of MIS 5e could have instigated rapid northern hemisphere ice sheet collapse and sea level rise (Kopp et al., 2009). A possible second MIS 5e sea level rise event due to retreat of the West Antarctic ice sheet may also be responsible (Hearty et al., 1992; Scherer et al., 1998; Dutton et al., 2015; Hansen et al., 2015), although the freshening of local waters seems to necessitate a northern source. Existing age data do not allow for differentiation between these hypotheses for GB shells. Our results nevertheless likely reflect major weakening of meridional heat transport at the onset of a LIG high stand.

5.7 An Enhanced MIS 5e North Atlantic Gyre?

In contrast, RB shells record similar to modern $\delta^{18}O$ water values and temperatures only slightly cooler than modern. This may conversely reflect a strengthened North Atlantic Gyre. When combined with warmer-than-modern temperatures reconstructed for the MIS 5e northern North Atlantic (Fig. 5.3), slightly cooler conditions in Bermuda are consistent with increased Gyre transport.

Notably, modern average annual SSTs in the eastern Atlantic at Bermuda's latitude are ~3° – 5 °C colder than in Bermuda (Fig. 5.3). If Gulf Stream transport were to be strengthened, enhancement of cool-water return flow via the diffuse Azores and Canary currents would result, thereby possibly supplanting the relatively stagnant warm pool in the Sargasso Sea today with cooler waters. This is consistent with the overall pattern of LIG SST proxy data, which shows

cooler tropics and a warm North Atlantic (Turney and Jones, 2010; Capron et al., 2014) (Fig. 5.3). $\delta^{13}C$ in the RB (and GB) shells is generally 2 – 4 ‰ higher relative to modern shells (Fig. 5.S3), which could also result from differences in water mass sourcing (Curry and Oppo, 2005).

These data are consistent, then, with enhanced North Atlantic Gyre transport during much of MIS 5e and also with Gyre weakening induced by rapid ice sheet collapse at the onset of the LIG. Regardless of implications for paleo-circulation patterns, however, our results indicate cold local conditions in Bermuda while sea levels were rising. They also demonstrate high sensitivity of local climate to global climate changes and imply that perturbations to Atlantic circulation via anthropogenic warming (Rahmstorf et al., 2015) could have dramatic local and regional climate effects.

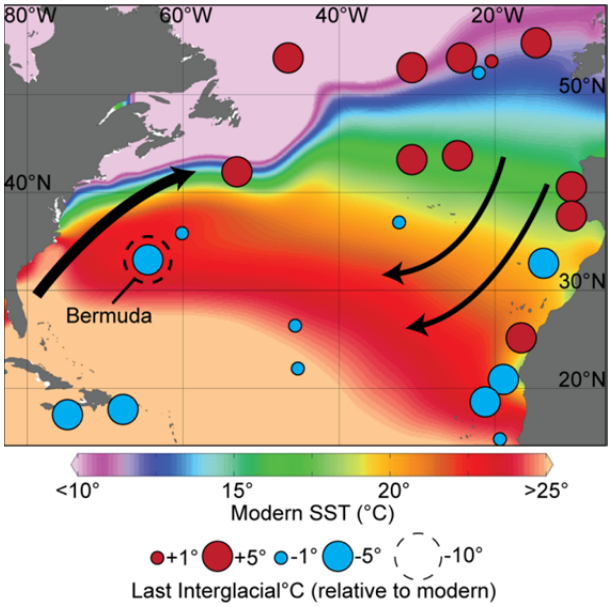

Figure 5.3. MIS 5e SST estimates from a variety of proxy sources, including this study. Arrows schematically indicate North Atlantic Gyre circulation. Ocean colors indicate modern average annual SST according to the 2009 World Ocean Atlas. Data from, and figure modified from, Turney and Jones (2010).

References

Adkins J. F., Boyle E. A., Keigwin L., Cortijo E., 1997. Variability of the North Atlantic thermohaline circulation during the last interglacial period. Nature 390, 154–156.

Alley R. B., 2007. Wally Was Right: Predictive Ability of the North Atlantic "Conveyor Belt" Hypothesis for Abrupt Climate Change. Annu. Rev. Earth Planet. Sci. 35, 241–272.

Böhm E., Lippold J., Gutjahr M., Frank M., Blaser P., Antz B., Fohlmeister J., Frank N., Andersen M. B. and Deininger M., 2015. Strong and deep Atlantic meridional overturning circulation during the last glacial cycle. Nature 517, 73–76.

Capron E., Govin A., Stone E. J., Masson-Delmotte V., Mulitza S., Otto-Bliesner B., Rasmussen T. L., Sime L. C., Waelbroeck C. and Wolff E. W., 2014. Temporal and spatial structure of multi-millennial temperature changes at high latitudes during the Last Interglacial. Quat. Sci. Rev. 103, 116–133.

Crowley T. J. and Kim K.-Y., 1994. Milankovitch forcing of the last interglacal sea level. Science 265, 1566–1568.

Curry W. B. and Oppo D. W., 2005. Glacial water mass geometry and the distribution of δ13C of ΣCO2 in the western Atlantic Ocean. Paleoceanography 20, 1–12.

Defliese W. F., Hren M. T., Lohmann K. C, 2015. Compositional and temperature effects of phosphoric acid fractionation on Δ47 analysis and implications for discrepant calibrations. Chem. Geol. 396, 51–60.

Defliese W. F. and Lohmann K. C., 2016. Evaluation of meteoric calcite cements as a proxy material for mass-47 clumped isotope thermometry. Geochim. Cosmochim. Acta 173, 126–141. Available at: http://dx.doi.org/10.1016/j.gca.2015.10.022.

Dennis K. J., Affek H. P., Passey B. H., Schrag D. P. and Eiler J. M., 2011. Defining an absolute reference frame for "clumped" isotope studies of CO2. Geochim. Cosmochim. Acta 75, 7117–7131.

Dutton A., Carlson A., Long A., Milne G., Clark P., DeConto R., Horton B., Rahmstorf S. and Raymo M., 2015. Sea-level rise due to polar ice-sheet mass loss during past warm periods. Science 349, doi: 153 aaa4019–1.

Eiler J. M., 2011. Paleoclimate reconstruction using carbonate clumped isotope thermometry. Quat. Sci. Rev. 30, 3575–3588. Fronval T. and Jansen E. 1996 Rapid changes in ocean circulation and heat flux in the Nordic seas during the last interglacial period. Nature 383, 806–810.

Grossman E. L. and Ku T.-L., 1986. Oxygen and carbon isotope fractionation in biogenic aragonite: temperature effects. Chem. Geol. 59, 59–74.

Hansen J., Sato M., Hearty P., Ruedy R., Kelley M., Masson-Delmotte V., Russell G., Tselioudis G., Cao J., Rignot E., Velicogna I., Kandiano E., von Schuckmann K., Kharecha P., Legrande a. N., Bauer M., Lo K.-W., 2015. Ice melt, sea level rise and superstorms: evidence from paleoclimate data, climate modeling, and modern observations that 2 °C global warming is highly dangerous. Atmos. Chem. Phys. Discuss. 15, 20059–20179.

Hearty P. J., Vacher H. L. and Mitterer R. M., 1992. Aminostratigraphy and ages of Pleistocene limestones of Bermuda. Geol. Soc. Am. Bull. 104, 471–480.

Hill J. C. and Condron A., 2014. Subtropical iceberg scours and meltwater routing in the deglacial western North Atlantic. Nat. Geosci. 7, 806–810.

Kim S., Mucci A. and Taylor B. E., 2007. Phosphoric acid fractionation factors for calcite and aragonite between 25 and 75 ° C : Revisited. Chem. Geol. 246, 135–146.

Kopp R. E., Simons F. J., Mitrovica J. X., Maloof A. C. and Oppenheimer M., 2009. Probabilistic assessment of sea level during the last interglacial stage. Nature 462, 863–867.

Lisiecki L. E. and Raymo M. E., 2005. A Pliocene-Pleistocene stack of 57 globally distributed benthic δ^{18}O records. Paleoceanography 20.

Muhs D. R., Simmons K. R. and Steinke B., 2002. Timing and warmth of the Last Interglacial period: New U-series evidence from Hawaii and Bermuda and a new fossil compilation for North America. Quat. Sci. Rev. 21, 1355–1383.

Olson S. L. and Hearty P. J., 2013. Periodicity of extinction and recolonization of the West Indian topshell Cittarium pica in the Quaternary of Bermuda Gastropoda : Trochoidea . Biol. J. Linn. Soc. 110, 235–243.

Otto-Bliesner B. L., 2006. Simulating Arctic Climate Warmth and Icefield Retreat in the Last Interglaciation. Science 311, 1751–1753.

Palter J. B., 2015. The role of the gulf stream in European climate. Ann. Rev. Mar. Sci. 7, 113–37.

Petersen S. V., Winkelstern I. Z., Lohmann K. C. and Meyer K. W., 2015. The effects of PorapakTM trap temperature on d18O, d13C, and D47 values in preparing samples for clumped isotope analysis. Rapid Commun. Mass Spectrom. 30, 1–10.

Rahmstorf S., 2002. Ocean circulation and climate during the past 120,000 years. Nature 419, 207–214.

Rahmstorf S., Box J. E., Feulner G., Mann M. E., Robinson A., Rutherford S. and Schaffernicht E. J., 2015. Exceptional twentieth-century slowdown in Atlantic Ocean overturning circulation. Nat. Clim. Chang. 5, 475–480.

Rowe M. P. and Bristow C. S., 2015. Sea-level controls on carbonate beaches and coastal dunes eolianite: Lessons from Pleistocene Bermuda. Geol. Soc. Am. Bull. 127, 1645–1665.

Scherer R. P., Aldahan A., Tulaczyk S., Engelhardt H. and Kamb B., 1998. Pleistocene Collapse of the West Antarctic Ice Sheet. Science 281, 82–85.

Steinberg D. K., Carlson C. a., Bates N. R., Johnson R. J., Michaels A. F. and Knap A. H., 2001. Overview of the US JGOFS Bermuda Atlantic Time-series Study BATS: A decade-scale look at ocean biology and biogeochemistry. Deep. Res. Part II Top. Stud. Oceanogr. 48, 1405–1447.

Turney C. S. M. and Jones R. T. 2010 Does the Agulhas Current amplify global temperatures during super-interglacials? J. Quat. Sci. 25, 839–843.

Vacher H. L. and Hearty P., 1989. History of stage 5 sea level in Bermuda: Review with new evidence of a brief rise to present sea level during Substage 5a. Quat. Sci. Rev. 8, 159–168.

Welch J. J., 2010. The "Island Rule" and Deep-Sea Gastropods : Re- Examining the Evidence. PLoS One 5.

Appendix 5.1 Materials And Methods

All fossil samples were taken from < 1 m of sedimentary section within the upper portion of the < 2 m thick Devonshire Marine member. Modern shells were collected live under permit in 2011 near Cooper's Island, Bermuda by Dr. Mark Outerbridge of the Bermuda Department of Conservation Services. 100% aragonitic composition was determined using a Rigaku XRD in the Michigan Electron Microprobe Analysis Laboratory.

Carbonate samples were measured for their stable and clumped isotopic composition at the University of Michigan Stable Isotope Laboratory. For clumped isotopes, ~20 mg of carbonate was sampled by chipping off the youngest end of a shell and powdering via mortar and pestle. The clumped isotope value of each sample (Δ_{47} in the absolute reference frame; see ref. 25) was replicated at least four times, with a minimum of 4 mg used for each measurement.

CO_2 was extracted from each carbonate sample using an offline sample preparation procedure (see Defliese et al., 2015, for additional details). Each aliquot was reacted individually in anhydrous phosphoric acid in a common acid bath at 75° C for 15 – 20 minutes (until completion). Residual water vapor was removed from resultant CO_2 via cryogenic distillation under vacuum conditions. To eliminate hydrocarbon and halocarbon contaminants, gas was passed through Porapak^{TM} resin held at -30° C for 15 minutes (shells RB1, RB3, and RB6) or at -15° C for 10 minutes (all other shells). Clumped isotope $\delta^{18}O$ values for those run at -30°C were corrected by +0.36 ‰ according to (Petersen et al., 2015). Replicates from modern shells were run under each Porapak temperature and time state, with no consistent $\delta^{18}O$ offset after correction.

CO_2 was measured on a Thermo Scientific MAT 253 Stable Isotope Ratio Mass Spectrometer configured for Δ_{47} analysis, where masses 44 through 49 were measured for 60-80 cycles. Heated CO_2 with stochastic isotopologue distributions and CO_2 equilibrated with water at 25° C were used to monitor machine conditions and establish the absolute reference frame. Final clumped isotope values incorporate an acid fractionation factor of 0.067‰ for a 75°C reaction temperature (Defliese et al., 2015). Temperature interpretations for Δ_{47} values were made using the >75° C acid compiled calibration of Defliese et al. (2015) because it it is based on compiled data from several calibration studies, and because it incorporates data measured on the same apparatus as these samples, thereby reducing the impacts of any unaccounted for laboratory-specific effects.

All clumped $\delta^{18}O$ values were corrected for acid fractionation as in Kim et al. (2007) and the isotopic composition of the water from which the shells precipitated was calculated using the fractionation factor of Grossman and Ku (1986). All carbonate $\delta^{18}O$ and $\delta^{13}C$ values are reported

relative to the Vienna Pee Dee Belemnite standard (VPDB), and all $\delta^{18}O$ water values are reported relative to the Vienna Standard Mean Ocean Water standard (VSMOW). Powders for high resolution $\delta^{18}O$ and $\delta^{13}C$ measurements were sampled from cut ~0.5 cm thick shell sections using a Micromill computerized sampling device. These were then measured using a Kiel IV automated preparation device coupled to a Thermo Scientific MAT 253 mass spectrometer (with analytical precision better than 0.1 ‰).

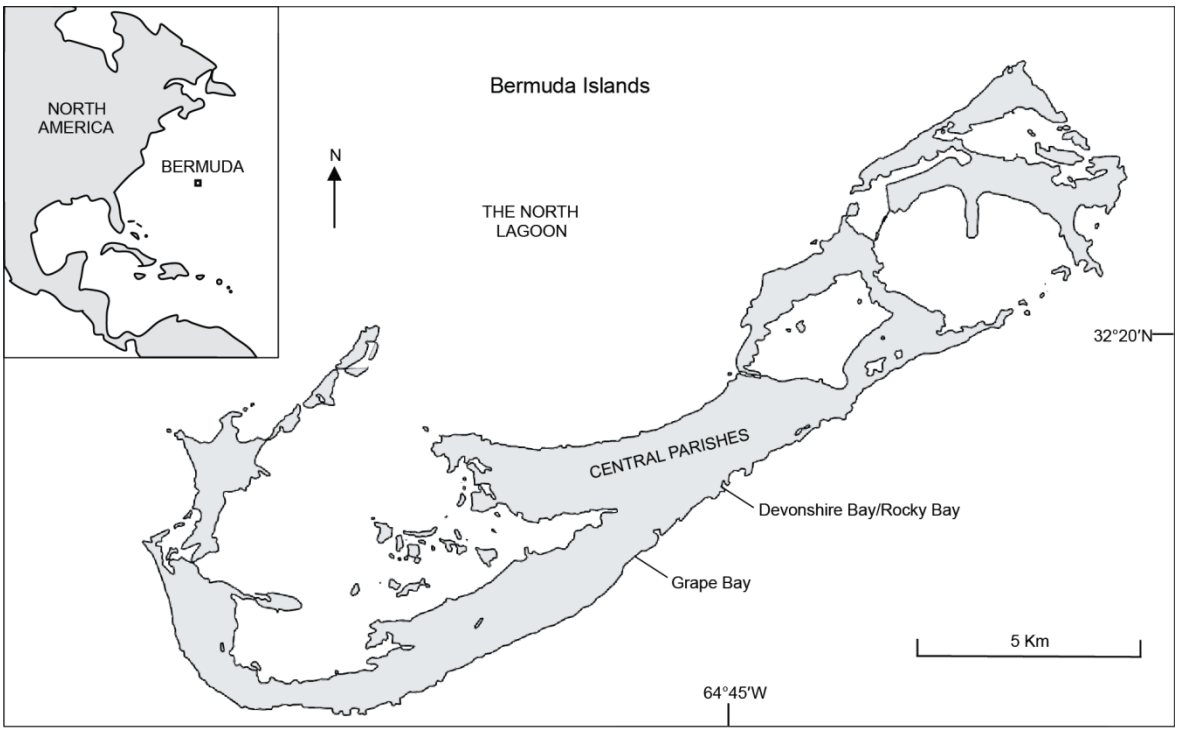

Figure 5.S1. Map of Bermuda indicating sampling locations. Modified from Rowe and Bristow (2015).

Figure 5.S2. Field photo from Rocky Bay showing MIS 5e transgressive Devonshire Marine member of the Rocky Bay Formation erosively overlying the MIS 7 Belmont Formation (at bottom), as indicated by rip-up clasts of the Belmont incorporated above the contact.

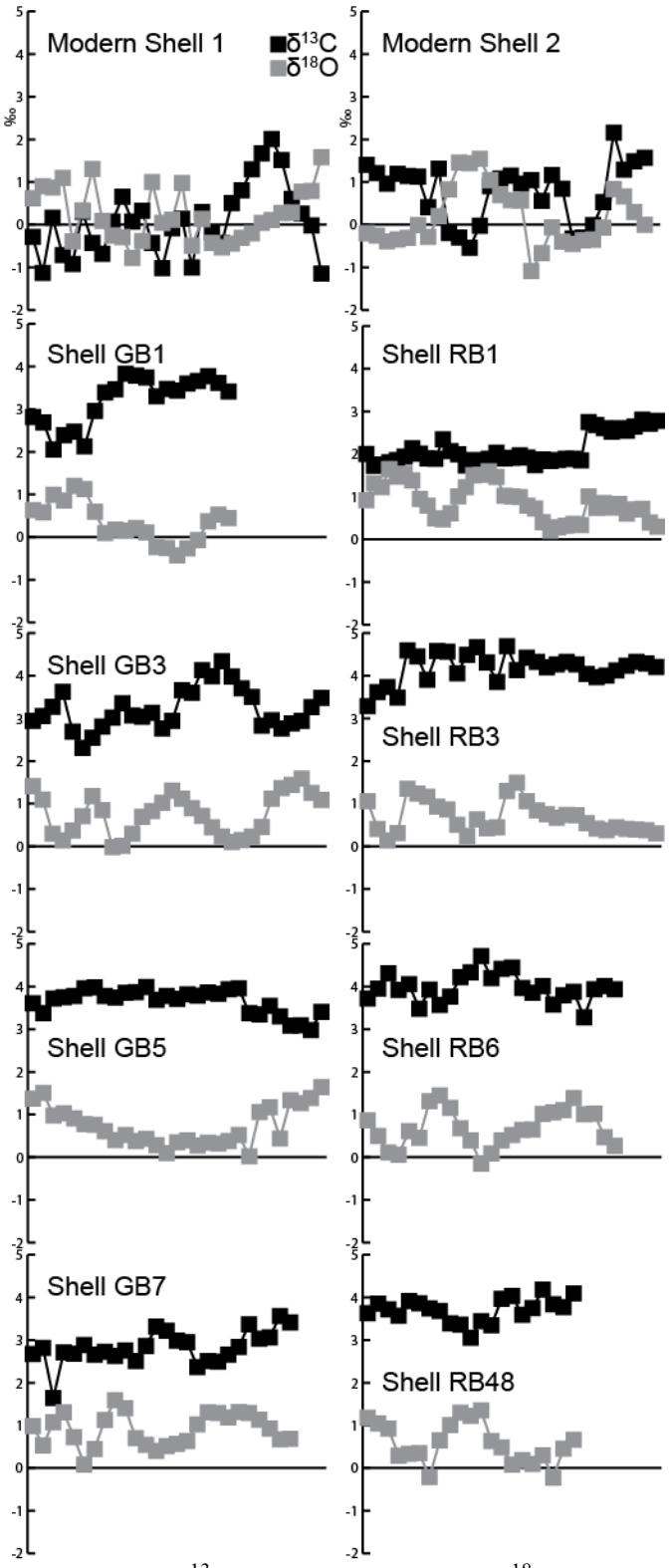

Figure 5.S3. $\delta^{13}C$ (black squares) and $\delta^{18}O$ (grey squares) data relative to VPDB for each shell. Vertical axis is in per mille, horizontal axis is distance along each shell's main growth axis and is variable for each shell. $\delta^{13}C$ in the GB and RB shells is generally 2 – 4 ‰ higher relative to modern shells, which could result from differences in water mass sourcing.

Table 5.S1. Clumped isotope measurments for each shell.

Shell	Δ^{47} (‰ ARF)[1]	Δ^{47} °C[2]	$\delta^{18}O_{H2O}$[3] (‰ VSMOW)
Modern1	0.6824 ± 0.0047	30.0° ± 1.0°	+1.7 ± 0.3
Modern2	0.6889 ± 0.0062	27.7° ± 1.3°	+1.5 ± 0.4
GB1	0.7192 ± 0.0102	17.3° ± 2.1°	-0.3 ± 0.7
GB3	0.7257 ± 0.0051	15.0° ± 1.0°	-0.9 ± 0.3
GB5	0.7280 ± 0.0110	14.5° ± 2.2°	-1.0 ± 0.8
GB7	0.7212 ± 0.0052	16.4° ± 1.1°	+0.1 ± 0.3
RB1	0.6982 ± 0.0068	24.3° ± 1.4°	+1.4 ± 0.5
RB3	0.6963 ± 0.0032	24.9° ± 0.7°	+2.1 ± 0.2
RB6	0.7150 ± 0.0119	18.8° ± 2.5°	+0.8 ± 0.8
RB48	0.7074 ± 0.0086	21.3° ± 1.8°	+1.1 ± 0.6

[1]Δ_{47} values are reported in the absolute reference frame of Dennis et al. (2011).
[2]Δ_{47} temperatures use the Defliese et al. (2015) calibration.
[3]Water $\delta^{18}O$ calculated from clumped isotope temperatures and carbonate $\delta^{18}O$, via the fractionation factor of Grossman and Ku (1986). All errors are one standard error of the mean.

Chapter 6

Summary and Conclusions

6.1 The Problems and Promise of Clumped Isotope Thermometry

This dissertation demonstrates the potential of clumped isotope thermometry to help solve longstanding diagenetic and paleoclimatic questions. It also shows that, in many geologic settings, original clumped isotope compositions may not be preserved. Much of the scientific interest in clumped isotope thermometry during its first few years was driven by the possibility of obtaining paleotemperatures from Paleozoic and even older rocks (e.g., Finnegan et al. 2011). I have shown here that obtaining 'deep time' paleoclimate data will be challenging, but also that the technique shows great promise for answering more geologically recent paleoclimatic questions.

In Chapter 2, for example, I demonstrated that carbonate clumped isotope compositions can be altered at relatively shallow burial depths (~1.3 km) and at remarkably cool geothermal conditions (~45° C). These results show that precautions must be taken in the use of other fine grained carbonates (e.g., lake micrites and soil nodules) for clumped isotope paleothermometry. This study also found that clumped isotope compositions in dolomite are not more resilient to diagenetic alteration than corresponding calcites. No significant difference in clumped isotope composition was found between dolomites and calcites thought to have formed at the same temperature.

These results inspired Chapter 3, which conclusively demonstrated that calcite and dolomite clumped isotope temperature calibrations are statistically indistinguishable. My results also suggest that the dolomite-specific acid fractionation shown by Murray et al. (2016) does not exist in all laboratories. These results are a clear example of lingering interlaboratory methodology issues facing clumped isotope thermometry, but they also lay the groundwork for many more studies utilizing dolomite as a paleotemperature resource.

Chapter 4 applied clumped isotopes as a part of a broad petrologic and geochemical study seeking to understand the diagenetic evolution of a Midwestern Silurian carbonate bioherm. Petrographic observations clearly bracket dolomite formation within a meteoric diagenetic system, and conventional isotope data support the idea that minor dolomitization of the Pipe Creek Junior complex was due to the mixing of fresh and saline waters. Clumped isotopes and fluid inclusion measurements show that, long after dolomitization, hot saline brines passed through the complex and likely altered the clumped isotope composition of the dolomites and original marine calcites. These waters also precipitated a calcite spar. Calculated water $\delta^{18}O$ values from this spar are consistent with brines in the Michigan Basin, and this event likely impacted Paleozoic sediments across the region.

The promise of clumped isotope thermometry as a paleoclimate indicator is clear in the results of Chapter 5, where I found Last Interglacial sea surface temperatures in Bermuda that were much colder than today. When combined with water $\delta^{18}O$ measurements that indicate reduced salinities, these results (from one locality, at least) are indicative of a large meltwater pulse in the North Atlantic. An important element of these data is that all shells, including modern, have similar carbonate $\delta^{18}O$ values. This means that if the clumped isotope thermometer had not been applied, calculated temperatures (using an assumed or modeled water $\delta^{18}O$ value)

would have been similar to modern. Instead, the application of clumped isotope thermometry here revealed a rapid climate change event.

6.2 Outlook for the Future

Clumped isotope thermometry is almost certainly the most important analytical development in carbonate geochemistry in more than six decades. The next few years will be an especially exciting time to be working in the field, as the number of laboratories coming online is increasing exponentially. Like any emergent technique, many analytical questions remain. Foremost among them is an unresolved discrepancy between the 'steep slope' temperature calibrations obtained by a few laboratories (e.g., Ghosh et al., 2006) and the 'shallow slope' temperature calibrations obtained by most others (e.g., Dennis and Schrag, 2010).

Other questions stem from the research presented here. The models and experimental data of Passey and Henkes (2012) and Stolper and Eiler (2015) essentially suggest that pristine carbonates never exposed to burial temperatures exceeding ~100° C should preserve original clumped isotope compositions over hundreds of millions of years. My data in Chapter 2 and Chapter 4 at least raise the possibility that solid state reordering can occur at much lower temperatures. Although recrystallization cannot be ruled out in either case, future detailed work on a range of diagenetic environments could place even better empirical constraints on when and how clumped isotope compositions are altered. These projects were among the first clumped isotope studies to specifically examine altered carbonates, and analyses from a diverse range of other diagenetic environments can refine the exact conditions of alteration.

Similarly, investigation into analytical and diagenetic effects specific to dolomite clumped isotope thermometry has only just begun. On the analytical side, apparent dolomite acid

fractionation differences between the results of Murray et al. (2016) and Defliese et al. (2015) remain entirely unresolved. Solving this interlaboratory discrepancy will likely require sample exchange and collaboration. More broadly, statistically identical calcite and dolomite calibrations mean that a wide array of dolomite-forming systems can now be reassessed with temperature constraints provided by clumped isotopes. The origin of much of Earth's dolomite is poorly understood, but the results of Chapter 2 show that many Cenozoic dolomites should preserve original formation temperatures and permit measurement of formation water $\delta^{18}O$. If applied widely, these geochemical constraints may be sufficient to answer longstanding questions about how this common mineral forms.

Finally, from a paleoclimate application perspective, my Last Interglacial study results from Bermuda indicate short term but dramatic shifts in ocean circulation and temperature. The effect of a large freshwater pulse entering the North Atlantic would undoubtedly affect climate across the basin, and future work could geographically expand my approach. Coeval transgressive deposits exist in eastern North America, Western Europe, and on other islands, and these could also be targeted for clumped isotope paleotemperature evaluation. Temporary shutdown or reductions in strength of the Gulf Stream would be expected to cool much of the North Atlantic while perhaps warming the tropics, and this hypothesis could be further tested.

A related question is whether melting of the Greenland ice sheet can cause similarly dramatic climate effects in the near future. Because clumped isotope thermometry enables direct measurement of the changes in seawater $\delta^{18}O$ that occur when ice sheets collapse, future work could perhaps more closely examine the conditions under which such events occur. Even if diagenetic issues mean the promise of deep-time clumped isotope paleoclimatology cannot be

fully realized, the technique will still play an integral role in enhancing knowledge about key paleoclimatic intervals for decades to come.

References

Defliese, W.F., Hren, M.T., Lohmann, K.C., 2015. Compositional and temperature effects of phosphoric acid fractionation on Δ_{47} analysis and implications for discrepant calibrations. Chemical Geology 396, 51-60.

Dennis, K.J., Schrag, D.P., 2010. Clumped isotope thermometry of carbonatites as an indicator of diagenetic alteration. Geochimica et Cosmochimica Acta 74, 4110-4122.

Finnegan, S. Bergmann, K., Eiler, J.M., Jones, D. S., Fike, D.A., Eisenman, I., Hughes, N. C., Tripati, A. K., Fischer, W. W., 2011. The Magnitude and Duration of Late Ordovician-Early Silurian Glaciation. Science 331, 903-906.

Ghosh, P., Adkins, J., Affek, H., Balta, B., Guo, W., Schauble, E. A., Schrag, D., and Eiler, J. M., 2006. 13C-18O bonds in carbonate minerals. A new kind of paleothermometer: Geochimica et Cosmochimica Acta 70, 1439–1456, doi:10.1016/j.gca.2005.11.014.

Murray, S.T., Arienzo, M.M., Swart, P.K., 2016. Determining the Δ_{47} acid fractionation in dolomites. Geochimica et Cosmochimica Acta 174, 42-53.

Passey, B. H., and Henkes, G. A., 2012. Carbonate clumped isotope bond reordering and geospeedometry. Earth and Planetary Science Letters 351, 223–236, doi:10.1016/j.epsl.2012.07.021.

Stolper, D. A., and Eiler, J. M., 2015. The kinetics of solid-state isotope-exchange reactions for clumped isotopes. A study of inorganic calcites and apatites from natural and experimental samples: American Journal of Science 315, 363-411, doi: 10.2475/05.2015.01.

Appendix 6.1 Raw Clumped Isotope Data

Raw data used to place clumped isotope data in the absolute reference frame is provided below.

Chapter 2 Raw Data

JUNE 2015 RUN

Samples:

Date	Name	d13C	d18O	d45	d46	d47	d48	D47	D48	window	D47rfac
6/15	AC33d-1	2.38	43.71	5.979	8.435	14.405	17.865	-0.108	0.908	1	0.704
6/15	AC33d-2	2.30	43.40	5.896	8.142	14.035	16.667	-0.102	0.312	1	0.717
6/30	AC33d-3	2.29	43.26	5.877	8.001	13.9	17.588	-0.078	1.497	3	0.722

Transfer Functions:

Window	Start date	end date	SlopeEGL	SlopeETF	IntETF
1	6/12/2015	06/17/15	0.01894	1.039	1.032
2	6/18/2015	06/26/15	0.02128	1.103	1.071
3	6/25/2015	06/29/15	0.02210	1.088	1.074

D47rfac = value with reference frame and acid fractionation

Equilibrated and Heated Gasses:

DATE	Name	d13C	d18O	d45	d46	d47	d48	D47	D48
6/12/2015	MDlWHG	-41.03	30.67	-35.197	-4.240	-42.07	-9.848	-1.833	-1.398
6/12/2015	CarraraHG	1.91	35.37	5.272	0.389	4.987	-1.516	-0.829	-2.292
6/12/2015	EvapHG	-41.22	41.84	-35.015	6.546	-31.44	12.113	-1.576	-1.01
6/13/2015	2xEVHG	-40.93	58.25	-34.216	22.383	-15.29	48.543	-1.241	3.135
6/15/2015	OoidsHG	4.33	31.43	7.415	-3.415	3.393	-6.361	-0.863	0.46
6/16/2015	MDlWHG	-40.92	26.44	-35.229	-8.322	-46	-22.09	-1.861	-5.603
6/12/2015	Heavy25C	4.75	70.96	9.069	34.745	44.632	79.739	0.755	8.445
6/12/2015	MDlW25C	-41.42	30.34	-35.568	-4.558	-41.86	-11.58	-0.896	-2.508
6/13/2015	Evap25C	-41.36	46.03	-35.009	10.582	-26.61	27.543	-0.544	6.135
6/13/2015	2XEV25C	-41.30	72.96	-34.093	36.575	-0.608	84.294	-0.126	9.126
6/14/2015	Heavy25C	4.78	73.43	9.178	37.127	47.077	84.074	0.719	7.848
6/16/2015	MDlW25C	-41.56	29.88	-35.717	-5.005	-42.46	-13.24	-0.920	-3.291
6/17/2015	Evap25C	-41.76	46.20	-35.377	10.745	-26.88	23.939	-0.593	2.283
6/18/2015	2xEVHG	-41.00	53.15	-34.449	17.460	-20.32	37.821	-1.371	2.509
6/19/2015	CarraraHG	2.30	30.46	5.481	-4.355	0.445	-13.1	-0.896	-4.45
6/20/2015	EvapHG	-40.73	41.73	-34.558	6.436	-31.13	12.276	-1.638	-0.63
6/23/2015	EvapHG	-40.99	44.92	-34.696	9.516	-28.3	19.749	-1.577	0.614
6/23/2015	CarraraHG	2.21	37.21	5.607	2.163	7.123	1.922	-0.792	-2.397
6/24/2015	2xEVHG	-41.04	68.37	-33.992	32.152	-5.666	75.201	-1.104	9.258
6/25/2015	OoidsHG	4.23	33.50	7.386	-1.416	5.413	-2.735	-0.794	0.095
6/18/2015	2xEV25C	-41.37	73.02	-34.161	36.635	-0.627	84.626	-0.129	9.317
6/20/2015	Heavy25C	4.75	71.40	9.088	35.172	45.113	81.335	0.790	9.102
6/20/2015	MDlW25C	-41.44	30.58	-35.581	-4.331	-41.78	-12.63	-1.029	-4.026
6/23/2015	Evap25C	-41.46	47.83	-35.046	12.327	-25.08	27.061	-0.628	2.2
6/24/2015	MDlW25C	-41.46	30.71	-35.595	-4.204	-41.68	-12.14	-1.031	-3.784
6/24/2015	2xEV25C	-41.32	71.55	-34.16	35.214	-2.017	83.033	-0.174	10.605
6/25/2015	Evap25C	-41.59	46.48	-35.215	11.016	-26.56	24.323	-0.695	2.122
6/26/2015	Heavy25C	4.94	74.56	9.363	38.220	48.551	90.61	0.900	11.79
6/25/2015	OoidsHG	4.23	33.50	7.386	-1.416	5.413	-2.735	-0.794	0.095
6/27/2015	EvapHG	-41.26	42.89	-35.013	7.551	-30.56	15.535	-1.649	0.37
6/28/2015	MDlWHG	-40.94	29.10	-35.162	-5.753	-43.6	-16.58	-1.969	-5.164
6/29/2015	CarraraHG	2.12	35.55	5.475	0.561	5.356	-1.341	-0.840	-2.461
6/25/2015	Evap25C	-41.59	46.48	-35.215	11.016	-26.56	24.323	-0.695	2.122
6/26/2015	Heavy25C	4.94	74.56	9.363	38.220	48.551	90.61	0.900	11.79
6/27/2015	MDlW25C	-41.54	30.27	-35.691	-4.625	-42.22	-13.49	-1.078	-4.303
6/29/2015	2xEV25C	-41.34	70.04	-34.23	33.762	-3.502	79.666	-0.209	10.295
6/29/2015	Evap25C	-41.76	46.18	-35.379	10.730	-27.03	24.386	-0.724	2.751

JANUARY 2015 RUN

Samples:

Date	Sample Name	d13C (pdb)	d18O (smow)	d45	d46	d47	d48	D47	D48	window	D47rfac
1/28	AC6 cal #3 IZW	1.66	35.98	5.05	0.973	5.936	1.848	-0.232	-0.098	1	0.663
1/30	AC29 cal #1 IZW	-0.51	36.74	3.042	1.707	4.566	5.394	-0.255	1.969	1	0.675
1/30	AC37 cal #1 IZW	2.04	39.20	5.519	4.084	9.595	13.578	-0.136	5.348	1	0.668
2/1	AC23 cal #1 IZW	2.53	38.83	5.961	3.729	9.737	12.853	-0.1	5.342	1	0.704
2/1	AC29 cal #2 IZW	-0.26	37.36	3.296	2.306	5.476	3.449	-0.198	-1.163	1	0.713
2/1	AC37 cal #2 IZW	1.87	39.24	5.358	4.125	9.494	7.362	-0.111	-0.898	1	0.698
2/2	AC5 dolo #1 IZW	0.86	41.35	4.478	6.153	10.47	27.19	-0.227	14.664	1	0.544
2/3	AC37 cal #3 IZW	2.02	39.11	5.495	3.997	9.501	6.698	-0.119	-1.301	1	0.689
2/3	AC 23 cal #2 IZW	2.82	40.33	6.283	5.176	11.573	10.215	-0.031	-0.162	1	0.729
2/7	AC5 dolo #2 IZW	1.05	40.73	4.637	5.556	10.079	16.703	-0.193	5.499	2	0.593
2/7	AC29 cal #3 IZW	-0.27	37.51	3.293	2.449	5.595	5.328	-0.218	0.421	2	0.693
2/9	AC5 dolo #3 IZW	1.02	41.02	4.617	5.841	10.387	17.277	-0.146	5.496	2	0.636
2/10	AC23 cal #3 IZW	2.46	38.74	5.892	3.638	9.55	14.675	-0.125	7.332	2	0.683
2/12	AC5 dolo #4 IZW	0.98	40.98	4.575	5.803	10.296	21.511	-0.156	9.758	3	0.625
2/13	AC37 cal #4 IZW	2.05	39.06	5.522	3.949	9.494	6.821	-0.106	-1.084	3	0.704
2/13	AC23 cal #4 IZW	2.58	38.89	6.012	3.785	9.828	16.832	-0.117	9.178	3	0.682

Transfer Functions:

Window	Start date	end date	SlopeEGL	SlopeETF	IntETF
1	1/26/2015	2/3/2015	0.02503	1.100	1.015
2	2/4/2015	2/11/2015	0.02581	1.096	1.023
3	2/12/2015	2/21/2015	0.02658	1.109	1.035

Equilibrated and Heated Gasses:

DATE	Name	d13C	d18O	d45	d46	d47	d48	D47	D48
26-Jan	MDlWHG	-41.36	25.22	-47.792	-25.590	7.945	-2.094	-6.812	67.592
26-Jan	CarraraHG1	2.06	35.21	5.057	-3.896	3.459	-0.743	-4.354	-2.737
26-Jan	CarraraHG2	2.11	35.17	5.066	-2.204	2.236	-0.751	-2.601	-3.942
26-Jan	2xEVHG1	-41.15	63.47	-10.447	63.008	1.107	-1.134	7.018	-14.78
27-Jan	2xEVHG2	-41.35	63.24	-10.897	65.083	0.295	-1.161	9.424	-14.94
28-Jan	EvapHG	-41.07	35.47	-37.556	-2.789	8.741	-1.817	-3.568	47.079
29-Jan	CarraraHG	2.13	37.04	6.921	2.405	3.033	-0.758	-1.601	-6.756
31-Jan	MDlWHG	-41.26	26.66	-46.322	-22.814	6.912	-2.081	-6.774	63.395
1-Feb	2xEVHG	-41.31	61.93	-12.17	59.389	3.808	-1.228	6.518	-9.07
2-Feb	OoidsHG	4.54	37.03	9.348	2.105	3.937	-0.662	-1.889	-8.225
3-Feb	MDlWHG	-41.21	28.94	-44.079	-17.453	6.959	-2.031	-5.729	58.699
27-Jan	Evap25C	-41.26	47.36	-25.409	25.022	3.606	-0.709	1.119	18.429
27-Jan	MDlW25C1	-41.38	30.55	-41.839	-16.860	8.831	-1.112	-8.233	57.543
27-Jan	2xEV25C1	-41.32	70.39	-3.068	81.246	-4.199	-0.134	11.113	-32.46
27-Jan	MDlW25C2	-41.49	29.87	-42.58	-14.297	6.061	-1.108	-4.337	56.146
27-Jan	2xEV25C2	-41.31	70.51	-2.996	82.182	-0.903	-0.175	11.767	-29.47
28-Jan	2xEV25C	-41.47	70.13	-3.505	82.290	-0.306	-0.174	12.579	-28.05
30-Jan	Evap25C	-41.30	47.21	-25.614	26.272	4.745	-0.734	2.627	19.919
31-Jan	MDlW25C	-41.40	30.65	-41.778	-12.907	7.356	-1.137	-4.451	55.797
1-Feb	2xEV25C	-41.30	70.53	-2.986	81.675	-0.323	-0.193	11.260	-28.95
2-Feb	MDlW25C	-41.36	30.03	-42.336	-14.116	6.682	-1.145	-4.472	56.321
4-Feb	CarraraHG	1.96	37.57	7.299	2.012	3.581	-0.738	-3.002	-7.055
4-Feb	CarraraHG	2.15	37.74	7.68	1.125	9.065	-0.704	-4.206	-2.138
7-Feb	EvapHG	-41.21	43.68	-29.79	17.667	2.992	-1.688	0.938	24.928
8-Feb	2xEVHG	-41.36	66.82	-7.42	74.362	-0.763	-1.064	11.403	-22.57
9-Feb	CarraraHG	2.05	38.09	7.942	0.387	7.342	-0.696	-5.617	-4.423
11-Feb	OoidsHG	4.53	38.09	10.426	1.154	7.736	-0.622	-4.863	-6.489
11-Feb	2XEVHG	-41.19	67.27	-6.896	72.911	8.161	-1.139	9.190	-14.84
4-Feb	Evap25C	-41.37	46.87	-26.008	24.686	4.814	-0.738	1.714	20.719
5-Feb	2xEV25C	-41.36	70.46	-3.078	82.456	0.418	-0.161	12.124	-28.04
8-Feb	MDlW25C	-41.37	30.69	-41.76	-11.458	7.337	-1.186	-3.070	55.661
9-Feb	Evap25C	-41.18	47.35	-25.398	25.331	6.956	-0.768	1.434	21.76
10-Feb	2xEV25C	-41.26	71.06	-2.404	83.858	-0.191	-0.165	12.287	-29.84
11-Feb	MDlW25C	-41.29	30.76	-41.567	-15.978	14.365	-1.136	-7.758	62.796

12-Feb	MDIWHG	-41.41	29.33	-43.958	-17.178	7.756	-2.094	-6.212	58.945
13-Feb	CarraraHG	2.06	37.38	7.232	2.583	1.837	-0.716	-2.072	-8.519
15-Feb	EVAPHG	-41.31	44.64	-28.954	15.011	12.547	-1.658	-3.508	32.902
16-Feb	CarraraHG	2.08	36.76	6.632	1.293	3.044	-0.712	-2.153	-6.141
18-Feb	2XEVHG	-41.27	62.95	-11.141	62.736	3.499	-1.202	7.755	-11.32
19-Feb	CarraraHG	2.00	37.56	7.331	3.530	2.084	-0.732	-1.473	-8.554
21-Feb	OoidsHG	4.61	37.78	10.172	3.526	3.387	-0.649	-1.913	-10.27
12-Feb	Evap25C	-41.31	71.54	-1.988	85.129	0.895	-0.158	12.563	-29.61
12-Feb	2xEV25C	-41.46	70.66	-2.997	83.409	0.568	-0.175	12.631	-28.17
14-Feb	MDIW25C	-41.29	30.19	-42.177	-15.417	8.711	-1.208	-6.098	58.041
15-Feb	Evap25C	-41.38	46.96	-25.962	26.593	3.13	-0.774	3.411	18.839
16-Feb	2xEV25C	-41.12	70.33	-2.978	81.657	2.933	-0.184	11.614	-25.62
19-Feb	EVAP25C	-41.41	46.65	-26.264	25.650	2.064	-0.748	3.085	18.397
20-Feb	MDIW25C	-41.24	31.03	-41.367	-11.976	6.898	-1.248	-4.243	54.36
21-Feb	2xEV25C	-41.28	71.43	-2.079	83.981	2.622	-0.169	11.707	-27.76

SEPTEMBER 2014 RUN

Samples:

Date	Sample	d13C	d18O	d45	d46	d47	d48	D47	D48	window	D47 rfac
09/18/14	Andros32 cal #1 IZW	-0.28	36.86	3.25471	1.818	4.9302	4.5959	-0.22	0.9528	1	0.6740
09/18/14	Andros6 cal #1 IZW	1.21	34.78	4.57567	-0.182	4.2914	-0.399	-0.246	-0.035	1	0.6656
09/22/14	Andros26 cal #1 IZW	-0.15	38.71	3.4399	3.607	6.9355	9.5759	-0.172	2.3326	2	0.6665
09/23/14	Andros32 cal #2 IZW	-0.32	36.87	3.21894	1.828	4.8804	4.3855	-0.243	0.7232	2	0.6818
09/23/14	Andros6 cal #2 IZW	1.50	35.93	4.88333	0.925	5.6796	8.6928	-0.269	6.83	2	0.6295
09/27/14	Andros15 dolo #1 IZW	1.31	40.93	4.87426	5.753	10.604	15.769	-0.11	4.1821	3	0.6584
09/27/14	Andros6 cal #3 IZW	1.56	35.62	4.92984	0.629	5.4473	1.6576	-0.257	0.3996	3	0.6557
09/29/14	Andros 32 cal #3 IZW	-0.24	37.17	3.30047	2.120	5.2739	5.1473	-0.222	0.8981	3	0.6977
09/29/14	Andros 27 dolo #1 IZW	3.25	43.29	6.76805	8.033	14.982	20.776	0.0439	4.5719	3	0.6915
09/29/14	Andros 2 dolo #1 IZW	3.63	41.59	7.06648	6.391	13.576	16.814	-0.044	3.9407	3	0.6405
10/02/14	Andros 26 cal#2 IZW	0.26	39.04	3.82837	3.925	7.6192	11.066	-0.204	3.1756	3	0.6476
10/02/14	Andro2 dolo#2 IZW	3.78	41.53	7.20723	6.337	13.684	17.317	-0.029	4.5452	3	0.6528
10/02/14	Andros27 dolo VER2 #1 IZW	2.66	42.53	6.19745	7.302	13.623	18.936	0.0023	4.2169	3	0.6877
10/03/14	Andros15 dolo #2 IZW	1.56	41.81	5.14189	6.605	11.737	17.79	-0.097	4.4777	4	0.6225
10/03/14	Andros 27 dolo ver2 #2 IZW	3.17	43.23	6.6946	7.975	14.849	20.557	0.0438	4.4711	4	0.6777
10/04/14	Andros 15 dolo #3 IZW	1.31	40.74	4.87422	5.573	10.428	16.294	-0.108	5.0609	4	0.6489
10/04/14	Andros 18 dolo #1 IZW	-1.30	35.96	2.26907	0.952	2.9649	1.9249	-0.313	0.0201	4	0.6529
10/07/14	Andros2 dolo #3 IZW	3.85	41.35	7.26731	6.169	13.575	14.782	-0.034	2.3778	4	0.6342
10/07/14	Andros 18 dolo #2 IZW	-1.47	36.16	2.11657	1.139	3.0059	1.6772	-0.299	-0.601	4	0.6658
10/07/14	Andros 26 cal #3 IZW	-0.01	38.83	3.57361	3.728	7.1704	12.897	-0.194	5.3876	4	0.6536
10/07/14	Andros18 cal #2 IZW	1.99	41.57	5.5307	6.375	11.945	18.657	-0.066	5.7919	4	0.6486
10/09/14	AC18 cal #3 IZW	1.99	41.67	5.54033	6.465	12.07	16.007	-0.04	2.9966	4.1	0.6456
10/10/14	AC18 dolo#3	-1.52	36.18	2.066	1.162	2.9781	2.2264	-0.297	-0.098	4.1	0.6667

Transfer Functions:

Window	Start date	end date	SlopeEGL	SlopeETF	IntETF
1	9/15/2014	9/21/2014	0.02929	0.988	0.946
2	9/22/2014	9/24/2014	0.02894	1.037	0.992
3	9/26/2014	10/2/2014	0.02976	1.024	0.993

4	10/1/2014	10/7/2014	0.030514	1.00273	0.968				
4.1	10/2/2014	##########	0.030564	1.01035	0.977				
Equilibrated and Heated Gasses:									
Date	**Sample**	**d13C**	**d18O**	**d45**	**d46**	**d47**	**d48**	**D47**	**D48**
09/09/14	MCB HG	-2.82	23.32	0.41	-11.256	-11.91	-14.71	-1.270	7.86
09/09/14	Mix HG	-3.06	25.14	0.25	-9.499	-10.25	-15.57	-1.173	3.41
09/09/14	Cararra HG	2.06	36.86	5.44	1.830	6.66	8.82	-0.753	5.14
09/09/14	Ooids HG	4.37	37.36	7.62	2.313	9.49	16.86	-0.654	12.17
09/10/14	Mix HG	-3.01	26.57	0.34	-8.113	-8.79	-17.45	-1.168	-1.31
09/10/14	MCB HG	-3.32	20.99	-0.14	-13.499	-14.70	-26.65	-1.295	0.17
09/10/14	MDIW HG	-41.48	28.97	-35.54	-5.883	-44.33	-13.70	-2.194	-1.99
09/11/14	Mix HG	-2.96	22.49	0.25075	-12.055	-12.87	-30.13	-1.279	-6.316
09/11/14	Cararra HG	2.12	36.73	5.48899	1.704	6.6046	5.1591	-0.737	1.7419
09/12/14	Mix HG	-2.93	27.52	0.45926	-7.200	-7.743	-16.28	-1.137	-1.958
09/14/14	MCB HG	-3.05	22.31	0.16	-12.229	-13.10	-32.32	-1.252	-8.21
09/15/14	Carrara HG	1.90	37.10	5.29739	2.058	6.7445	6.3545	-0.749	2.2253
09/16/14	Cararra HG	2.13	37.61	5.52665	2.552	7.4752	7.9366	-0.744	2.8111
09/18/14	Mix HG	-3.06	24.95	0.24375	-9.677	-10.48	-24.86	-1.224	-5.713
09/19/14	MCB HG	-3.02	21.82	0.17168	-12.699	-13.61	-31.36	-1.306	-6.278
09/19/14	MCB HG	-3.02	21.82	0.17	-12.699	-13.61	-31.36	-1.306	-6.28
09/20/14	AAS HG	-41.66	16.41	-36.1416	-18.005	-56.78	-46.34	-2.602	-11.05
09/22/14	MDIW HG	-41.38	26.67	-35.5242	-8.105	-46.49	-20.76	-2.276	-4.69
09/23/14	Cararra HG	2.04	33.60	5.31231	-1.318	3.3354	-3.535	-0.836	-0.902
09/26/14	MDIW HG	-41.29	29.37	-35.3485	-5.499	-43.79	-15.19	-2.217	-4.272
09/27/14	AAS HG	-41.46	16.96	-35.9329	-17.472	-56.07	-44.06	-2.600	-9.761
09/28/14	Mix HG	-3.33	26.44	0.03982	-8.247	-9.255	-21.55	-1.192	-5.207
09/27/14	AAS HG	-41.46	16.96	-35.9329	-17.472	-56.07	-44.06	-2.600	-9.761
09/29/14	Carrara 2 HG	2.38	35.20	5.679	0.223	5.2582	-0.597	-0.815	-1.043
10/01/14	Evap HG	-41.51	39.76	-35.1943	4.534	-33.89	11.114	-1.950	2.006
10/02/14	AAS HG	-41.42	17.18	-35.8868	-17.264	-55.89	-45.72	-2.667	-11.9
10/04/14	Carrara2 HG	3.21	38.77	6.57962	3.677	9.7682	9.2174	-0.653	1.836
10/07/14	Evap HG	-41.35	42.58	-34.9505	7.256	-30.99	18.458	-1.874	3.836
10/09/14	AAS HG	-41.53	17.14	-35.9865	-17.299	-55.99	-46.17	-2.636	-12.29
10/13/14	Carrara2 HG	1.85	34.23	5.149	-0.711	3.814	-2.854	-0.790	-1.435
10/13/14	Carrara2 HG (rerun)	1.84	34.23	5.148	-0.712	3.795	-2.780	-0.807	-1.358
09/09/14	AAS 25C	-41.63	17.02	-36.09	-17.422	-55.16	-35.22	-1.533	-0.70
09/10/14	AAS 25C	-41.31	17.96	-35.76	-16.509	-54.05	-33.31	-1.614	-0.58
09/10/14	Evap 25C	-40.61	47.16	-34.10	11.674	-24.83	35.80	-0.748	12.03
09/10/14	MDIW 25C	-41.64	30.58	-35.63	-4.327	-42.07	-8.09	-1.275	0.55
09/11/14	Evap 25C	-40.62	46.65	-34.13	11.177	-25.35	33.49	-0.764	10.77
09/11/14	MDIW 25C	-41.57	30.67	-35.5607	-4.244	-41.88	-9.768	-1.236	-1.308
09/12/14	MDIW 25C	-41.67	30.26	-35.6701	-4.637	-42.37	-9.213	-1.240	0.0401
09/12/14	MDIW 25C	-41.49	30.81	-35.4829	-4.111	-41.67	-8.524	-1.229	-0.322
09/14/14	AAS 25 BL	-41.77	15.35	-36.2802	-19.028	-56.98	-48.44	-1.637	-11.17
09/15/14	AAS 25C	-41.60	17.31	-36.0542	-17.138	-54.98	-43.09	-1.654	-9.423
09/16/14	Evap 25	-40.68	46.97	-34.1715	11.490	-25.11	30.507	-0.776	7.2279
09/17/14	Evap 25C	-41.57	46.41	-35.03	10.948	-26.55	28.88	-0.816	6.72
09/19/14	MDIW 25C	-41.52	29.27	-35.56	-5.595	-43.21	-14.26	-1.283	-3.14
09/20/14	AAS 25C	-41.48	17.11	-35.9443	-17.328	-55.08	-45.27	-1.692	-11.3
09/22/14	AAS 25	-41.57	17.38	-36.0214	-17.072	-54.90	-45.65	-1.676	-12.21
09/23/14	Evap 25C	-41.53	46.74	-34.9774	11.270	-26.22	29.66	-0.845	6.8368
09/24/14	AAS 25	-41.58	17.51	-36.03	-16.944	-54.78	-44.18	-1.674	-10.95
09/26/14	AAS 25C	-41.69	17.25	-36.1344	-17.199	-55.15	-43.67	-1.688	-9.905
09/27/14	Evap 25C	-41.49	47.04	-34.9282	11.560	-25.9	31.689	-0.849	8.2437
09/28/14	AAS 25C	-41.45	17.71	-35.8961	-16.754	-54.52	-43.93	-1.724	-11.07
09/29/14	MDIW 25C	-41.41	30.66	-35.4127	-4.249	-41.86	-11.47	-1.362	-3.015
09/28/14	AAS 25C	-41.45	17.71	-35.90	-16.754	-54.52	-43.93	-1.724	-11.07
10/03/14	AAS 25	-41.54	17.97	-35.9759	-16.503	-54.37	-42.82	-1.725	-10.42
10/04/14	Evap 25C	-41.43	47.02	-34.8786	11.539	-25.88	30.291	-0.856	6.9187

10/07/14	MDIW 25C	-41.46	29.58	-35.4969	-5.296	-42.95	-14.65	-1.375	-4.129		
10/08/14	AAS 25C	-41.47	17.85	-35.9137	-16.615	-54.45	-44.08	-1.768	-11.5		
10/11/14	Evap 25C	-41.56	45.15	-35.0645	9.736	-27.78	25.201	-0.861	5.527		

MARCH 2014 RUN

Date	Sample	d13C	d18O	d45	d46	d47	d48	D47	D48	window	D47 rfac
03/25/14	AC31 dolo #1 IZW	1.93	43.02	5.531	7.769	13.334	19.398	-0.056	3.742	1	0.6764
03/25/14	AC30 dolo #2 IZW	1.88	42.67	5.465	7.436	12.952	18.310	-0.040	3.333	1	0.7034
03/25/14	AC30 dolo #1 IZW	1.86	42.83	5.458	7.589	13.095	19.134	-0.042	3.839	1	0.6984
03/26/14	AC31 dolomite #2 IZW	1.77	41.87	5.343	6.661	12.034	16.461	-0.063	3.055	1	0.6932
03/28/14	AC7-A dolo #1 IZW	2.05	40.12	5.542	4.973	10.513	12.496	-0.122	2.501	2	0.6371
03/28/14	AC7-A calcite #1 IZW	2.11	36.10	5.464	1.093	6.473	3.323	-0.242	1.134	2	0.6141
03/28/14	AC1 deep dolo #1 IZW	2.63	39.35	6.055	4.230	10.263	11.315	-0.167	2.814	2	0.5970
03/31/14	AC7-A calcite #2 IZW	2.10	36.47	5.463	1.453	6.876	3.908	-0.194	0.997	3	0.6662
03/31/14	AC 30 dolo #3 IZW	1.03	41.68	4.637	6.481	11.142	17.046	-0.046	3.991	3	0.7129
04/01/14	AC7-A dolo #2 IZW	2.32	40.95	5.826	5.773	11.639	14.505	-0.082	2.892	3	0.6538
04/01/14	AC31 dolo #3 IZW	1.88	42.87	5.480	7.626	13.175	19.375	-0.021	4.003	3	0.6778
04/01/14	AC1-deep dolo #2 IZW	2.95	40.51	6.396	5.349	11.876	13.743	-0.017	2.984	3	0.7140
04/02/14	AC7-A dolo #3 IZW	2.32	40.61	5.811	5.451	11.281	14.032	-0.106	3.068	4	0.6101
04/02/14	AC7-A calcite #3 IZW	1.78	35.94	5.146	0.936	6.013	2.598	-0.218	0.724	4	0.6396
04/02/14	AC1 deep dolo #3 IZW	2.32	39.39	5.768	4.272	10.047	10.690	-0.128	2.110	4	0.6215
04/03/14	AC7-A dolo #4 IZW	1.40	35.97	4.794	0.964	5.766	2.651	-0.131	0.722	4	0.7377
04/03/14	AC7-A calcite #4 IZW	2.09	35.95	5.435	0.952	6.338	3.074	-0.208	1.166	4	0.6412
04/03/14	AC31 dolo #4 IZW	1.94	42.93	5.536	7.682	13.300	19.711	-0.010	4.223	4	0.6543
04/03/14	AC30 dolo #4 IZW	2.00	42.91	5.587	7.667	13.326	19.505	-0.022	4.050	4	0.6417
04/04/14	AC1 deepdolo #4 IZW	2.23	39.67	5.697	4.543	10.214	11.068	-0.155	1.944	4	0.5884
04/08/14	AC1 deep dolo #5 IZW	2.55	40.30	6.017	5.149	11.188	13.218	-0.114	2.864	5	0.6315
04/14/14	AC15 dolo #1 IZW	1.51	41.59	5.088	6.393	11.453	16.955	-0.115	4.075	6	0.6050
04/14/14	AC26 calcite #1 IZW	-0.13	39.11	3.468	3.990	7.356	10.863	-0.159	2.844	6	0.6708
04/15/14	AC26 calcite #2 IZW	0.20	39.66	3.797	4.530	8.215	13.494	-0.173	4.375	6	0.6328

Transfer Functions:

Window	Start date	end date	SlopeEGL	SlopeETF	IntETF	
1	3/18/2014	3/25/2014	0.02253	1.083	0.980	
2	3/21/2014	3/28/2014	0.02424	1.008	0.936	
3	3/24/2014	3/31/2014	0.02431	1.021	0.953	
4	4/2/2014	4/8/2014	0.029592	1.37523	1.003	
5	4/7/2014	4/11/2014	0.028009	2.0919	1.308	
6	3/26/2015	4/15/2014	0.027038	1.10306	0.974	*few standards at end of run; used long-term data

Equilibrated and Heated Gasses:

Date	Sample	d13C	d18O	d45	d46	d47	d48	D47	D48
03/16/14	Ooids HG	-1.35	34.90	2.19	-0.071	1.32	-0.64	-0.865	-0.50
03/16/14	MIX HG	-3.27	29.69	0.21	-5.105	-5.79	-12.90	-0.989	-2.74
03/16/14	MCB HG IZW	-5.96	22.29	-2.56	-12.256	-15.90	-30.16	-1.251	-5.94
03/16/14	Carerra HG	2.12	38.22	5.54	3.139	8.11	7.19	-0.706	0.90
03/16/14	Carerra HG	2.15	35.65	5.49	0.664	5.55	1.32	-0.764	-0.01
03/17/14	Ooids HG	-1.47	36.19	2.11	1.175	2.51	2.63	-0.829	0.28

03/17/14	Ooids HG	-1.50	36.26	2.1	1.237	2.5	2.7	-0.843	0.2
03/17/14	MCB HG	-5.88	22.44	-2.47	-12.111	-15.64	-29.57	-1.218	-5.63
03/17/14	Cararra HG	2.10	38.24	5.53	3.163	8.12	7.35	-0.708	1.01
03/18/14	Mix HG	-3.44	30.72	0.08743	-4.112	-4.934	-10.15	-0.982	-1.958
03/19/14	Ooids HG	-1.59	34.03	1.93	-0.914	0.18	-2.56	-0.909	-0.73
03/19/14	MCB HG	-6.00	23.36	-2.56	-11.224	-14.83	-27.55	-1.192	-5.35
03/20/14	Mix HG	-2.84	31.17	0.67	-3.678	-3.83	-8.30	-0.903	-0.99
03/21/14	Cararra HG	2.04	37.67	5.45	2.610	7.48	6.21	-0.720	0.98
03/22/14	Carrara HG	2.00	37.86	5.42	2.792	7.61	6.72	-0.739	1.12
03/23/14	MCB HG	-5.81	24.14	-2.36	-10.467	-13.89	-26.13	-1.206	-5.42
03/24/14	MIX HG	-3.34	29.84	0.15	-4.957	-5.74	-12.78	-1.021	-2.92
03/26/14	Ooids HG	-1.50	36.43	2.10	1.406	2.73	3.28	-0.821	0.46
03/27/14	Carerra HG	2.02	37.55	5.42	2.490	7.30	6.42	-0.748	1.43
03/28/14	carrara HG BL	2.03	37.29	5.43	2.239	7.06	4.42	-0.750	-0.06
03/30/14	Evap HG	-41.28	43.93	-34.84	8.556	-29.42	21.21	-1.639	3.96
03/31/14	MCB HG	-5.91	23.70	-2.47	-10.893	-14.47	-27.80	-1.254	-6.27
04/01/14	MCB HG	-5.92	23.77	-2.47	-10.828	-14.43	-27.47	-1.279	-6.06
04/02/14	MCB HG	-41.60	16.87	-36.06	-17.564	-56.07	-44.30	-2.378	-9.82
04/03/14	Mix HG	-3.87	29.48	-0.35	-5.312	-6.65	-13.81	-1.070	-3.25
04/05/14	MDIW HG	-41.38	28.77	-35.4553	-6.074	-44.31	-15.23	-2.073	-3.159
04/06/14	MCB HG BL	-4.50	22.94	-1.17025	-11.620	-13.61	-29.69	-0.999	-6.748
04/08/14	Evap HG	-19.52	41.84	-14.56	6.582	-9.54	16.99	-0.880	3.72
04/12/14	MDIW HG	-41.38	29.93	-35.41	-4.956	-43.27	-13.53	-2.146	-3.68
04/14/14	Ooids HG	-1.44	35.25	2.11	0.266	1.54	0.22	-0.896	-0.31
03/17/14	MDIW 25C	-41.42	31.50	-35.39	-3.439	-40.71	-8.04	-0.984	-1.18
03/18/14	MDIW 25C	-41.32	31.28	-35.31	-3.654	-40.82	-8.70	-0.974	-1.41
03/18/14	Evap 25C	-41.54	47.52	-34.96	12.021	-25.28	29.59	-0.626	5.27
03/18/14	AAS 25C	-41.37	17.58	-35.83	-16.879	-54.14	-40.69	-1.266	-7.46
03/19/14	Evap 25C	-41.53	47.51	-34.95	12.005	-25.29	29.37	-0.635	5.10
03/20/14	MDIW 25C	-41.36	31.49	-35.34	-3.455	-40.67	-8.57	-0.994	-1.68
03/21/14	Evap 25C	-41.66	46.41	-35.11	10.944	-26.49	27.43	-0.661	5.30
03/23/14	AAS 25C	-40.99	18.66	-35.44	-15.830	-52.80	-38.88	-1.320	-7.72
03/24/14	EVAP 25	-41.51	45.76	-34.99	10.324	-26.98	26.02	-0.688	5.16
03/26/14	MDIW 25C	-41.43	29.67	-35.4697	-5.211	-42.51	-12.95	-1.035	-2.578
03/27/14	Evap 25C	-41.59	46.12	-35.06	10.670	-26.71	26.95	-0.671	5.38
03/28/14	25C AAS	-41.43	17.05	-35.90	-17.385	-54.83	-42.60	-1.409	-8.43
03/30/14	Evap 25C	-41.37	46.53	-34.84	11.062	-26.15	28.03	-0.711	5.66
03/31/14	Evap 25C	-41.45	47.01	-34.89	11.528	-25.77	29.20	-0.720	5.87
04/01/14	MDIW 25C	-41.43	31.14	-35.42	-3.786	-41.18	-9.31	-1.109	-1.76
04/03/14	Evap 25C	-41.39	47.28	-34.83	11.790	-25.46	30.02	-0.731	6.15
04/03/14	AAS 25C	-41.29	17.09	-35.76	-17.350	-54.71	-43.40	-1.468	-9.32
04/05/14	AAS 25	-28.47	20.22	-23.6729	-14.300	-39.24	-36.1	-1.222	-7.96
04/07/14	AAS 25C	-41.32	30.96	-35.32	-3.959	-41.75	-9.97	-1.640	-2.41
04/11/14	Evap 25C	-41.45	47.33	-34.88	11.833	-25.53	30.68	-0.781	6.71
04/11/14	AAS 25C	-41.41	16.22	-35.91	-18.183	-55.78	-46.86	-1.608	-11.23
04/13/14	Evap 25C	-41.41	47.56	-34.84	12.056	-25.29	31.33	-0.798	6.90
04/14/14	AAS 25C	-41.29	17.19	-35.77	-17.251	-54.75	-44.04	-1.607	-10.19

SAMPLE	**d13RAWc**	**d18ORAWc**	**δ18O and δ13C corrections for -30°C Porapak**
AC30 dolo #2 IZW	1.98	43.03	See Petersen et al. (2015), *RCMS*, for details
AC30 dolo #1 IZW	1.96	43.19	
AC30 dolo #4 IZW	2.10	43.27	*+.1 for δ13C and +.36 for δ18O
AC31 dolo #1 IZW	2.03	43.38	
AC31 dolo #3 IZW	1.98	43.23	
AC31 dolo #4 IZW	2.04	43.29	
AC31 dolomite	1.87	42.23	

#2 IZW		
Andros 27 dolo #1 IZW	3.35	43.65
Andros27 dolo VER2 #1 IZW	2.76	42.89
Andros 27 dolo ver2 #2 IZW	3.27	43.59
Andros 18 cal #1 IZW DOLO	2.13	42.02
Andros18 cal #2 IZW DOLO	2.09	41.93
AC18 cal #3 IZW DOLO	2.09	42.03
Andros15 dolo #1 IZW	1.41	41.29
Andros15 dolo #2 IZW	1.66	42.17
Andros 15 dolo #3 IZW	1.41	41.10
AC15 dolo #1 IZW	1.61	41.95
AC7-A dolo #2 IZW	2.42	41.31
AC7-A dolo #3 IZW	2.42	40.97
AC7-A dolo #1 IZW	2.15	40.48
Andros 2 dolo #1 IZW	3.73	41.95
Andro2 dolo#2 IZW	3.88	41.89
Andros2 dolo #3 IZW	3.95	41.71
AC1 deep dolo #3 IZW	2.42	39.75
AC1 deepdolo #4 IZW	2.33	40.03
AC1 deep dolo #5 IZW	2.65	40.66
AC1 deep dolo #1 IZW	2.73	39.71
Andros 32 cal #3 IZW	-0.14	37.53
Andros32 cal #1 IZW	-0.18	37.22
Andros32 cal #2 IZW	-0.22	37.23
Andros 26 cal#2 IZW	0.36	39.40
Andros 26 cal #3 IZW	0.09	39.19
Andros26 cal #1 IZW	-0.05	39.07
AC26 calcite #1 IZW	-0.03	39.47
AC26 calcite #2 IZW	0.30	40.02
Andros 18 dolo #1 IZW CAL	-1.20	36.32
Andros 18 dolo #2 IZW CAL	-1.37	36.52
(AC18 dolo#3) CAL	-1.42	36.54
Andros6 cal #3 IZW	1.66	35.98
Andros6 cal #1 IZW	1.31	35.14
AC7-A calcite #1 IZW	2.21	36.46
AC7-A calcite #2 IZW	2.20	36.83
AC7-A calcite #3 IZW	1.88	36.30
AC7-A calcite #4 IZW	2.19	36.31

Chapter 3 Raw Data

SEPTEMBER 2015 RUN

Samples:

Date	Sample Name	d13C (pdb)	d18O (smow)	d45	d46	d47	d48	D47	D48	window	D47rfac
09/13/15	235-O-12-1	3.792	13.344	6.324	-20.868	-15.13	-47.15	-0.990	-6.104	2	0.3921
09/16/15	235-O-12-2	4.205	13.411	6.713	-20.803	-14.64	-49.7	-0.964	-8.895	3	0.4312
09/18/15	235-O-12-3	4.058	13.626	6.583	-20.596	-14.54	-39.37	-0.930	1.452	3	0.4643
09/21/15	235-O-12-4	4.349	12.928	6.833	-21.268	-15.04	-50.67	-1.020	-8.962	3	0.3817
09/23/15	235-O-12-5	4.228	13.454	6.737	-20.762	-14.6	-51.21	-0.979	-10.55	4	0.4502
09/12/15	Barb110-1	-7.568	42.896	-3.386	7.633	3.648	15.824	-0.341	0.493	2	0.6956
09/13/15	Barb110-2	-7.299	42.707	-3.14	7.450	3.746	25.838	-0.320	10.721	2	0.7159
09/18/15	Barb110-3	-7.378	43.017	-3.204	7.750	3.997	18.56	-0.296	2.954	3	0.7197
09/22/15	BarbDolo110-4	-7.404	42.191	-3.255	6.952	3.121	15.418	-0.338	1.445	4	0.7044
09/13/15	MIZd-1	-0.154	32.173	3.229	-2.702	0.143	1.54	-0.519	6.974	2	0.5786
09/18/15	MIZd-2	-0.487	31.609	2.898	-3.248	-0.756	-7.322	-0.540	-0.843	3	0.5696
09/21/15	MIZd-3	-0.427	31.57	2.953	-3.284	-0.707	-8.872	-0.511	-2.33	3	0.5986
09/13/15	O-H-2-1	4.358	13.624	6.864	-20.597	-14.27	-46.1	-0.948	-5.555	2	0.4191
09/19/15	O-H-2-2	4.337	13.98	6.856	-20.254	-13.94	-48.55	-0.948	-8.803	3	0.4326
09/22/15	O-H-2-3	4.244	13.793	6.763	-20.434	-14.21	-49.54	-0.941	-9.471	4	0.4808
09/23/15	O-H-2-4	4.403	13.78	6.911	-20.447	-14.09	-50.06	-0.966	-9.986	4	0.4521
09/19/15	O-T-5-1	3.513	13.449	6.065	-20.768	-15.3	-49.86	-0.997	-9.131	3	0.4112
09/21/15	O-T-5-2	3.449	13.601	6.01	-20.621	-15.2	-50.3	-0.993	-9.883	3	0.4133

Transfer Functions:

Window	Start date	end date	SlopeEGL	SlopeETF	IntETF
1	9/9/2015	9/10/2015	0.018546	0.99608	1.016
2	9/11/2015	9/15/2015	0.019341	1.06189	1.066
3	9/16/2015	9/21/2015	0.020947	1.03936	1.047
4	9/22/2015	9/29/2015	0.022432	1.04356	1.063

Equilibrated and Heated Gasses:

DATE	Name	d13C	d18O	d45	d46	d47	d48	D47	D48
09/09/15	Carrara HG	1.93	33.565	5.23	-1.354	3.107	-4.842	-0.944	-2.142
09/09/15	Evap HG	-41.025	43.044	-34.792	7.705	-30.06	15.227	-1.520	-0.239
09/10/15	2xEV HG	-41.124	62.552	-34.262	26.534	-11.39	58.422	-1.227	4.412
09/10/15	Evap 25C #1	-41.578	46.483	-35.202	11.023	-26.44	22.836	-0.590	0.653
09/10/15	MDIW 25C	-41.514	30.727	-35.649	-4.184	-41.6	-11.7	-0.909	-3.374
09/10/15	2xEV 25C #1	-41.651	70.564	-34.501	34.266	-3.265	76.926	-0.160	6.749
09/10/15	Evap 25C #2	-41.393	46.823	-35.017	11.352	-25.94	23.926	-0.602	1.068
09/11/15	2xEV 25C #2	-41.46	71.026	-34.308	34.712	-2.678	77.957	-0.201	6.845
09/11/15	Ooids HG	4.211	37.333	7.494	2.287	9.176	6.244	-0.811	1.657
09/13/15	2xEV 25C	-41.414	71.086	-34.262	34.770	-2.579	78.415	-0.206	7.16
09/13/15	Evap HG	-40.955	37.782	-34.896	2.626	-35.1	3.582	-1.657	-1.669
09/14/15	Evap 25C	-41.12	47.187	-34.749	11.704	-25.37	25.145	-0.645	1.563
09/14/15	Carrara HG	2.047	30.272	5.235	-4.532	-0.057	-12.24	-0.970	-3.225
09/15/15	MDIW 25C	-41.497	30.287	-35.646	-4.608	-42.06	-12.98	-0.970	-3.819
09/16/15	MDIW HG	-40.948	28.142	-35.201	-6.678	-44.47	-18.21	-1.920	-4.965
09/17/15	Evap 25C	-41.779	46.155	-35.4	10.706	-27.03	23.638	-0.676	2.066
09/18/15	2xEV 25C	-41.396	71.57	-34.231	35.237	-2.112	81.743	-0.216	9.356
09/18/15	Evap HG	-40.836	35.306	-34.864	0.237	-37.44	-1.935	-1.768	-2.408
09/19/15	MDIW 25C	-41.481	30.102	-35.638	-4.788	-42.28	-13.15	-1.038	-3.628
09/20/15	2xEV HG	-40.944	54.811	-34.34	19.063	-18.7	42.465	-1.387	3.827
09/20/15	Evap 25C	-41.688	46.366	-35.309	10.911	-26.75	23.461	-0.692	1.487
09/21/15	Carrara HG	1.664	35.612	5.047	0.622	4.957	-0.077	-0.857	-1.319
09/21/15	MDIW 25C	-41.514	30.119	-35.667	-4.771	-42.28	-12.58	-1.019	-3.089
09/22/15	MDIW HG	-41.182	28.147	-35.42	-6.674	-44.75	-17.23	-1.981	-3.978
09/23/15	Evap 25C	-41.353	46.822	-34.979	11.351	-25.99	24.656	-0.687	1.784
09/24/15	Evap HG	-40.961	43.721	-34.711	8.359	-29.44	17.528	-1.611	0.728
09/24/15	2xEV 25C	-41.087	70.614	-33.97	34.315	-2.683	80.946	-0.191	10.41
09/25/15	Ooids HG	4.404	34.39	7.58	-0.552	6.422	-2.179	-0.842	-1.076

09/26/15	MDIW 25C	-41.211	30.517	-35.371	-4.386	-41.71	-11.5	-1.123	-2.772
09/26/15	Carrara HG	2.253	32.121	5.487	-2.747	1.994	-9.737	-0.943	-4.275
09/27/15	Evap 25C	-41.134	46.685	-34.778	11.219	-25.95	25.769	-0.732	3.134
09/28/15	Carrara HG	2.304	34.739	5.619	-0.220	4.655	-3.147	-0.917	-2.708
09/28/15	2xEV 25C	-41.052	71.223	-33.919	34.903	-2.118	82.517	-0.239	10.73
09/29/15	MDIW HG	-41.205	23.629	-35.588	-11.035	-49.19	-28.89	-2.133	-7.101
09/29/15	MDIW 25C	-41.303	30.925	-35.444	-3.992	-41.38	-11.69	-1.091	-3.754
09/30/15	2xEV HG	-41.185	60.442	-34.386	24.497	-13.54	55.367	-1.316	5.501
10/01/15	Evap 25C	-41.313	46.206	-34.961	10.757	-26.54	23.783	-0.698	2.108
10/01/15	Evap HG	-41.227	41.378	-35.036	6.097	-31.97	12.756	-1.670	0.517
10/02/15	2xEV 25C	-41.274	70.704	-34.143	34.402	-2.796	81.087	-0.201	10.373
10/03/15	Carrara HG	2.011	32.542	5.274	-2.342	2.238	-8.564	-0.881	-3.904
10/04/15	MDIW 25C	-41.049	30.358	-35.223	-4.539	-41.69	-13.85	-1.113	-4.841
10/06/15	Evap 25C	-41.267	0.7	2.1	-34.909	11.03	-26.28	14.901	10.2

JUNE 2015 RUN

Samples:

Date	Sample Name	d13C (pdb)	d18O (smow)	d45	d46	d47	d48	D47	D48	window	D47rfac
02/11/15	250-I-7-d-1	4.212	12.285	6.683	-21.890	-15.72	-52.15	-0.933	-9.247	1	0.439
03/14/15	250-I-7-d-2	4.336	12.364	6.803	-21.813	-15.55	-52.42	-0.961	-9.690	2	0.443
03/15/15	O-T-5-d-1	3.612	13.256	6.151	-20.953	-15.35	-50.21	-0.954	-9.118	2	0.446
03/16/15	200-p-30-d-1	4.543	15.45	7.097	-18.834	-12.22	-46.34	-0.875	-9.382	2	0.46
03/17/15	250-I-7-d-3	4.301	12.065	6.76	-22.102	-15.9	-52.91	-0.981	-9.609	2	0.429
03/18/15	O-T-5-d-2	3.55	13.337	6.096	-20.876	-15.36	-50.77	-0.982	-9.860	2	0.416
03/19/15	200-p-30-d-2	4.557	15.609	7.115	-18.680	-12.04	-45.21	-0.863	-8.509	2	0.469
03/28/15	250-I-7-d-4	4.062	12.683	6.555	-21.506	-15.49	-52.07	-0.957	-9.942	2	0.446
03/29/15	O-T-5-d-3	3.512	13.526	6.066	-20.693	-15.19	-50.42	-0.962	-9.863	2	0.434
03/30/15	200-P-30-d-3	4.555	15.674	7.115	-18.617	-11.97	-45.7	-0.860	-9.148	2	0.471
07/15/15	IODP-d-2	12.417	39.19	15.258	4.097	19.875	28.424	0.046	20.048	3	0.713
07/17/15	200-P-30-d-4	4.53	15.808	7.096	-18.488	-11.89	-44.87	-0.888	-8.543	3	0.461
07/18/15	O-T-5-d-4	3.437	13.568	5.997	-20.653	-15.23	-50.64	-0.974	-10.177	3	0.448
07/20/15	IODP-d-4	12.599	38.832	15.417	3.752	19.706	31.674	0.056	23.975	3	0.728
07/22/15	IODP-d-3	12.702	38.753	15.511	3.676	19.717	37.955	0.046	30.366	3	0.717

Transfer Functions:

Window	Start date	end date	SlopeEGL	SlopeETF	IntETF
1	6/12/2015	06/17/15	0.01894	1.039	1.032
2	6/18/2015	06/26/15	0.02128	1.103	1.071
3	6/25/2015	06/29/15	0.02210	1.088	1.074

Equilibrated and Heated Gasses:

DATE	Name	d13C	d18O	d45	d46	d47	d48	D47	D48
6/12/2015	MDIWHG	-41.031	30.668	-35.197	-4.240	-42.07	-9.848	-1.833	-1.398
6/12/2015	CarraraHG	1.912	35.371	5.272	0.389	4.987	-1.516	-0.829	-2.292
6/12/2015	EvapHG	-41.221	41.844	-35.015	6.546	-31.44	12.113	-1.576	-1.01
6/13/2015	2xEVHG	-40.929	58.25	-34.216	22.383	-15.29	48.543	-1.241	3.135
6/15/2015	OoidsHG	4.33	31.425	7.415	-3.415	3.393	-6.361	-0.863	0.46
6/16/2015	MDIWHG	-40.92	26.438	-35.229	-8.322	-46	-22.09	-1.861	-5.603
6/12/2015	Heavy25C	4.745	70.958	9.069	34.745	44.632	79.739	0.755	8.445
6/12/2015	MDIW25C	-41.416	30.339	-35.568	-4.558	-41.86	-11.58	-0.896	-2.508
6/13/2015	Evap25C	-41.358	46.026	-35.009	10.582	-26.61	27.543	-0.544	6.135
6/13/2015	2XEV25C	-41.296	72.956	-34.093	36.575	-0.608	84.294	-0.126	9.126
6/14/2015	Heavy25C	4.777	73.426	9.178	37.127	47.077	84.074	0.719	7.848
6/16/2015	MDIW25C	-41.558	29.877	-35.717	-5.005	-42.46	-13.24	-0.920	-3.291
6/17/2015	Evap25C	-41.755	46.195	-35.377	10.745	-26.88	23.939	-0.593	2.283
6/18/2015	2xEVHG	-41.004	53.15	-34.449	17.460	-20.32	37.821	-1.371	2.509
6/19/2015	CarraraHG	2.303	30.456	5.481	-4.355	0.445	-13.1	-0.896	-4.45
6/20/2015	EvapHG	-40.73	41.729	-34.558	6.436	-31.13	12.276	-1.638	-0.63
6/23/2015	EvapHG	-40.987	44.92	-34.696	9.516	-28.3	19.749	-1.577	0.614
6/23/2015	CarraraHG	2.206	37.208	5.607	2.163	7.123	1.922	-0.792	-2.397
6/24/2015	2xEVHG	-41.035	68.373	-33.992	32.152	-5.666	75.201	-1.104	9.258

6/25/2015	OoidsHG	4.228	33.496	7.386	-1.416	5.413	-2.735	-0.794	0.095
6/18/2015	2xEV25C	-41.372	73.019	-34.161	36.635	-0.627	84.626	-0.129	9.317
6/20/2015	Heavy25C	4.749	71.401	9.088	35.172	45.113	81.335	0.790	9.102
6/20/2015	MDIW25C	-41.437	30.575	-35.581	-4.331	-41.78	-12.63	-1.029	-4.026
6/23/2015	Evap25C	-41.459	47.833	-35.046	12.327	-25.08	27.061	-0.628	2.2
6/24/2015	MDIW25C	-41.457	30.706	-35.595	-4.204	-41.68	-12.14	-1.031	-3.784
6/24/2015	2xEV25C	-41.32	71.546	-34.16	35.214	-2.017	83.033	-0.174	10.605
6/25/2015	Evap25C	-41.593	46.475	-35.215	11.016	-26.56	24.323	-0.695	2.122
6/26/2015	Heavy25C	4.936	74.559	9.363	38.220	48.551	90.61	0.900	11.79
6/25/2015	OoidsHG	4.228	33.496	7.386	-1.416	5.413	-2.735	-0.794	0.095
6/27/2015	EvapHG	-41.255	42.885	-35.013	7.551	-30.56	15.535	-1.649	0.37
6/28/2015	MDIWHG	-40.94	29.1	-35.162	-5.753	-43.6	-16.58	-1.969	-5.164
6/29/2015	CarraraHG	2.123	35.549	5.475	0.561	5.356	-1.341	-0.840	-2.461
6/25/2015	Evap25C	-41.593	46.475	-35.215	11.016	-26.56	24.323	-0.695	2.122
6/26/2015	Heavy25C	4.936	74.559	9.363	38.220	48.551	90.61	0.900	11.79
6/27/2015	MDIW25C	-41.544	30.27	-35.691	-4.625	-42.22	-13.49	-1.078	-4.303
6/29/2015	2xEV25C	-41.344	70.041	-34.23	33.762	-3.502	79.666	-0.209	10.295
6/29/2015	Evap25C	-41.757	46.179	-35.379	10.730	-27.03	24.386	-0.724	2.751

MARCH 2014 RUN

Date	Sample	d13C	d18O	d45	d46	d47	d48	D47	D48	window	D47rfac
03/25/14	AC30 dolo #2 IZW	1.875125	42.672	5.46516	7.436	12.952	18.31	-0.04	3.3329	1	0.7034
03/25/14	AC30 dolo #1 IZW	1.861625	42.8305	5.45824	7.589	13.095	19.134	-0.042	3.8393	1	0.6984
03/31/14	AC 30 dolo #3 IZW	1.025125	41.68325	4.63699	6.481	11.142	17.046	-0.046	3.9908	3	0.7129
04/03/14	AC30 dolo #4 IZW	1.99725	42.911	5.58739	7.667	13.326	19.505	-0.022	4.0498	4	0.6417

Transfer Functions:

Window	Start date	end date	SlopeEGL	SlopeETF	IntETF
1	3/18/2014	3/25/2014	0.02253	1.083	0.980
2	3/21/2014	3/28/2014	0.02424	1.008	0.936
3	3/24/2014	3/31/2014	0.02431	1.021	0.953
4	4/2/2014	4/8/2014	0.029592	1.37523	1.003

Equilibrated and Heated Gasses:

Date	Sample	d13C	d18O	d45	d46	d47	d48	D47	D48
03/16/14	Ooids HG	-1.35	34.90	2.19	-0.071	1.32	-0.64	-0.865	-0.50
03/16/14	MIX HG	-3.27	29.69	0.21	-5.105	-5.79	-12.90	-0.989	-2.74
03/16/14	MCB HG IZW	-5.96	22.29	-2.56	-12.256	-15.90	-30.16	-1.251	-5.94
03/16/14	Carerra HG	2.12	38.22	5.54	3.139	8.11	7.19	-0.706	0.90
03/16/14	Carerra HG	2.15	35.65	5.49	0.664	5.55	1.32	-0.764	-0.01
03/17/14	Ooids HG	-1.47	36.19	2.11	1.175	2.51	2.63	-0.829	0.28
03/17/14	Ooids HG	-1.5	36.3	2.1	1.237	2.5	2.7	-0.843	0.2
03/17/14	MCB HG	-5.88	22.44	-2.47	-12.111	-15.64	-29.57	-1.218	-5.63
03/17/14	Cararra HG	2.10	38.24	5.53	3.163	8.12	7.35	-0.708	1.01
03/18/14	Mix HG	-3.440625	30.71888	0.08743	-4.112	-4.934	-10.15	-0.982	-1.958
03/19/14	Ooids HG	-1.59	34.03	1.93	-0.914	0.18	-2.56	-0.909	-0.73
03/19/14	MCB HG	-6.00	23.36	-2.56	-11.224	-14.83	-27.55	-1.192	-5.35
03/20/14	Mix HG	-2.84	31.17	0.67	-3.678	-3.83	-8.30	-0.903	-0.99
03/21/14	Cararra HG	2.04	37.67	5.45	2.610	7.48	6.21	-0.720	0.98
03/22/14	Carrara HG	2.00	37.86	5.42	2.792	7.61	6.72	-0.739	1.12
03/23/14	MCB HG	-5.81	24.14	-2.36	-10.467	-13.89	-26.13	-1.206	-5.42
03/24/14	MIX HG	-3.34	29.84	0.15	-4.957	-5.74	-12.78	-1.021	-2.92
03/26/14	Ooids HG	-1.50	36.43	2.10	1.406	2.73	3.28	-0.821	0.46
03/27/14	Carerra HG	2.02	37.55	5.42	2.490	7.30	6.42	-0.748	1.43
03/28/14	carrara HG BL	2.03	37.29	5.43	2.239	7.06	4.42	-0.750	-0.06
03/30/14	Evap HG	-41.28	43.93	-34.84	8.556	-29.42	21.21	-1.639	3.96
03/31/14	MCB HG	-5.91	23.70	-2.47	-10.893	-14.47	-27.80	-1.254	-6.27
04/01/14	MCB HG	-5.92	23.77	-2.47	-10.828	-14.43	-27.47	-1.279	-6.06
04/02/14	MCB HG	-41.60	16.87	-36.06	-17.564	-56.07	-44.30	-2.378	-9.82

04/03/14	Mix HG	-3.87	29.48	-0.35	-5.312	-6.65	-13.81	-1.070	-3.25
04/05/14	MDIW HG	-41.38475	28.7725	-35.4553	-6.074	-44.31	-15.23	-2.073	-3.159
04/06/14	MCB HG BL	-4.500875	22.94225	-1.17025	-11.620	-13.61	-29.69	-0.999	-6.748
04/08/14	Evap HG	-19.52	41.84	-14.56	6.582	-9.54	16.99	-0.880	3.72

Chapter 5 Raw Data

JUNE 2015 RUN

Samples:

Date	Sample Name	d13C (pdb)	d18O (raw)	d45	d46	d47	d48	D47	D48	window	D47rfac
06/16/16	B14_Mod1x-1	-0.85	39.292	2.805	4.168	6.747	8.611	-0.256	0.255	1	0.700
06/16/16	B11_RB48x-2	3.094	40.49	6.547	5.333	11.872	9.908	-0.158	-0.777	1	0.701
06/16/15	B14_GB1x-1	2.053	39.858	5.549	4.72	10.237	9.610	-0.153	0.147	1	0.739
06/16/16	B14_Mod1x-2	-0.75	39.378	2.901	4.251	6.923	7.673	-0.262	-0.839	1	0.691
06/17/15	B11-RB48x-1	3.105	40.48	6.556	5.323	11.91	10.375	-0.122	-0.297	1	0.738

Transfer Functions:

Window	Start date	end date	SlopeEGL	SlopeETF	IntETF
1	6/12/2015	06/17/15	0.01894	1.039	1.032

Equilibrated and Heated Gasses:

DATE	Name	d13C	d18O	d45	d46	d47	d48	D47	D48
6/12/15	Carrara HG - old	2.295	37.973	5.716	2.902	7.987	9.769	-0.772	3.935
6/12/15	Ooids HG - old	4.487	40.106	7.842	4.965	12.359	12.141	-0.644	2.165
6/12/15	MDIW HG	-41.031	30.668	-35.197	-4.240	-42.07	-9.848	-1.833	-1.398
6/12/15	Carrara HG	1.912	35.371	5.272	0.389	4.987	-1.516	-0.829	-2.292
6/12/15	Evap HG	-41.221	41.844	-35.015	6.546	-31.44	12.113	-1.576	-1.01
6/13/15	2xEV HG	-40.929	58.25	-34.216	22.383	-15.29	48.543	-1.241	3.135
6/15/15	Ooids HG	4.33	31.425	7.415	-3.415	3.393	-6.361	-0.863	0.46
6/16/15	MDIW HG	-40.92	26.438	-35.229	-8.322	-46	-22.09	-1.861	-5.603
6/18/15	2xEV HG	-41.004	53.15	-34.449	17.460	-20.32	37.821	-1.371	2.509
6/19/15	Carrara HG	2.303	30.456	5.481	-4.355	0.445	-13.1	-0.896	-4.45
6/20/15	Evap HG	-40.73	41.729	-34.558	6.436	-31.13	12.276	-1.638	-0.63
6/23/15	Evap HG	-40.987	44.92	-34.696	9.516	-28.3	19.749	-1.577	0.614
6/23/15	Carrara HG	2.206	37.208	5.607	2.163	7.123	1.922	-0.792	-2.397
6/24/15	2xEV HG	-41.035	68.373	-33.992	32.152	-5.666	75.201	-1.104	9.258
6/25/15	Ooids HG	4.228	33.496	7.386	-1.416	5.413	-2.735	-0.794	0.095
6/27/15	Evap HG	-41.255	42.885	-35.013	7.551	-30.56	15.535	-1.649	0.37
6/28/15	MDIW HG	-40.94	29.1	-35.162	-5.753	-43.6	-16.58	-1.969	-5.164
6/29/15	Carrara HG	2.123	35.549	5.475	0.561	5.356	-1.341	-0.840	-2.461
6/30/15	OoidsHG	4.059	30.368	7.127	-4.436	2.059	3.906	-0.890	12.871
7/1/15	MDIW HG	-41.082	29.545	-35.281	-5.324	-43.35	-14.16	-2.005	-3.574
7/3/15	Carrara HG	2.071	36.685	5.464	1.658	6.452	2.403	-0.818	-0.913
7/5/15	Evap HG	-41.146	41.914	-34.942	6.614	-31.45	13.864	-1.734	0.583
6/12/15	Heavy 25C	4.745	70.958	9.069	34.745	44.632	79.739	0.755	8.445
6/12/15	MDIW 25C	-41.416	30.339	-35.568	-4.558	-41.86	-11.58	-0.896	-2.508
6/13/15	Evap 25C	-41.358	46.026	-35.009	10.582	-26.61	27.543	-0.544	6.135
6/13/15	2X EV 25C	-41.296	72.956	-34.093	36.575	-0.608	84.294	-0.126	9.126
6/14/15	Heavy 25	4.777	73.426	9.178	37.127	47.077	84.074	0.719	7.848
6/16/15	MDIW 25C	-41.558	29.877	-35.717	-5.005	-42.46	-13.24	-0.920	-3.291
6/17/15	Evap 25C	-41.755	46.195	-35.377	10.745	-26.88	23.939	-0.593	2.283
6/18/15	2xEV 25C	-41.372	73.019	-34.161	36.635	-0.627	84.626	-0.129	9.317
6/20/15	Heavy 25C	4.749	71.401	9.088	35.172	45.113	81.335	0.790	9.102
6/20/15	MDIW 25C	-41.437	30.575	-35.581	-4.331	-41.78	-12.63	-1.029	-4.026
6/23/15	Evap 25C	-41.459	47.833	-35.046	12.327	-25.08	27.061	-0.628	2.2
6/24/15	MDIW 25C	-41.457	30.706	-35.595	-4.204	-41.68	-12.14	-1.031	-3.784
6/24/15	2xEV 25C	-41.32	71.546	-34.16	35.214	-2.017	83.033	-0.174	10.605
6/25/15	Evap 25C	-41.593	46.475	-35.215	11.016	-26.56	24.323	-0.695	2.122
6/26/15	Heavy 25C	4.936	74.559	9.363	38.220	48.551	90.61	0.900	11.79
6/27/15	MDIW 25C	-41.544	30.27	-35.691	-4.625	-42.22	-13.49	-1.078	-4.303
6/29/15	2xEV 25C	-41.344	70.041	-34.23	33.762	-3.502	79.666	-0.209	10.295

6/29/15	Evap25C	-41.757	46.179	-35.379	10.730	-27.03	24.386	-0.724	2.751
7/1/15	Heavy25C	4.885	74.247	9.305	37.920	48.179	95.575	0.889	16.984
7/3/15	MDIW 25C	-41.522	30.248	-35.671	-4.646	-42.26	-12.95	-1.121	-3.714
7/4/15	2x EV 25C	-41.362	71.92	-34.188	35.575	-1.719	85.643	-0.188	12.334

JANUARY 2015 RUN

Samples:

Date	Sample Name	d13C (pdb)	d18O (smow)	d45	d46	d47	d48	D47	D48	window	D47rfac
1/31/15	B11 RB48 #1 IZW	2.985	40.467	6.443	5.31	11.863	10.628	-0.04	-0.021	1	0.711
1/31/15	B14 GB3 #1 IZW	2.324	39.668	5.797	4.538	10.398	9.153	-0.07	0.056	1	0.718
1/31/15	B14 GB5 #1 IZW	3.354	39.68	6.765	4.551	11.472	8.788	-0.013	-0.332	1	0.752
2/1/15	B14 RB6 #1 IZW	2.982	40.749	6.450	5.582	12.164	11.033	-0.016	-0.161	1	0.729
2/1/15	B14 GB7 #1 IZW	2.23	40.352	5.731	5.198	10.992	10.844	-0.061	0.417	1	0.712
2/3/15	B14 GB5 #2 IZW	3.32	39.697	6.733	4.568	11.45	8.489	-0.018	-0.662	1	0.747
2/3/15	B14 GB3 #2 IZW	2.331	39.71	5.805	4.578	10.447	9.289	-0.069	0.111	1	0.718
2/3/15	B11 RB48 #2 IZW	2.819	40.328	6.283	5.176	11.573	10.215	-0.031	-0.162	1	0.729
2/10/15	B14 GB7 #2 IZW	2.261	40.392	5.761	5.236	11.083	7.266	-0.039	-3.2	2	0.734
2/10/15	B14 GB5 #3 IZW	3.292	39.663	6.706	4.534	11.342	8.258	-0.064	-0.823	2	0.699
2/10/15	B14 GB3 #3 IZW	2.426	39.765	5.896	4.631	10.602	10.640	-0.061	1.344	2	0.723
2/10/15	B14 GB1 #2 IZW	2.05	40.001	5.551	4.858	10.453	10.076	-0.077	0.333	2	0.710
2/11/15	B11 RB48 #3 IZW	2.953	40.29	6.407	5.139	11.622	11.103	-0.074	0.791	2	0.680
2/11/15	B14 RB6 #2 IZW	3.023	40.53	6.481	5.371	12.008	10.007	0.004	-0.756	2	0.755
2/12/15	B14 GB7 #3 IZW	2.241	40.416	5.743	5.259	11.068	10.372	-0.059	-0.172	3	0.710
2/13/15	B14 RB6 #3 IZW	3.07	40.785	6.534	5.617	12.281	11.536	-0.02	0.268	3	0.717
2/13/15	B14 GB1 #3 IZW	2.03	39.778	5.525	4.643	10.235	10.260	-0.056	0.943	3	0.738
2/18/15	B14 Mod2 Ver2 #4 IZW	0.063	39.222	3.660	4.103	7.642	7.991	-0.182	-0.23	3	0.675
2/18/15	B14 GB3 #4 IZW	2.33	39.717	5.804	4.585	10.478	11.433	-0.045	2.222	3	0.743
2/20/15	B14 GB7 #4 IZW	2.258	40.623	5.766	5.46	11.314	11.742	-0.035	0.784	3	0.729
2/20/15	B14 RB3 #4 IZW	2.457	40.568	5.951	5.407	11.436	12.509	-0.053	1.648	3	0.706
2/24/15	B14 RB6 #4 IZW	3.058	40.665	6.519	5.501	12.151	10.106	-0.019	-0.916	4	0.697
2/24/15	B14 Mod1 #5 IZW	-0.79	39.251	2.860	4.128	6.832	6.097	-0.189	-2.159	4	0.669
2/24/15	B14 Mod2 #5 IZW	0.555	39.856	4.142	4.716	8.84	10.049	-0.09	0.59	4	0.717
2/24/15	B14 GB1 #4 IZW	1.95	39.917	5.454	4.777	10.274	11.712	-0.076	2.114	4	0.690
2/24/15	B14 GB5 #4 IZW	3.349	39.752	6.762	4.621	11.532	9.741	-0.019	0.473	4	0.715
2/24/15	B11 RB48 #4 IZW	3.087	40.547	6.542	5.387	12.05	11.232	-0.032	0.423	4	0.685
2/26/15	B14 Mod1 #6 IZW	-0.928	39.181	2.728	4.061	6.63	7.179	-0.189	-0.951	4	0.675
2/26/15	B14 Mod2 #6 IZW	0.528	39.822	4.116	4.682	8.749	8.597	-0.12	-0.782	4	0.687

Transfer Functions:

Window	Start date	end date	SlopeEGL	SlopeETF	IntETF
1	1/26/2015	2/3/2015	0.025025	1.099500	1.015
2	2/4/2015	2/11/2015	0.025807	1.096200	1.023
3	2/12/2015	2/21/2015	0.026576	1.108800	1.035
4	2/22/2015	3/3/2015	0.027203	1.079100	1.007

Equilibrated and Heated Gasses:

DATE	Name	d13C	d18O	d45	d46	d47	d48	D47	D48
1/26/15	MDIWHG	-41.36	25.221	-47.792	-25.590	7.945	-2.094	-6.812	67.592
1/26/15	CarraraHG1	2.063	35.206	5.057	-3.896	3.459	-0.743	-4.354	-2.737
1/26/15	CarraraHG2	2.114	35.173	5.066	-2.204	2.236	-0.751	-2.601	-3.942
1/26/15	2xEVHG1	-41.145	63.474	-10.447	63.008	1.107	-1.134	7.018	-14.78
1/27/15	2xEVHG2	-41.349	63.242	-10.897	65.083	0.295	-1.161	9.424	-14.94
1/28/15	EvapHG	-41.069	35.466	-37.556	-2.789	8.741	-1.817	-3.568	47.079
1/29/15	CarraraHG	2.129	37.044	6.921	2.405	3.033	-0.758	-1.601	-6.756
1/31/15	MDIWHG	-41.261	26.661	-46.322	-22.814	6.912	-2.081	-6.774	63.395
2/1/15	2xEVHG	-41.309	61.925	-12.17	59.389	3.808	-1.228	6.518	-9.07

2/2/15	OoidsHG	4.539	37.033	9.348	2.105	3.937	-0.662	-1.889	-8.225
2/3/15	MDIWHG	-41.213	28.935	-44.079	-17.453	6.959	-2.031	-5.729	58.699
1/27/15	Evap25C	-41.258	47.356	-25.409	25.022	3.606	-0.709	1.119	18.429
1/27/15	MDIW25C1	-41.384	30.545	-41.839	-16.860	8.831	-1.112	-8.233	57.543
1/27/15	2xEV25C1	-41.316	70.391	-3.068	81.246	-4.199	-0.134	11.113	-32.46
1/27/15	MDIW25C2	-41.491	29.867	-42.58	-14.297	6.061	-1.108	-4.337	56.146
1/27/15	2xEV25C2	-41.314	70.508	-2.996	82.182	-0.903	-0.175	11.767	-29.47
1/28/15	2xEV25C	-41.467	70.132	-3.505	82.290	-0.306	-0.174	12.579	-28.05
1/30/15	Evap25C	-41.297	47.207	-25.614	26.272	4.745	-0.734	2.627	19.919
1/31/15	MDIW25C	-41.401	30.652	-41.778	-12.907	7.356	-1.137	-4.451	55.797
2/1/15	2xEV25C	-41.304	70.526	-2.986	81.675	-0.323	-0.193	11.260	-28.95
2/2/15	MDIW25C	-41.362	30.031	-42.336	-14.116	6.682	-1.145	-4.472	56.321
2/4/15	CarraraHG	1.962	37.57	7.299	2.012	3.581	-0.738	-3.002	-7.055
2/4/15	CarraraHG	2.15	37.737	7.68	1.125	9.065	-0.704	-4.206	-2.138
2/7/15	EvapHG	-41.206	43.683	-29.79	17.667	2.992	-1.688	0.938	24.928
2/8/15	2xEVHG	-41.359	66.822	-7.42	74.362	-0.763	-1.064	11.403	-22.57
2/9/15	CarraraHG	2.051	38.091	7.942	0.387	7.342	-0.696	-5.617	-4.423
2/11/15	OoidsHG	4.529	38.09	10.426	1.154	7.736	-0.622	-4.863	-6.489
2/11/15	2XEVHG	-41.185	67.27	-6.896	72.911	8.161	-1.139	9.190	-14.84
2/4/15	Evap25C	-41.374	46.874	-26.008	24.686	4.814	-0.738	1.714	20.719
2/5/15	2xEV25C	-41.36	70.455	-3.078	82.456	0.418	-0.161	12.124	-28.04
2/8/15	MDIW25C	-41.374	30.694	-41.76	-11.458	7.337	-1.186	-3.070	55.661
2/9/15	Evap25C	-41.182	47.35	-25.398	25.331	6.956	-0.768	1.434	21.76
2/10/15	2xEV25C	-41.259	71.062	-2.404	83.858	-0.191	-0.165	12.287	-29.84
2/11/15	MDIW25C	-41.29	30.761	-41.567	-15.978	14.365	-1.136	-7.758	62.796
2/12/15	MDIWHG	-41.412	29.329	-43.958	-17.178	7.756	-2.094	-6.212	58.945
2/13/15	CarraraHG	2.062	37.381	7.232	2.583	1.837	-0.716	-2.072	-8.519
2/15/15	EVAPHG	-41.312	44.644	-28.954	15.011	12.547	-1.658	-3.508	32.902
2/16/15	CarraraHG	2.077	36.755	6.632	1.293	3.044	-0.712	-2.153	-6.141
2/18/15	2XEVHG	-41.274	62.948	-11.141	62.736	3.499	-1.202	7.755	-11.32
2/19/15	CarraraHG	1.999	37.56	7.331	3.530	2.084	-0.732	-1.473	-8.554
2/21/15	OoidsHG	4.611	37.781	10.172	3.526	3.387	-0.649	-1.913	-10.27
2/12/15	Evap25C	-41.306	71.544	-1.988	85.129	0.895	-0.158	12.563	-29.61
2/12/15	2xEV25C	-41.458	70.658	-2.997	83.409	0.568	-0.175	12.631	-28.17
2/14/15	MDIW25C	-41.293	30.193	-42.177	-15.417	8.711	-1.208	-6.098	58.041
2/15/15	Evap25C	-41.375	46.961	-25.962	26.593	3.13	-0.774	3.411	18.839
2/16/15	2xEV25C	-41.118	70.329	-2.978	81.657	2.933	-0.184	11.614	-25.62
2/19/15	EVAP25C	-41.408	46.65	-26.264	25.650	2.064	-0.748	3.085	18.397
2/20/15	MDIW25C	-41.236	31.03	-41.367	-11.976	6.898	-1.248	-4.243	54.36
2/21/15	2xEV25C	-41.278	71.43	-2.079	83.981	2.622	-0.169	11.707	-27.76

SEPTEMBER 2014 RUN

Samples:

Date	Sample	d13C	d18O (raw)	d45	d46	d47	d48	D47	D48	window	D47rfac
09/14/14	B2014 RB_shell_hash #1 IZW	-3.99475	37.42313	-0.202	2.35736	1.8027	7.642	-0.307	2.9077	1	0.6928
09/15/14	B2014 RB shell hash #2 IZW	-4.371625	36.91963	-0.571	1.87078	0.9479	5.117	-0.302	1.3665	1	0.7227
09/18/14	B2104 Mod2 Ver2 #2 IZW	-0.787875	38.84525	2.845	3.73651	6.4404	10.321	-0.18	2.8135	1	0.6932
09/18/14	B2104 Mod1 Ver2 #1 IZW	-0.7055	38.79975	2.920	3.69335	6.4723	9.332	-0.183	1.9178	1	0.6889
09/18/14	B2014 RB_shell_hash #3 IZW	-4.152375	35.87625	-0.402	0.86391	0.1343	2.390	-0.301	0.66	1	0.7474
09/22/14	B2104 Mod1 Ver2 #3 IZW	-1.554	38.097	2.104	3.013	4.937	7.271	-0.203	1.228	2	0.7017
09/23/14	B2014 Mod1 VER2 #2 IZW	-0.638	38.787	2.983	3.682	6.522	15.395	-0.187	7.959	2	0.6704
09/26/14	B2014 RB6 VER2 #1 IZW	2.589	40.183	6.048	5.036	11.177	25.051	-0.046	14.804	2	0.6771
09/26/14	B2014 RB3 #1	2.193	40.305	5.682	5.152	10.914	14.753	-0.043	4.378	2	0.6875

	IZW										
09/26/14	B2014 Mod2 VER2 #1 IZW	-0.188	38.839	3.406	3.732	7.045	10.557	-0.151	3.057	2	0.6916
10/02/14	B2014 RB3 #2 IZW	2.394	40.261	5.869	5.110	11.086	13.523	-0.023	3.244	3	0.6964
10/07/14	B2014 RB3 #3 IZW	2.323	40.268	5.803	5.117	11.023	13.521	-0.026	3.227	3	0.6957

	δ13C*	**δ18O***
B2014 RB_shell_hash #1 IZW	-3.89	-2.27
B2014 RB shell hash #2 IZW	-4.27	-2.75
B2104 Mod2 Ver2 #2 IZW	-0.69	-0.90
B2104 Mod1 Ver2 #1 IZW	-0.61	-0.95
B2014 RB_shell_hash #3 IZW	-4.05	-3.76
B2104 Mod1 Ver2 #3 IZW	-1.45	-1.62
B2014 Mod1 VER2 #2 IZW	-0.54	-0.96
B2014 RB6 VER2 #1 IZW	2.69	0.38
B2014 RB3 #1 IZW	2.29	0.50
B2014 Mod2 VER2 #1 IZW	-0.09	-0.91
B2014 RB3 #2 IZW	2.49	0.46
B2014 RB3 #3 IZW	2.42	0.47

*Corrected δ18O and δ13C for -30C Porapak fractionation
(see Petersen et al., 2015, *RCMS,* for details)

Transfer Functions:

Window	**Start date**	**end date**	**SlopeEGL**	**SlopeETF**	**IntETF**
1	9/12/2014	9/18/2014	0.02929	0.988	0.946
2	9/22/2014	9/26/2014	0.02894	1.037	0.992
3	9/27/2014	##########	0.02976	1.024	0.993

Equilibrated and Heated Gasses:

Date	**Sample**	**d13C**	**d18O**	**d45**	**d46**	**d47**	**d48**	**D47**	**D48**
09/09/14	MCB HG	-2.82	23.32	0.41	-11.256	-11.91	-14.71	-1.270	7.86
09/09/14	Mix HG	-3.06	25.14	0.25	-9.499	-10.25	-15.57	-1.173	3.41
09/09/14	Cararra HG	2.06	36.86	5.44	1.830	6.66	8.82	-0.753	5.14
09/09/14	Ooids HG	4.37	37.36	7.62	2.313	9.49	16.86	-0.654	12.17
09/10/14	Mix HG	-3.01	26.57	0.34	-8.113	-8.79	-17.45	-1.168	-1.31
09/10/14	MCB HG	-3.32	20.99	-0.14	-13.499	-14.70	-26.65	-1.295	0.17
09/10/14	MDIW HG	-41.48	28.97	-35.54	-5.883	-44.33	-13.70	-2.194	-1.99
09/11/14	Mix HG	-2.96425	22.48875	0.25075	-12.055	-12.87	-30.13	-1.279	-6.316
09/11/14	Cararra HG	2.11675	36.73188	5.48899	1.704	6.6046	5.1591	-0.737	1.7419
09/12/14	Mix HG	-2.9255	27.51875	0.45926	-7.200	-7.743	-16.28	-1.137	-1.958
09/14/14	MCB HG	-3.05	22.31	0.16	-12.229	-13.10	-32.32	-1.252	-8.21
09/15/14	Carrara HG	1.89875	37.09925	5.29739	2.058	6.7445	6.3545	-0.749	2.2253
09/16/14	Cararra HG	2.125125	37.61063	5.52665	2.552	7.4752	7.9366	-0.744	2.8111
09/18/14	Mix HG	-3.061875	24.95313	0.24375	-9.677	-10.48	-24.86	-1.224	-5.713
09/19/14	MCB HG	-3.02425	21.82213	0.17168	-12.699	-13.61	-31.36	-1.306	-6.278
09/19/14	MCB HG	-3.02	21.82	0.17	-12.699	-13.61	-31.36	-1.306	-6.28
09/20/14	AAS HG	-41.66488	16.4115	-36.1416	-18.005	-56.78	-46.34	-2.602	-11.05
09/22/14	MDIW HG	-41.38	26.67	-35.5242	-8.105	-46.49	-20.76	-2.276	-4.69
09/23/14	Cararra HG	2.042625	33.60113	5.31231	-1.318	3.3354	-3.535	-0.836	-0.902
09/27/14	AAS HG	-41.46075	16.96313	-35.9329	-17.472	-56.07	-44.06	-2.600	-9.761
09/28/14	Mix HG	-3.334375	26.4355	0.03982	-8.247	-9.255	-21.55	-1.192	-5.207

09/27/14	AAS HG	-41.46075	16.96313	-35.9329	-17.472	-56.07	-44.06	-2.600	-9.761
09/29/14	Carrara 2 HG	2.376125	35.19738	5.679	0.223	5.2582	-0.597	-0.815	-1.043
10/01/14	Evap HG	-41.5075	39.76438	-35.1943	4.534	-33.89	11.114	-1.950	2.006
10/02/14	AAS HG	-41.4205	17.1775	-35.8868	-17.264	-55.89	-45.72	-2.667	-11.9
10/04/14	Carrara2 HG	3.208875	38.77438	6.57962	3.677	9.7682	9.2174	-0.653	1.836
10/07/14	Evap HG	-41.34875	42.5835	-34.9505	7.256	-30.99	18.458	-1.874	3.836
10/09/14	AAS HG	-41.52575	17.14313	-35.9865	-17.299	-55.99	-46.17	-2.636	-12.29
10/13/14	Carrara2 HG	1.845	34.230	5.149	-0.711	3.814	-2.854	-0.790	-1.435
10/13/14	Carrara2 HG (rerun)	1.844	34.231	5.148	-0.712	3.795	-2.780	-0.807	-1.358
09/09/14	AAS 25C	-41.63	17.02	-36.09	-17.422	-55.16	-35.22	-1.533	-0.70
09/10/14	AAS 25C	-41.31	17.96	-35.76	-16.509	-54.05	-33.31	-1.614	-0.58
09/10/14	Evap 25C	-40.61	47.16	-34.10	11.674	-24.83	35.80	-0.748	12.03
09/10/14	MDIW 25C	-41.64	30.58	-35.63	-4.327	-42.07	-8.09	-1.275	0.55
09/11/14	Evap 25C	-40.62	46.65	-34.13	11.177	-25.35	33.49	-0.764	10.77
09/11/14	MDIW 25C	-41.56725	30.66838	-35.5607	-4.244	-41.88	-9.768	-1.236	-1.308
09/12/14	MDIW 25C	-41.66813	30.262	-35.6701	-4.637	-42.37	-9.213	-1.240	0.0401
09/12/14	MDIW 25C	-41.4885	30.806	-35.4829	-4.111	-41.67	-8.524	-1.229	-0.322
09/14/14	AAS 25 BL	-41.77425	15.35225	-36.2802	-19.028	-56.98	-48.44	-1.637	-11.17
09/15/14	AAS 25C	-41.60338	17.30925	-36.0542	-17.138	-54.98	-43.09	-1.654	-9.423
09/16/14	Evap 25	-40.67513	46.96838	-34.1715	11.490	-25.11	30.507	-0.776	7.2279
09/17/14	Evap 25C	-41.57	46.41	-35.03	10.948	-26.55	28.88	-0.816	6.72
09/19/14	MDIW 25C	-41.52	29.27	-35.56	-5.595	-43.21	-14.26	-1.283	-3.14
09/20/14	AAS 25C	-41.47925	17.11188	-35.9443	-17.328	-55.08	-45.27	-1.692	-11.3
09/22/14	AAS 25	-41.57	17.38	-36.0214	-17.072	-54.90	-45.65	-1.676	-12.21
09/23/14	Evap 25C	-41.52913	46.7425	-34.9774	11.270	-26.22	29.66	-0.845	6.8368
09/24/14	AAS 25	-41.58	17.51	-36.03	-16.944	-54.78	-44.18	-1.674	-10.95
09/26/14	AAS 25C	-41.6875	17.24575	-36.1344	-17.199	-55.15	-43.67	-1.688	-9.905
09/27/14	Evap 25C	-41.48763	47.04338	-34.9282	11.560	-25.9	31.689	-0.849	8.2437
09/28/14	AAS 25C	-41.44938	17.70738	-35.8961	-16.754	-54.52	-43.93	-1.724	-11.07
09/29/14	MDIW 25C	-41.40875	30.66475	-35.4127	-4.249	-41.86	-11.47	-1.362	-3.015
09/28/14	AAS 25C	-41.45	17.71	-35.90	-16.754	-54.52	-43.93	-1.724	-11.07
10/03/14	AAS 25	-41.54475	17.967	-35.9759	-16.503	-54.37	-42.82	-1.725	-10.42
10/04/14	Evap 25C	-41.43375	47.02113	-34.8786	11.539	-25.88	30.291	-0.856	6.9187
10/07/14	MDIW 25C	-41.45788	29.57975	-35.4969	-5.296	-42.95	-14.65	-1.375	-4.129
10/08/14	AAS 25C	-41.47375	17.85088	-35.9137	-16.615	-54.45	-44.08	-1.768	-11.5
10/11/14	Evap 25C	-41.56475	45.15313	-35.0645	9.736	-27.78	25.201	-0.861	5.527

MARCH 2014 RUN

Samples:

Date	Sample	d13C	d18O (raw)	d45	d46	d47	d48	D47	D48	window	D47rfac
04/07/14	B11 RB1 #2 IZW	2.390375	39.71875	5.847	4.58664	10.494	11.934	-0.075	2.7152	1	0.6915
04/08/14	B11 RB1 #3 IZW	2.37225	40.06625	5.841	4.92343	10.83	13.132	-0.066	3.2293	1	0.6906
04/08/14	B11 RB1 #4 IZW	2.071125	39.56275	5.543	4.4359	10.048	11.927	-0.057	3.0089	1	0.7218
04/08/14	B11 RB1 #1 IZW	2.495375	39.68038	5.943	4.55007	10.557	11.960	-0.075	2.8132	1	0.6889

Transfer Functions:

Window	Start date	end date	SlopeEGL	SlopeETF	IntETF
1	4/7/2014	4/11/2014	0.028009	2.0919	1.308

	δ13C*	δ18O*	*Corrected δ18O and δ13C for -30C Porapak fractionation
B11 RB1 #2 IZW	2.49	-0.06	(see Petersen et al., in review, *RCMS,* for details)
B11 RB1 #3 IZW	2.47	0.27	
B11 RB1 #4 IZW	2.17	-0.21	
B11 RB1 #1 IZW	2.60	-0.10	

Equilibrated and Heated Gasses:

Date	Sample	d13C	d18O	d45	d46	d47	d48	D47	D48
03/30/14	Evap HG	-41.27538	43.9305	-34.8366	8.556	-29.42	21.208	-1.639	3.9553

03/31/14	MCB HG	-5.91425	23.69825	-2.46552	-10.893	-14.47	-27.8	-1.254	-6.272
04/01/14	MCB HG	-5.91725	23.7665	-2.46607	-10.828	-14.43	-27.47	-1.279	-6.061
04/02/14	MCB HG	-41.59838	16.8685	-36.0641	-17.564	-56.07	-44.3	-2.378	-9.818
04/03/14	Mix HG	-3.867875	29.47713	-0.35419	-5.312	-6.653	-13.81	-1.070	-3.245
04/05/14	MDIW HG	-41.38475	28.7725	-35.4553	-6.074	-44.31	-15.23	-2.073	-3.159
04/06/14	MCB HG BL	-4.500875	22.94225	-1.17025	-11.620		-29.69	-0.999	-6.748
04/05/14	MDIW HG	-41.38475	28.7725	-35.4553	-6.074	-44.31	-15.23	-2.073	-3.159
04/06/14	MCB HG BL	-4.500875	22.94225	-1.17025	-11.620		-29.69	-0.999	-6.748
04/08/14	Evap HG	-41.40713	43.60513	-34.9703	8.241	-29.95	20.979	-1.742	4.3562
04/12/14	MDIW HG	-41.37575	29.9325	-35.4075	-4.956	-43.27	-13.53	-2.146	-3.684
04/14/14	Ooids HG	-1.439625	35.25113	2.11329	0.266	1.5437	0.2214	-0.896	-0.311
03/30/14	Evap 25C	-41.37425	46.52688	-34.8408	11.062	-26.15	28.031	-0.711	5.6576
03/31/14	Evap 25C	-41.44638	47.0115	-34.8914	11.528	-25.77	29.197	-0.720	5.872
04/01/14	MDIW 25C	-41.43088	31.14238	-35.4173	-3.786	-41.18	-9.307	-1.109	-1.762
04/03/14	Evap 25C	-41.38763	47.28213	-34.8267	11.790	-25.46	30.02	-0.731	6.1539
04/03/14	AAS 25C	-41.28563	17.08938	-35.7636	-17.350	-54.71	-43.4	-1.468	-9.323
04/05/14	AAS 25	-28.46867	20.22025	-23.6729	-14.300	-39.24	-36.1	-1.222	-7.96
04/05/14	AAS 25	-28.46867	20.22025	-23.6729	-14.300	-39.24	-36.1	-1.222	-7.96
04/07/14	AAS 25C	-41.227	18.3215	-35.6665	-16.160	-53.55	-41.16	-1.540	-9.401
04/09/14	AAS 25C	-41.36888	17.24725	-35.8364	-17.198	-54.71	-43.83	-1.547	-10.07
04/11/14	Evap 25C	-41.448	47.32588	-34.8818	11.833	-25.53	30.681	-0.781	6.7135
04/11/14	AAS 25C	-41.41	16.22388	-35.9099	-18.183	-55.78	-46.86	-1.608	-11.23
04/13/14	Evap 25C	-41.40788	47.55813	-34.8363	12.056	-25.29	31.329	-0.798	6.9044
04/14/14	AAS 25C	-41.29413	17.1915	-35.7685	-17.251	-54.75	-44.04	-1.607	-10.19